Optische-val-gecontroleerde elektroforese van individuele colloïdale deeltjes

Optical Trapping Electrophoresis of Single Colloidal Particles

Caspar Schreuer

Promotoren: prof. dr. ir. F. Beunis, prof. dr. ir. K. Neyts
Proefschrift ingediend tot het behalen van de graad van
Doctor in de ingenieurswetenschappen: fotonica

Vakgroep Elektronica en Informatiesystemen
Voorzitter: prof. dr. ir. K. De Bosschere
Faculteit Ingenieurswetenschappen en Architectuur
Academiejaar 2017 - 2018

UNIVERSITEIT
GENT

ISBN 978-94-6355-118-2
NUR 910, 950
Wettelijk depot: D/2018/10.500/36

Universiteit Gent
Faculteit Ingenieurswetenschappen en Architectuur
Vakgroep Elektronica en Informatiesystemen

Promotoren:

prof. Filip Beunis
prof. Kristiaan Neyts

Examencommissie:

prof. Filip De Turck (Voorzitter)	Universiteit Gent
prof. Filip Beunis (promotor)	Universiteit Gent
prof. Kristiaan Neyts (promotor)	Universiteit Gent
prof. Filip Strubbe	Universiteit Gent
prof. Thomas Palberg	Johannes Gutenberg-Universität
prof. Peter Bienstman	Universiteit Gent
prof. Kevin Braeckmans	Universiteit Gent

Dit werk kwam tot stand in het kader van een beurs van het agentschap voor Innovatie door Wetenschap en Technologie (IWT)

Dankwoord

In 2012 ben ik begonnen aan dit doctoraat en uiteindelijk heeft het 5 volle jaren in beslag genomen. Het werd een werk van veel vallen en opstaan, waar zeldzame eureka-momenten omringd werden door eindelooslijkende wetenschappelijke droogtes. Zo is dan ook de aard van wetenschappelijk onderzoek. En waar opluchting dan wel het eerste gevoel is dat het afronden van dit doctoraat in mij oproept, is een oprecht gevoel van dankbaarheid de nipte tweede. Dankbaarheid aan tal van mensen, die mij elk op zijn of haar manier hebben bijgestaan. Zonder hen was geen letter van dit doctoraat geschreven.

Eerst en vooral wil ik mijn promotoren bedanken. Trouw aan zijn stijl, bood Filip me de positie van doctoraatstudent aan op café. Het zou niet de laatste keer zijn dat we na het werk iets gingen drinken. Als promotor was je steeds aanspreekbaar en behulpzaam. Ik heb een goede vriend overgehouden aan jou. Ook mijn promotor Kristiaan heeft me dikwijls bijgestaan met advies en correcties, waarvoor dank.

Stijn, voor talloze gesprekken over werk en leven, voor de technische ondersteuning, voor het gezelschap tot in de vroege uurtjes op kantoor en voor de vriendschap, bedankt! Succes met de laatste loodjes. Filip Strubbe, voor vele discussies en voor goede suggesties. Toon, jij leerde mij het ABC van OTE. Bavo, voorzie tijdig opvolging, zodat de kajakroute niet onbevaren achterblijft! Samira, ever so upbeat, tu me manqueras.

Thanks to all the colleagues who have made this place into what it is, I will always remember you for it. In particular to John, Oliver, Glenn and Lieven and also to Michiel, prof. Lauwaert, Varsenik, Yerzhan, Natalia, Sheng, Frederik, Boxuan, Gilles, Brecht, Jeroen, Ingrid, Inge, Woestie, Tom, Xi, Aimi, prof. De Vos, prof. De Visschere, prof. Burgelman, Manoj, Masoumeh and Oksana.

Aan mijn vrienden, die er ook zijn wanneer het even serieus moet zijn. Omdat ik aan de voorbije 10 jaar in Gent niets zou veranderen.

Sacha, Lara, Milan en Max, mijn broers en zus die me dierbaar zijn. Alsook mijn nieuwe broers en zussen Nils, Oriane, Inès, Rikke, Niels, Lotte en Davy. Patrick en Kristien, betere schoonouders kan een mens niet wensen.

Aan mijn ouders, die me meer dan wie ook gevormd hebben tot wie ik vandaag ben. Jullie boden me een warme thuis en onvoorwaardelijke steun. Jullie leerden me het belang van inzet en kritisch denken. Mama en papa, bedankt er om altijd te zijn.

Sanne,
mijn vrouw,
mijn steun en toeverlaat,
bedankt voor je begrip die laatste 6 maanden.
Ik zie je graag.

Ellis,
aan wie ik dit werk opdraag.

Contents

List of symbols

Symbol	Unit	Description
A_{Lamp}	-	Aperture for the lamp
A_{QPD}	-	Aperture for the QPD
c	m/s	Speed of light in vacuum
d	µm	Particle's diameter
d_{CM}	m	Inverse micelle's diameter
D	m²/s	Diffusion coefficient
e	C	Elementary charge
E_0	V/m	Amplitude of the electric field
f_E	Hz	Frequency of the electric field
f_s	Hz	Sampling rate of the QPD
f_c	Hz	Corner frequency
f_Q	Hz	Rate at which the particle's charge is calculated
F	N	A force. F_B *Brownian* force, F_{drag} drag force, F_{part} force exerted on the particle, F_{trap} trapping force, F_{tot} total force.
h	m²kg/s	*Planck's* constant
k_B	J/K	*Boltzmann* constant
m	kg	Particle's mass
m_n	-	Ratio of the refractive index of the particle over the refractive index of the medium
n	-	Refractive index
$n_+, n_-, n_0, n_{\mathrm{ion}}$	m^{-3}	concentration of positively charged, negatively charged and neutral inverse micelles and ions of unspecified polarity
N_{el}	-	Number of elementary charging events
p	kg m/s	Momentum
Q	C	The particle's charge. For Chapters 4 and 5 $Q = Q_f = Q_{\mathrm{part}}$.
Q_f	C	Final calculated charge value

$Q_{\mathrm{i}}, Q_{\mathrm{final}}$	C	Respectively the first value and the last value of the particle's charge from the measurement
Q_j	C	First, intermediate calculated charge value
Q_{part}	C	The particle's charge
r	m	Displacement
R^2	-	Name of a function used to analyze the charge
R_-^2	-	Variation of the R^2 -function
S_{zz}	m²s	Power spectral density of z
$S_{z,VV}$	V²s	Power spectral density of V_z
t	s	Time
T	K	Temperature
u	-	Correction factor as a parameter
u_{el}	-	Effective correction factor
v	m/s	Velocity
V_1, V_2, V_3, V_4	V	Voltages of individual photodiodes of the QPD
V_x, V_y, V_z	V	Voltages containing information on x, y, z movement respectively
x, y, z	m	Positional coordinate
$\dot{z}$	m/s	Time derivative of positional coordinate
$\ddot{z}$	m/s²	Time derivative of $\dot{z}$
Z	-	Valence number of an ion or a particle
$\beta_x, \beta_y, \beta_z$	-	Conversion factors
Δt	s	Duration of a measurement
Δt_s	s	Sampling time
Δt_Q	s	Time window for which a single calculation of the charge is performed
χ	-	Fraction of charged inverse micelles over uncharged inverse micelles
ε_0	F/m	Permittivity of vacuum
ε_i	-	Variation of the normalized charge around integer values
ε_r	-	Relative dielectric permittivity
Φ_{d}	V	*Stern* potential
Φ_s	V	Surface potential

γ	Pa m s	*Stokes* drag coefficient
η	Pa s	Dynamic viscosity
κ^{-1}	m	Debye length
κ_F	N/m	Stiffness of the optical trap
λ_B	m	*Bjerrum* length
μ_e	m²/Vs	Electrophoretic mobility
θ	-	Angle
σ^2	C²	Variance, σ_R^2 the variance calculated from the R^2 -function
σ_m	C/m²	Surface charge density
τ	s	Time constant
ω	rad/s	$\omega = 2\pi f$
ξ	$Hz^{-1/2}$	*Gaussian* noise term
ζ	V	Zeta-potential

List of Abbreviations

Abbreviation	Full text
AC	Alternating current
CMC	Critical micelle concentration
DC	Direct current
DFT	Discrete *Fourier* transform
DP-OCT	Differential phase optical coherence tomography
ITO	Indium Tin Oxide
LDE	Laser Doppler electrophoresis
NA	Numerical aperture
OLOA	Oronite Lubricating Oil Additive, OLOA 11000 is a surfactant.
OTE	Optical trapping electrophoresis
PALS	Phase analysis light scattering
PHSA	Poly-12-hydroxystearic, a type of steric stabilizing coating for colloidal particles.
PMMA	Poly(methyl methacrylate)
SNR	Signal-to-noise ratio
QPD	Quadrant photodiode

Nederlandstalige samenvatting

Een colloïdale suspensie is een mengeling waarin microscopische of nanoscopische deeltjes verspreid zijn doorheen een vloeistof. Melk is een colloïdale suspensie van vetdruppels in water en printer inkt is een colloïdale suspensie van vaste inkt partikels in olie. Een belangrijke eigenschap van colloïdale suspensies is hun stabiliteit. De stabiliteit van een colloïdale suspensie kan in het gedrang komen door zowel aggregatie als sedimentatie. Dit komt voor wanneer aantrekkende inter-deeltjes krachten het winnen van afstotende inter-deeltjes krachten. Een veelgebruikte wijze om aggregatie te voorkomen bestaat uit het verhogen van de afstotende inter-deeltjes krachten door de elektrische lading van de deeltjes te laten toenemen. Coulomb krachten verhinderen de deeltjes dan om contact te maken met elkaar of met het substraat.

Elektrische fenomenen vormen een fundamenteel aspect van colloïdale suspensies en deze zijn reeds goed begrepen in waterachtige systemen. Hetzelfde kan niet gezegd worden van colloïdale suspensies in olieachtige vloeistoffen. Het verschillend gedrag tussen waterachtige en olieachtige systemen is vooral te wijten aan hun sterk verschillende relatieve diëlektrische constanten. Door zijn hoge relative diëlektrische constante (ε_{r,H_2O} = 80) is water een geschikt medium voor ionen. Olieachtige vloeistoffen zoals n-dodecaan ($\varepsilon_{r,C_{12}H_{26}}$ = 2) daarentegen zijn dat niet. Vloeistoffen met een hoge diëlektrische constante heten polaire vloeistoffen en vloeistoffen met een lage diëlektrische constante heten niet-polaire vloeistoffen. Ten gevolge van hun lage diëletrische constante reiken elektrostatische interacties in niet-polaire vloeistoffen veel verder dan in polaire vloeistoffen, waardoor ionen in niet-polaire vloeistoffen een grotere waarschijnlijkheid hebben om elkaar te neutraliseren. Colloïdale deeltjes in

niet-polaire vloeistoffen zijn gewoonlijk niet sterk genoeg geladen om elkaar af te stoten, waardoor ze aggregeren of sedimenteren.

Er bestaan chemische substanties die, wanneer ze toegevoegd worden aan niet-polaire vloeistoffen, ervoor zorgen dat de colloïdale deeltjes sterk geladen worden. Deze chemische substanties heten tensiden. Ze bestaan gewoonlijk uit polaire kopstukken gekoppeld aan een lange niet-polaire staart. Boven een zekere concentratie vormen tensiden sferische structuren, inverse micellen genoemd, waarin de polaire kopstukken naar binnen wijzen en de niet-polaire staarten naar de vloeistof toe wijzen. Deze concentratie heet de kitische micelle concentratie.

Het mechanisme waardoor deeltjes in niet-polaire vloeistoffen geladen worden is echter nog steeds het onderwerp van hevig debat en van wetenschappelijke studies. Verscheidene mogelijke tenside gerelateerde ladingsmechanismen zijn reeds voorgesteld en in het geval van enkele specifieke deeltje-vloeistof-tenside systemen is het reeds bepaald welk ladingsmechanisme het dominante is. Het is echter tot op heden vaak onmogelijk om op voorhand uit te maken welk mechanisme het dominante zal zijn voor een gegeven colloïdaal systeem. Dit is deels te wijten aan de complexiteit van landingsprocessen in tenside-verrijkte systemen, maar eveneens aan het beperkte bereik van de huidige meettechnieken die we ter beschikking hebben.

Optische-val-gecontroleerde elektroforese blijft tot op heden de enige experimentele techiek waarvan aangetoond is dat ze in staat is om de elektrische lading van een colloïdaal deeltje te meten met een precisie zodanig dat elementaire ladingsstappen gemeten kunnen worden zonder dat er daarop tijdsrestricties heersen. De eigenschap om elementaire landingsstappen te detecteren opent een nieuw perspectief op de studie van ladingsfenomenen in niet-polaire vloeistoffen. In voorafgaand werk werd aangetoond dat optische-val-gecontroleerde elektroforese elementaire landingsstappen kan detecteren op individuele deeltjes in zuivere, niet-polaire vloeistoffen. Het opzet van dit werk is om deze techniek te verbeteren, zodanig dat elementaire ladingsstappen van deeltjes gedetecteerd kunnen worden in niet-polaire vloeistoffen die verrijkt zijn met

tensiden. Een belangrijke mijlpaal is elementaire ladingsdetectie in vloeistoffen met een concentratie aan tensiden boven de kritische micelle concentratie.

Om dat doel te bereiken heb ik aan alle niveaus van de techniek gesleuteld. Ik heb de microfluïdische cel waarin de suspensies onderzocht worden opnieuw ontworpen. De huidige cel bestaat uit twee glasplaten die bedekt zijn met ITO elektroden. Het elektrische veld staat nu dwars op het vloeistof-substraat interface, zodat vloeistofstromingen, veroorzaakt door een elektrisch veld, vermeden worden. Een tweede voordeel aan deze cellen is dat ze gemaakt worden in de cleanroom, zodat contaminatie geminimaliseerd wordt. Ik heb ook een alignatie protocol opgesteld dat dient uitgevoerd te worden voorafgaand aan elke meting. Ten laatste, heb ik de bestaande analyse procedure verder uitgediept, zodat de elementaire stappen in de experimentele data correct gedetecteerd kunnen worden.

Eerst heb ik PHSA-bedekte PMMA deeltjes van micrometer grootte bestudeerd in dodecaan zonder surfactant. Experimenten toonden aan dat de lading van zo'n deeltje niet stabiel was over de tijd, maar toenam in positieve oppervlaktelading. Geconfronteerd met dit niet-geanticipeerde ladingsgedrag heb ik onderzocht wat de invloed is op de ladingssnelheid van factoren zoals de amplitude en de frequentie van het elektrische veld, de diameter van het deeltje, het elektrodemateriaal, de afwezigheid van een AC elektrisch veld en de aanwezigheid van een DC elektrisch veld. Ook onderzocht ik de saturatie van dit proces over lange termijn. Tesamen leidde deze set aan experimenten mij ertoe te besluiten dat de deeltjes negatieve ionen afstoten onder de invloed van het elektrische veld.

Daarna heb ik bestudeerd hoe het ladingsproces verandert wanneer een tenside toegevoegd wordt. In dit werk heb ik exclusief gewerkt met tenside OLOA 11000. Door het opleggen van een DC spanning van 1 V, ben ik erin geslaagd om het bereik van optische-val-gecontroleerde elektroforese waarin het elementaire ladingsstappen kan detecteren uit te breiden naar een tenside concentratie van 0.05 wt%, hetgeen een factor 10 boven de kritische micelle concentratie van OLOA 11000 in dodecaan ligt. Dit is het eerste experimentele werk waarin elementaire ladingsstappen in tenside

verreikte colloïdale systemen zijn waargenomen. Eén reden waardoor het aanleggen van een DC spanning hierbij helpt, is omdat het alle ionen uit de bulk van de vloeistof verwijdert. De aanwezigheid van ionen dempt immers de oscillerende beweging van een deeltje in een AC elektrisch veld. In deze omstandigheden toonde ik aan dat het deeltje zijn ladingssnelheid toeneemt met toenemende concentraties aan tenside. Rond de kritische micelle concentratie stabiliseert de elektrische lading van het deeltje en fluctueert ze rond een vaste, gemiddelde waarde.

Als besluit kan ik stellen dat ik het concentratie bereik van optische-val-gecontroleerde electrophorese waarin een deeltje zijn lading met een resolutie van minder dan één elementaire lading gemeten kan worden uitgebreid en dus het bereik waarin elementaire op- en ontladingen kunnen worden waargenomen uitgebreid. Ik heb getoond hoe de techniek kan ingezet worden om nieuwe inzichten te verwerven over de landingsmechanismen van colloïdale deeltjes in zowel zuivere niet-polaire vloeistoffen als in niet-polaire vloeistoffen die verrijkt zijn met tensiden in concentraties boven de kritische micelle concentratie.

English summary

A colloid or a colloidal suspension is a mixture in which microscopic or nanoscopic particles are dispresed throughout a liquid medium. Milk is a colloidal suspension of fat droplets in water and printer ink is a colloidal suspension of solid ink particles in oil. An important characteristic of colloidal suspensions is its stability. The stability of colloidal suspensions is hindered by aggregation and sedimentation. This occurs when attractive interparticle forces prevail over repulsive interparticle forces. A common way to prevent aggregation and sedimentation is to increase repulsive forces by increasing the particle's electric charge. Coulombic forces then prevent particles from making contact with each other or with the substrate interface.

Electric phenomena form a fundamental aspect of colloidal suspensions and they are well-understood in aqueous suspensions. The same is not true for colloidal suspensions in oily liquids. A key difference between oils and water lies in their respective dielectric constants. Due to its high relative dielectric constant ($\varepsilon_{r,\mathrm{H_2O}}$ = 80), water provides a suitable host medium for ionic molecules where they can be freely dispersed. Oily liquids such as n-dodecane ($\varepsilon_{r,C_{12}H_{26}}$ = 2) on the other hand do not. Liquids with high relative dielectric constants, such as water, are called polar liquids and liquids with low dielectric constants, such as dodecane, are called nonpolar liquids. Due to the low relative dielectric constant, electrostatic interactions in nonpolar liquids are long ranged when compared to water, which is why oppositely charged ions are more likely to neutralize each other. Colloidal particles in pure nonpolar liquids commonly are not sufficiently charged to repel each other, causing aggregation or sedimentation.

There exist chemical compounds that, when added to a nonpolar colloidal suspension, cause the colloidal particles to become highly charged. These chemical compounds are called surfactants. Surfactant molecules typically consist of polar head groups with long nonpolar tails. Above a certain concentration, surfactants in nonpolar liquids form spherical structures,

called inverse micelles, where the polar head groups of the molecules are pointed inwards and the nonpolar tails are pointed toward the liquid medium. This concentration is called the critical micelle concentration.

The mechanism through which particles in nonpolar liquids become charged by surfactants however, is still the subject of much debate and scientific research. Different possible surfactant related charging mechanisms have been put forward and in several specific particle-liquid-surfactant combinations it has been determined what the dominant charging mechanism is. However, to date, it is often still impossible to state in advance what the dominant charging mechanism will be for a colloidal system. This is partly due to the complexity of surfactant-enriched colloidal nonpolar systems, but also partly due to the limited scope of currently available measurement techniques.

Optical trapping electrophoresis remains the only experimental technique that has demonstrated the capabilty of measuring the charge of colloidal particles with such precision that single elementary charging and discharging events can be detected and that can do so without time restrictions. The ability to resolve elementary (dis)charging events on a single particle opens up new avenues to study colloidal charging phenomena. In previous work, the detection of elementary charging events on single particles has been achieved for particles in a pure nonpolar liquid. The aim of this work is to improve optical trapping electrophoresis as a technique, so that single charging events can be detected on particles in nonpolar liquids with surfactants. An important milestone is the detection of elementary charging events at surfactant concentrations above the critical micelle concentration.

In order to achieve that goal, all stages that together make up optical trapping electrophoresis are revisited. I redesigned the microfluidic cell in which the colloids are examined. The cell consists of two parallel glass plates that are covered with a thin ITO electrode. The electric field is now perpendicular to the liquid-solid interface of the cell. This has the advantage that liquid flows generated by the presence of an electric field are prevented. Another advantage is that the cells are now created under cleanroom conditions to prevent contamination by undetermined species. I also put

forward a protocol to align the laser prior to each measurement. Finally, I extended the analysis method that is used to resolve elementary charging events from the measurement data.

First, I studied micrometer sized PHSA-coated PMMA particles in dodecane without surfactant. Experiments revealed that the particle's charge was not stable over time. Instead, particles accumulated positive surface charge over time. Confronted by this unanticipated phenomenon, I investigated how the particle's charging rate changed when factors such as the amplitude and the frequency of an AC electric field, the particle's diameter, the electrode material, the absence of an electric field and the presence of a DC electric field are changed. I also studied the long-term saturation of this effect. Through the ensemble of these experiments, I concluded that these particles shed negatively charged ions under the influence of an electric field.

Then, I studied how the charging mechanism changes when surfactant is introduced. In this work, we used OLOA 11000 as surfactant. By applying a DC voltage of 1 V, the concentration range in which the particle's charge can be measured with a charge resolution smaller than the elementary charge was extended to 0.05 wt% OLOA in dodecane, which encompasses the critical micelle concentration of OLOA 11000 in dodecane. This marks the first experimental demonstration of elementary event monitoring in surfactant-enriched environments. One contributing reason why a DC voltage helps increase this range, is because it depletes the bulk of the liquid from ionic species. The presence of ions impedes the oscillatory motion of a particle in an AC electric field through the retardation effect. Under these conditions, I showed that the particle's charging frequency increases as the surfactant concentration increases. Around the critical micelle concentration, the particle's charge stabilizes and fluctuates around a mean charge value.

In summary, in this work, I extended the concentration range in which optical trapping electrophoresis can be used to monitor a particle's charge with a charge resolution smaller than the elementary charge and thus to detect elementary charging events. I demonstrated how this can be used to gain new insights in the charging mechanisms of colloidal particles both in pure

nonpolar liquids and in surfactant-enriched nonpolar systems at concentrations above the critical micelle concentration.

Chapter 1.

Background & Outline

1.1 Introduction

The aim of this dissertation is to demonstrate that optical trapping electrophoresis (OTE) is a valuable characterization tool for fundamental research into the charging behavior of colloidal particles in nonpolar liquids. To that effect, I elaborate on the innovations in the technique, both experimentally and analytically. I apply OTE to a model system of micrometer sized poly-12-hydroxystearic-coated (PHSA) poly(methyl methacrylate) (PMMA) particles in n-dodecane both with and without surfactant OLOA 11000 and demonstrate new findings that are relevant to the broader scientific community whose work is focused on the study of colloidal charging mechanisms.

1.2 Background and motivation

Colloidal particles form an essential element in several industrial applications ranging from electrophoretic image displays[1, 2], printing toners[3] and drug delivery systems[4]. It is the electric charge of the colloidal particles that largely determines their functionality and stability. Because nonpolar liquids have a low relative dielectric permittivity ($\varepsilon_{r,C_{12}H_{26}} = 2$) compared for instance to water with $\varepsilon_{r,H_2O} = 80$ at T = 298 K, electrostatic interactions are present over a longer range, which leads to low charge densities in nonpolar liquids.

To stabilize the particle's charge, most nonpolar dispersions contain added chemical substances such as surfactants[5-10]. Though the relation between the surfactant concentration and the charge density in nonpolar liquids is well documented, the nature of charging mechanisms in nonpolar colloidal systems continues to be an active area of research[11-16]. Several distinct charging mechanisms have been identified in surfactant-enriched nonpolar colloidal systems, but due to the complex nature of the interaction between surfactants and colloidal particles, it is not always clear in advance which mechanism will be dominant.

This difficulty to forecast the charging behavior of colloidal systems is partly due to a lack of accurate measurement tools. Different types of experimental techniques exist that directly measure the particle's velocity from which the

charge or the zeta-potential of colloidal particles such as optical tracking microelectrophoresis[17], blinking optical tweezers[18], laser Doppler electrophoresis[19], phase analysis light scattering[20], differential-phase optical coherence tomography[21] and electroacoustics[22] and they all have their own benefits. In contrast to these techniques however, OTE is the only technique that can measure the charge of colloidal particles in nonpolar liquids with elementary charge resolution over extended time periods. It is this ability to resolve individual charging and discharging events that allows me to study different aspects of the charging behavior besides the mean charge. For instance, I report on how the charging frequency of a particle varies with the surfactant concentration or how the charging mechanism is affected by the magnitude of the applied electric field.

In conclusion, I am convinced that OTE has a trove of unexplored information on the charging behavior to offer and that it has the possibility to shed new light on colloidal charging phenomena.

1.3 Outline

Chapter 2: Colloidal particles in nonpolar liquids

This chapter serves as an introductory chapter that offers a theoretical background for the subsequent chapters. The main subjects in this chapter are *Brownian* motion, optical trapping, surfactants and colloid stability.

Chapter 3: Measurement and analysis method

First, the working of the experimental setup is explained. This is followed by a thorough review of the analysis method that is used to detect elementary charging events in charge data.

Chapter 4: Electric field-induced charging

I examine the charge of PMMA particles in dodecane and encounter unanticipated charging behavior. Further experiments are conducted that shed light on this phenomena

Chapter 5: Surfactant and particle charging

I present experimental observations on how the presence of the surfactant OLOA 11000 influences the charging behavior.

Chapter 6: Conclusions & future prospects

Summary of the main conclusions of this work and an outlook on what optical trapping electrophoresis has to offer in the (hopefully near) future.

Chapter 2.

Background & Theory

2.1 Introduction

The goal of this dissertation is to present advances in optical trapping electrophoresis as a technique and to demonstrate its capabilities as a tool to investigate charging properties of colloidal particles in nonpolar liquids. To do so requires to first establish a comprehensive framework of the current state of the art, about theories that have been developed and about alternative techniques in this field. This chapter serves to point out the relevance of this work and to underscore that this work is not the product of my isolated research efforts, but instead is built upon the results of a broader scientific community.

In brief, this chapter addresses the objectives:

- To provide the theoretical background necessary to understand the work presented in subsequent chapters.
- To highlight existing challenges in understanding charge behavior in nonpolar liquids.
- To highlight advantages of optical trapping electrophoresis with respect to other existing tools.

Before delving into this, I will explain, in short, what constitutes optical tapping electrophoresis.

2.1.1 Optical trapping electrophoresis

In this work, I study charge phenomena of colloidal particles. I use an optical trap to confine a single colloidal particle to a small volume of space around the focus of the laser beam. The same beam is also used to measure that particle's movement within the optical trap. The application of an electric field exerts a force on the particle that induces electrophoretic motion. This way, the recorded motion contains information on the charge of the particle. A schematic representation of this principle is shown in Figure 2-1.

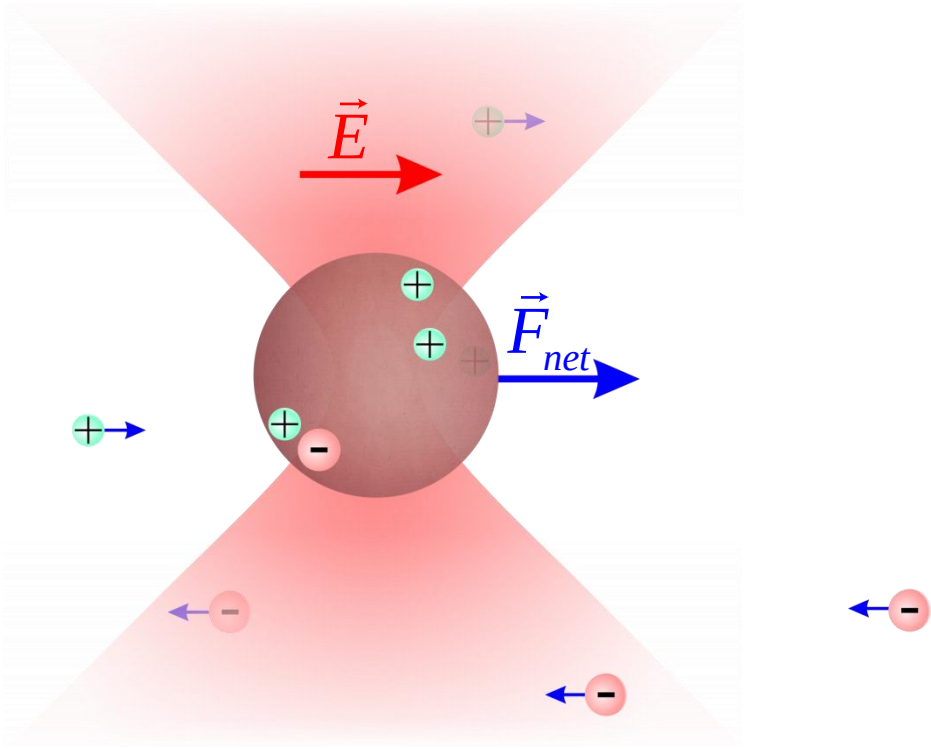

Figure 2-1 Schematic representation of a charged colloidal particle trapped in the focus of a laser beam. In the presence of an electric field $\vec{E}$ all charged species experience a force (blue arrows) that is proportional in magnitude to their net charge and directed along (positive) or opposite (negative) to the direction of the electric field. The laser may serve the dual purpose of containing the particle to a small volume around the laser focus and, at the same time, of detecting the particle's movement. From the motion analysis of the particle, information on the particle's charge is obtained.

The objective is not just to obtain an estimate of the particle's charge, but to create a measurement technique that can generate time-dependent charge measurements of particles in non-ideal nonpolar liquids where surfactants are introduced with such an accuracy that single elementary charging and discharging events can be resolved.

A detailed exposition of optical trapping electrophoresis is given in Chapter 3, where both the experimental setup and the analysis method will be discussed. This chapter will provide the necessary, information that is required to better understand the work presented in the following chapters.

This includes an analysis of *Brownian* motion of freely moving colloidal particles, a qualitative explanation about the principle of optical trapping and a background about colloid stability, surfactants and particle charging. Lastly, this chapter also covers a number of other, competing measurement techniques and compares how optical trapping electrophoresis holds up against these techniques.

2.2 Particles

There exists a wide variety of particles that are commonly used in both academia and in industrial applications. Some notable examples include polystyrene[23], silica[24, 25] and Poly(methyl methacrylate) (PMMA)[13, 23]. Here, I exclusively use one variant of PMMA particles, namely poly-12-hydroxystearic-coated (PHSA) PMMA particles. The particles from this work were provided by dr. *Schofield*[26].

PMMA particles are chosen here, because they are commonly used in both aqueous[27] and in nonpolar liquids[28]. Furthermore, they are easy to optically trap in the nonpolar liquid of choice, dodecane, due to its relative refractive index with respect to dodecane. Finally, they can be immersed in nonpolar liquids without the need for added surfactants, which allows me to study them in pure nonpolar liquids.

2.2.1 Brownian Motion

A homogenous liquid consists of a large number of identical molecules close to each other. Typically, these molecules are on the order of 0.1 nm apart by a combination of intermolecular forces; *ion-induced dipole forces, ion-dipole forces*, *hydrogen bonding* and *Van der Waals forces*. The presence and relative strength of these forces depends on the nature of the molecules.

Though liquid molecules are packed closely together, unlike in a solid, they are not held in fixed positions. Every molecule moves through the liquid and collides with other molecules or with larger entities, such as colloidal particles. Due to the statistical independence of collision directions of liquid molecules, suspended particles are pushed about randomly through the medium[29], as illustrated in Figure 2-2. This random movement of particles in liquids is called a *Random walk* or *Brownian motion*, after botanist Robert

Brown who, in 1827, was the first to discover and accurately report this phenomenon. A detailed analysis followed later by *Einstein* in 1905.

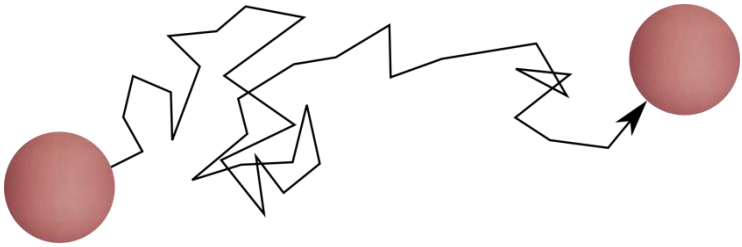

Figure 2-2 Random walk of a colloidal particle. Though the time average of the *Brownian force* is zero, $\langle F_B \rangle = 0$, the mean squared displacement of the particle is not, $\left\langle \left(z(t) - z_0 \right)^2 \right\rangle > 0$, where $z(t)$ is the particle's position in function of time and z_0 is the initial position.

The forces acting on a particle are the viscous drag force F_{drag} and the random Brownian force F_B, which is a stochastic force. The sum of these two forces is the total force F_{tot}.

$$F_{\text{tot}} = F_{drag}(t) + F_B(t) \qquad 2\text{-}1$$

According to *Newton's* second law, the total force can be written as $F_{\text{tot}} = m\ddot{z}$, where z denotes an arbitrary direction and where $\ddot{z}$ is the second time derivative of the particle's position and m is the particle's mass.

The drag force on a spherical object with small Reynolds number, *Re* << 1, in a viscous fluid is given by *Stokes's law* $F_{drag} = -\gamma \dot{z}$, where $\gamma = 3\pi\eta d$ with η the viscosity of the liquid and d the diameter of the particle. Implementing *Stokes' Law*, this transforms equation 2-1 into equation 2-2 below. Equation 2-2 is also known as the *Langevin equation*.

$$m\ddot{z} + \gamma \dot{z} = F_B(t) \qquad 2\text{-}2$$

Substituting $\dot{z}$ for v, this equation 2-2can be rewritten as $\dot{v}+\frac{1}{\tau}v=\frac{F_B(t)}{m}$, with the characteristic time constant $\tau=m/\gamma$, for which the general solution is:

$$v=v_0e^{-t/\tau}+\frac{1}{m}e^{-t/\tau}\int_0^t e^{u/\tau}F_B(u)\,du \qquad 2\text{-}3$$

As the *Brownian force* is a random force $\langle F_B\rangle=0$, $\langle v\rangle=v_0e^{-t/\tau}$ drops to zero exponentially at long timescales. The mean square velocity however, does not.

$$\begin{aligned} v^2 &= v_0^2e^{-2t/\tau}+\frac{2}{m}v_0e^{-t/\tau}\int_0^t e^{(u-t)/\tau}F_B(u)du \\ &+\frac{1}{m^2}\int_0^t e^{(u-t)/\tau}F_B(u)du\int_0^t e^{(w-t)/\tau}F_B(w)dw \end{aligned} \qquad 2\text{-}4$$

Taking the time average, this becomes:

$$\begin{aligned} \langle v^2\rangle &= \langle v_0^2e^{-2t/\tau}\rangle+\left\langle\frac{2}{m}v_0e^{-t/\tau}\int_0^t e^{(w-t)/\tau}F_B(u)dw\right\rangle \\ &+\left\langle\int_0^t e^{(u-t)/\tau}F_B(u)du\int_0^t e^{(w-t)/\tau}F_B(w)dw\right\rangle \\ &= v_0^2e^{-2t/\tau}+\frac{2}{m}v_0e^{-t/\tau}\int_0^t e^{(w-t)/\tau}\langle F_B(u)\rangle\,dw \\ &+\left\langle\int_0^t\int_0^t e^{(u-t)/\tau}F_B(u)e^{(w-t)/\tau}F_B(w)dudw\right\rangle \end{aligned} \qquad 2\text{-}5$$

The first term in equation 2-5 drops to zero exponentially at long time intervals $t\gg\tau$ and because $\langle F_B\rangle=0$ the second term is also zero. This leaves:

$$\langle v^2\rangle=\int_0^t\int_0^t e^{(u-t)/\tau}e^{(w-t)/\tau}\langle F_B(u)F_B(w)\rangle\,dudw \qquad 2\text{-}6$$

Due to the stationarity of the fluctuations of the random force, the autocorrelation function of that force is time-independent, $\langle F_B(u+\tau)F_B(w+\tau)\rangle = \langle F_B(u)F_B(w)\rangle$, and its power spectral density is constant $\langle F_B(u)F_B(w)\rangle = \sigma^2\delta(u-w)$. For time scales much longer than the characteristic time scale τ, the mean squared velocity from equation 2-6 now becomes

$$\langle v^2\rangle = \frac{\sigma^2}{2m\gamma} \qquad 2\text{-}7$$

The mean kinetic energy of the particle is $\frac{1}{2}m\langle v^2\rangle = \frac{1}{2}k_BT$. Substituting this into the relation equation 2-7, I get the power spectral density of the *Brownian force* $\sigma = \sqrt{2k_BT\gamma}$, which leads to the general form of the *Brownian force* itself

$$F_B(t) = \sqrt{2k_BT\gamma}\,\xi(t), \qquad 2\text{-}8$$

where $\xi(t)$ is a random *Gaussian* process with a white spectrum and normalized amplitude.

At time scales much larger than the characteristic time constant $\Delta t \gg \tau$, the inertial term in the *Langevin equation* can be neglected and the equation reduces to $\gamma\dot{z} = \sqrt{2k_BT\gamma}\,\xi(t)$. After integration this becomes

$$z(t) = z_0 + \frac{\sqrt{2k_BT\gamma}}{\gamma}\int_0^t \xi(u)du \qquad 2\text{-}9$$

Calculating the expected variance of the particle's position is now trivial

$$\langle (z(t)-z_0)^2\rangle = \frac{2k_BT}{\gamma}t \qquad 2\text{-}10$$

The diffusion coefficient D is defined as

$$D = \frac{k_BT}{\gamma} \qquad 2\text{-}11$$

Equation is 2-11 is the famous *Stokes-Einstein relation*.

2.3 Optical trapping

The theoretical framework for stimulated emission, which would later form the basis for laser theory was established by *Albert Einstein* in 1917[30]. Successful laser operation was only achieved four decades later by *Maiman* in 1960[31]. Next came the first gas laser (He-Ne), followed by the semiconductor laser diode in 1962. At first, the laser had no practical applications and was even described as '*A solution looking for a problem.*', though that changed quickly. Eventually, the laser came to enjoy a broad spectrum of applications, including spectroscopy, interferometry, lithography, laser cutting, laser welding and many more.

One such application came into light in 1970, when *Arthur Ashkin* made the first experimental observation of a laser's ability to confine the movement of a colloidal particle through optical scattering and gradient forces[32]. Later, he demonstrated the first successful three-dimensional optical tweezers from a single, tightly focused laser beam[33]. *Steven Chu*, who coauthored that publication, would go on to use optical trapping in his work to trap and cool neutral atoms in vacuum[34], for which he earned the 1997 Nobel Prize in Physics. Optical tweezers are now an important tool in various fields, such as physical chemistry[35, 36], cell biology[37, 38] soft matter physics[39-41].

In this work in particular, optical trapping constitutes an essential element of the technique. The laser has a dual purpose in the technique in that it is used both as tweezers and as part of the detection method. Here, I will focus on the characteristics of a laser trap and related phenomena.

2.3.1 Basic properties of photons

In this work, the aim is to harness the properties of light to confine the movement of colloidal particles. To understand the interaction between photons and matter, it is useful to recapitulate the basic properties of light.

the *Planck-Einstein* equation, states that the energy E of a photon is proportional to its frequency f, as shown in equation 2-12.

$$E = hf \qquad 2\text{-}12$$

With h, *Planck's* constant.

Though photons are massless, they have momentum. The momentum p of a photon is equal to its energy E divided by the speed of light in vacuum c, $p = E/c$. Or as this relation is more commonly notated:

$$p = hf/c \qquad 2\text{-}13$$

The knowledge that photons carry momentum is key to a qualitative understanding of optical tweezers. When a photon is deflected by its interaction with matter by deflection, refraction or reflection, the propagation direction of the photon has changed. This change in direction implies that also the momentum of the photon has changed. Conservation of momentum therefore dictates that an equal, but oppositely directed momentum is transferred to the matter the photon interacted with.

The momentum associated with a single photon is very small. However, through this interaction principle, a large stream of photons, such as a laser beam, can exert a measurable force on a colloidal particle. As by *Newton's 3rd Law*, the force F is defined as the time derivative of momentum, as expressed in equation 2-13.

$$F = dp/dt \qquad 2\text{-}14$$

The concept behind optical tweezers, is to configure a three dimensional photon stream, such that a displacement of the particle away from a single point in space results in a force exerted on the particle by the deflected photon stream that draws the particle back to that same point. The magnitude of the associated force has to be sufficiently strong in order to overcome the random *Brownian* force from the liquid molecules onto the particle. When a photon stream can accomplish those requirements, then the particle is trapped.

Such a configuration can be obtained and is most commonly created by tightly focusing a laser beam, though other methods have more recently been proposed[41, 42]. The forces on the particle indeed arise from reflection and deflection of the laser light by the particle. The theoretical

framework to derive the forces inside an optical trap is generally divided into two categories.

Particles with diameter d much larger than the wavelength λ of the laser bundle ($d \gg \lambda$), are considered to be in the *Ray optics* regime[43] where ray optics can be used to work out the optical forces. When the particle's diameter is much smaller than the wavelength of the laser ($d \ll \lambda$), the optics is better described by the *Rayleigh* regime[44]. While the electromagnetic field model from the *Rayleigh regime* is generally highly complex, the ray optics model provides an insightful model that can be understood from basic particle-photon interactions with transfer of momentum introduced above.

In this work, the size of the particles is of the same order of magnitude as the photon wavelength ($d \approx \lambda$), which is outside the scope of both theories.

2.3.2 Ray optics

For particles with a diameter much larger than the wavelength of the trapping beam $d \gg \lambda$, the refraction of the beam can be computed by *Snell's law* for light rays.

$$n_1 \sin(\theta_1) = n_2 \sin(\theta_2), \qquad 2\text{-}15$$

where θ_1 is the angle between the incident ray and the normal to the boundary between the media and n_1 is the refractive index of medium 1 and analogously for medium 2. This is depicted in Figure 2-3.

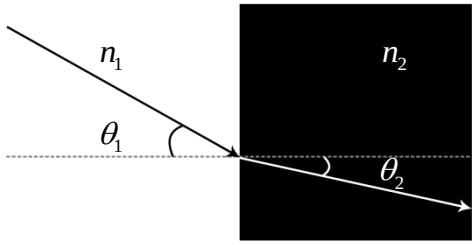

Figure 2-3 *Snell's law* for refraction of rays.

Neglecting reflection, the refraction of a laser beam by a spherical particle is shown in Figure 2-4. If the center of the particle coincides with focus of the

beam as in Figure 2-4 (b), the beam is not deflected. Since the beam is not deflected, its momentum has not been altered by the presence of the particle and it does exert a force onto the particle. The particle and the laser are in equilibrium.

In Figure 2-4 (a), the particle is laterally displaced to the left with respect to the focus of the beam. The laser beam is deflected in the same direction as the displacement of the particle and, hence, the beam exerts a force onto the particle in the opposite direction, towards its focal point.

A particle that is displaced along the propagation direction of the laser narrows or widens the beam for a forward displaced and backward displaced particle respectively. Figure 2-4 (c) depicts the former. Here too, the laser beam exerts a force on the beam that points back towards the focal point.

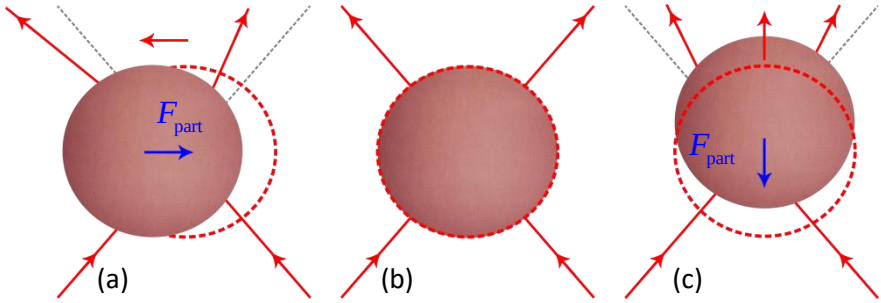

Figure 2-4 A *Gaussian* laser beam (red line) comes in from underneath and is deflected after it passes through a spherical particle. The grey, dotted lines represent the unperturbed trajectory of the laser beam. The position of the particle relative to the focus of the beam is shown for 3 cases: (a) lateral displacement (b) center and focus coincide (c) displacement along the propagation direction. The red, dotted circle is centered around the laser focus. The red arrow indicates the direction in which the beam is deflected. The blue arrow indicates the direction of the force of the beam onto the particle.

The change in momentum of the laser increases as the particle moves further. Hence, the particle feels a linearly increasing force in every direction.

Note: Here, for brevity and clarity, the workings of the optical trap has been explained phenomenologically through the ray approximation model. In practice, it is important to know two additional features of the focused *Gaussian* optical trap. First, because the intensity gradient is stronger in

lateral direction with respect to longitudinal direction, the trapping strength is typically much stronger in the lateral direction (x10). Second, due to the refractive index mismatch between the particle and the surrounding medium, part of the laser light is reflected. The backscattered photons result in a photon pressure on the particle along the laser's propagation direction[45]. In my experiments, this refractive index difference is very small ($\Delta n \approx 0.06$), thus in reality, the trapped particle in Figure 2-4 (b) would be centered just above the focus of the laser.

2.3.3 Rayleigh scattering

The forces exerted by a highly focused laser beam on a colloidal particle can be calculated with the Rayleigh scattering model in the case that the radius of the particle is much smaller than the wavelength of the laser. In this work, I will not delve into the specifics of this model, but I will state some of its relevant results. I refer to [44], where this is worked out in detail. This model shows that the particle is trapped inside a potential well $V(\vec{r})$

$$V(\vec{r}) = -\frac{2\pi n_{\mathrm{md}} r^3}{c}\left(\frac{m_n^2 - 1}{m_n^2 + 2}\right) I(\vec{r}), \qquad 2\text{-}16$$

where n_{md} is the refractive index of the liquid medium, r is the radius of the particle, m_n is the ratio of the refractive index of the particle n_{particle} divided by the refractive index of the medium ($m_n = n_{\mathrm{particle}} / n_{\mathrm{md}}$) and $I(\vec{r})$ is the spatial intensity distribution of the focused *Gaussian* laser beam.

Particles with a higher refractive index than the surrounding medium feel an attractive force that is proportional with the gradient of the laser intensity.

$$\vec{F}_{grad}(\vec{r}) = \frac{2\pi n_{\mathrm{md}} r^3}{c}\left(\frac{m_n^2 - 1}{m_n^2 + 2}\right) \nabla I(\vec{r}) \qquad 2\text{-}17$$

Figure 2-5 displays the gradient force along the propagation direction z of a beam associated with equation 2-17 for a focused Gaussian laser beam with wavelength λ = 975 nm and 60 mW optical power. The beam is focused by 100 X lens with numerical aperture NA = 1.3 and traps a particle with

diameter d = 1 µm and refractive index n_{particle} = 1.49 in a medium with refractive index n_{md} = 1.42. This shows that the trapped particle always experiences a force directed towards the focus of the beam and experiences forces in the order of several picoNewtons.

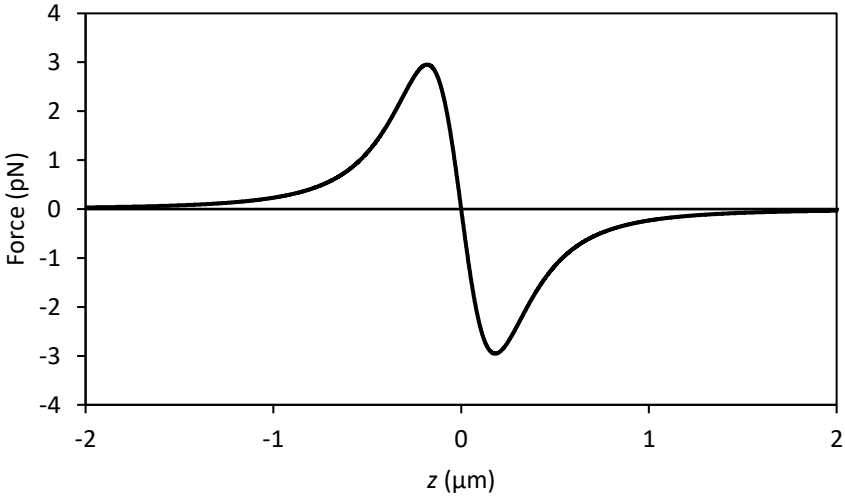

Figure 2-5 Gradient force experienced by a 1 µm PMMA particle (n_{particle} = 1.49) in an optical trap of a laser beam with wavelength λ = 975 nm, laser power of 60 mW and numerical aperture NA = 1.3 in dodecane (n_{md} = 1.42). The trapped particle experiences a force that is directed towards the focus of the laser.

2.3.4 Particle motion in an optical trap

In my analysis of particle movement in an optical trap, I limit myself to the one-dimensional treatment of the particle's movement along the propagation direction of the trapping beam. This direction is referred to as the z-direction. The movement in the lateral directions is analogous, with the simplification that no electric field is present in these directions.

A colloidal particle confined in an optical trap moves like an over-damped oscillator. The forces acting on the particle are the viscous drag force F_{drag}, the trapping force F_{trap} and the random Brownian force F_B, which is a

stochastic force. Continuing on the analysis from section 2.2.1, this can be written as

$$m\ddot{z} = -\gamma \dot{z}(t) + F_{trap}(t) + \sqrt{2k_B T\gamma}\xi(t) \qquad 2\text{-}18$$

Which is basically the *Langevin* equation, equation 2-2 from section 2.2.1, with an added term to account for the trapping force.

Due to the small size of the particles (d ~ 1 μm), the inertial term $m\ddot{z}$ is much smaller than the other terms in this equation. Therefore, equation 2-18 can be reduced to

$$\gamma \dot{z} + \kappa_F z = \sqrt{2k_B T\gamma}\xi(t), \qquad 2\text{-}19$$

where a linearized trapping force $F_{\text{trap}} = \kappa_F z$ is introduced with κ_F the stiffness of the trap. When a sinusoidal electric field is applied with amplitude E_0 and frequency f_E, $E(t) = E_0 \cos(2\pi f_E t)$, an extra force term appears that is proportional to both the electric field $E(t)$ and the charge of the particle Q_{part}:

$$Q_{\text{part}} E(t) + \sqrt{2k_B T\gamma}\xi(t) - \gamma \dot{z} - \kappa_F z = 0 \qquad 2\text{-}20$$

2.4 Colloidal stability

Early research into electrokinetic phenomena was spurred by an interest in colloidal stability. Most of this research was focused on aqueous media, which culminated in the well-known DLVO theory, named after the researchers behind its inception *Derjaguin*, *Landau*, *Verwey*, and *Overbeek*. In an earlier model that *Debye* and *Hückel* proposed, free ions feel an electrostatic attraction or repulsion by a charged surface that competes with the thermal energy of the liquid[46]. *Derjaguin* and *Landau* extended this theory by including *Van der Waals* forces[47]. This model was later independently developed by *Verwey*, and *Overbeek*[48]. While theory has much progressed since, DLVO theory still forms the basis for modern electrokinetic phenomena in colloidal suspensions and colloidal stability.

A colloidal suspension is said to be stable if the colloidal particles in the solvent aggregate at a sufficiently slow rate. When two colloidal particles are separated by only a few nanometers, attractive molecular dipole forces will pull the particles toward each other.

Rapid aggregation of colloidal particles can be prevented in several ways. One way is by electrically charging the particles. Electrostatic repulsion acts to drive same-charged particles away from each other, thereby effectively stabilizing the suspension. Another way is by coating the particles with long polymer chains that act as a physical barrier to prevent close approximation of oppositely charged particles.

The electrostatic and –kinetic phenomena are markedly different in polar (aqueous) and nonpolar (oils) liquids.

2.4.1 Charge and potential of particles in polar liquids

The physical property representing the chemical polarity of a solvent is the relative dielectric permittivity ε_r. The relative permittivity is a dimensionless material constant defined as the ratio of the material's permittivity $\varepsilon_{\mathrm{mat}}$ divided by the permittivity of vacuum ε_0, $\varepsilon_r = \varepsilon_{\mathrm{mat}} / \varepsilon_0$, with = ε_0 = 8.85*10^{-12} F/m. Polar media have a high relative permittivity, such as water $\varepsilon_{r,\mathrm{H_2O}}$ = 80 or glycerol $\varepsilon_{r,\mathrm{glycerol}}$ = 42 at room temperature, in contrast to nonpolar solvents like n-dodecane $\varepsilon_{r,C_{12}H_{26}}$ = 2.

The large difference in ε_r manifests itself in a qualitatively different charge behavior. A general representation of the charge distribution around a colloidal particle in polar liquids and the corresponding potential is shown in Figure 2-6. The particle has a positive surface charge density σ_m. Around the particle, a double layer is formed to screen the electric field of the charged sphere, which in turn causes an elektrokinetic potential between the particle and any point in the liquid. The corresponding voltage difference is called the surface potential Φ_S. Part of the negative ions of the double layer adhere directly to the particle's surface, resulting in an internal *Stern* layer[49].

Inside the *Stern* layer, the potential drops linearly from Φ_S to Φ_D, the *Stern* layer potential. Beyond the *Stern* layer, the potential drops exponentially with factor $\mathrm{e}^{-\kappa r}$, where the *Debye* length is defined as

$$\kappa^{-1} = \sqrt{\frac{\varepsilon_r \varepsilon_0 k_B T}{2e^2 z^2 n_{\mathrm{ion}}}}, \qquad 2\text{-}21$$

where k_B is *Boltzmann's* constant, T is the temperature (in Kelvin), e is the elementary charge, z is the valence number of the free ions and n_{ion} is the equilibrium concentration of free ions. As the particle's potential drops a factor $1/\mathrm{e}$ over κ^{-1}, the *Debye* length is a characteristic length scale for ionic liquids.

In the direct vicinity of the particle's surface, the fluid is not mobile, but instead, moves together with the particle. At a certain distance is the slipping plane, which separates the mobile fluid from the fluid that remains attached to the particle's surface. The potential at this point is called the zeta-potential ζ.

For polar liquids and high charge density nonpolar liquids, it is the zeta potential ζ that can be probed by electrophoresis, electroacoustic phenomena, streaming potential, and electro-osmotic flow. Due to the unknown relation between the measured mobilities and the ζ-potential[50] as well as the unknown position of the ζ-radius[51], the obtained mobilities cannot be accurately into a value for the electric surface charge.

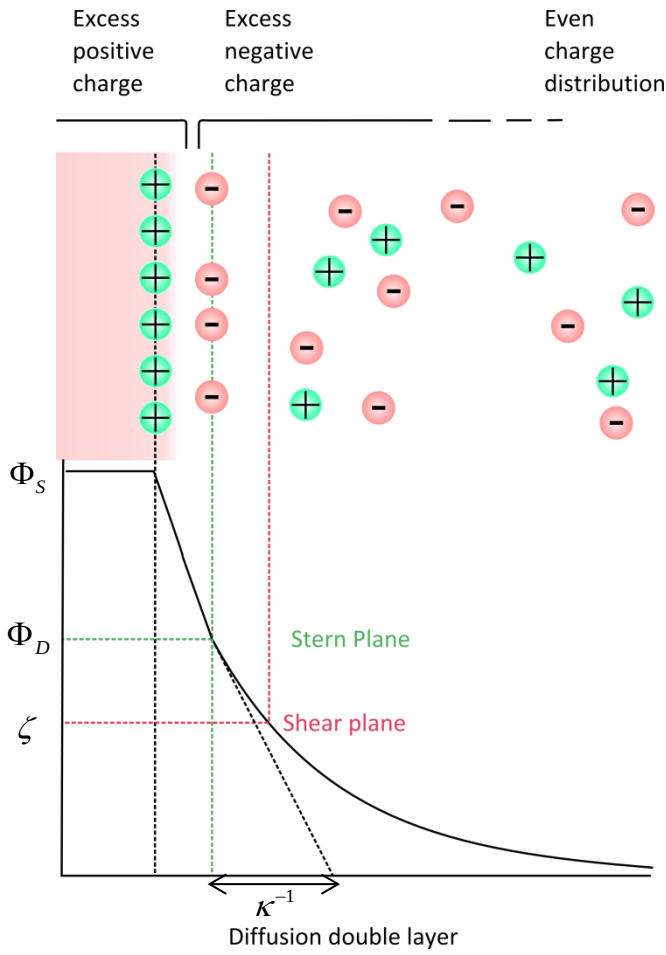

Figure 2-6 Schematic representation of the interfacial double layer for particles in polar liquids. Counter ions adhere directly to the particle's surface in the *Stern* layer, where the potential drops linearly from Φ_S to Φ_D. From there on, the potential drops exponentially. The external potential that can be probed experimentally is ζ, the value of the potential at the slipping plane.

2.4.2 Charge in nonpolar liquids

For nonpolar liquids, a commonly used characteristic length is the *Bjerrum* length λ_B. The *Bjerrum* length is defined as the separation between two ions at which the attractive or repulsive electrostatic energy between these ions is equal to the thermal energy $\kappa_B T$.

$$\lambda_B = \frac{Z^2 e^2}{4\pi\varepsilon_r\varepsilon_0 k_B T} \qquad 2\text{-}22$$

Two free ions of opposite polarity, separated by less than the *Bjerrum* length are likely to neutralize each other. Note that the main parameter is a material constant, the relative dielectric permittivity ε_r. For comparison, the *Bjerrum* length of water is $\lambda_{B,\mathrm{H_2O}}$ = 0.7 nm, for dodecane it is $\lambda_{B,C_{12}\mathrm{H}_{26}}$ = 28 nm.

Equation 2-23 expresses the fraction of charged versus uncharged inverse micelles in a nonpolar liquid[52]:

$$\chi = \frac{n_+ + n_-}{n_0} = 2\mathrm{e}^{-\frac{Z^2\lambda_B}{d_{\mathrm{CM}}}}, \qquad 2\text{-}23$$

where n_+, n_- and n_0 represent the concentration of positively charged, negatively charged and neutral inverse micelles, d_{CM} is the diameter of an inverse micelle and Z is the valence number of the charged inverse micelles. Through equation 2-23, the fraction of charged inverse micelles can be calculated as a function of the *Bjerrum* length. Hence, the *Bjerrum* length is a good indicator for determining the degree of charging for particles in a liquid.

Equation 2-21 shows that the *Debye* length κ^{-1} is inversely proportional to the square root of the concentration of free ions in the liquid $1/\sqrt{n}$. Because charge densities in nonpolar liquids are typically very low, the ratio of the particle radius over the *Debye* length is commonly much smaller than 1, $\kappa r_{\mathrm{particle}} \ll 1$.

2.4.3 Surfactants and inverse micelles

Surfactant molecules are made up of hydrophilic head groups and oil soluble tails. In nonpolar liquids, the hydrophilic head groups preferentially stick to solid interfaces, such as a glass interface or the surface of a colloidal particle, while the tail group is then directed towards the nonpolar solvent, as is shown in Figure 2-7 (left). This happens at low surfactant concentrations.

When the available surfaces are filled with a monolayer of surfactant, the surfactant concentration of the liquid bulk increases. At a threshold concentration, the surfactant molecules aggregate and form spherical structures, called inverse micelles. This concentration is called the critical micelle concentration (CMC). Inverse micelles are well-suited to stabilize charge in the liquid. By encapsulating a free ion in its core, it can presents an obstacle for the ion from approaching an oppositely charged ion and reduces the rate at which oppositely charged ions neutralize each other. This concept is called steric stabilization and is shown in Figure 2-7 (right).

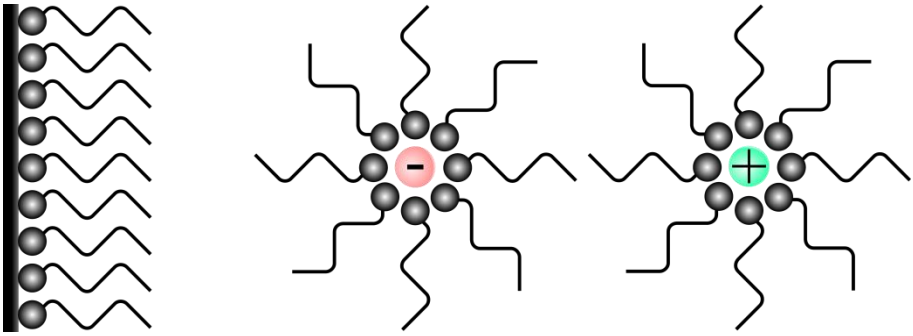

Figure 2-7 (left) Polar head groups of single surfactant molecules preferentially stick to solid surfaces, as opposed to being immersed in the nonpolar solvent. (right) Two inverse micelles sterically stabilize oppositely charged ions.

2.4.4 Applications of surfactants

Surfactants enjoy a diverse set of applications. As it is well established that the charge density of nonpolar liquids increases with increasing surfactant concentrations[53], even below the CMC[18], surfactants are frequently used to suppress aggregation caused by collisions due to *Brownian* motion of colloidal particles[54, 55] by stabilizing the electric charge. Perhaps the first widely known industrial use of surfactants was the prevention of explosions in the petroleum industry[56]. Now, surfactant-based solutions are found in drug delivery[57, 58], detergents[59], electro-rheological fluids[60], ink-jet printing[61] and electronic paper[1, 62]. In this work, we will refer to colloidal suspensions containing any concentration of surfactant as surfactant-enriched, as opposed to colloidal suspensions consisting only of a pure liduid and particles.

Some of the most widely used commercial surfactants for nonpolar liquids are SPAN[63, 64], AOT[65, 66] and OLOA 11000[67-69]. In this work, I have chosen to limit myself to the use of the commercial surfactant OLOA 11000 by Chevron because it is one of the most widely used surfactants. The precise chemical composition of OLOA 11000 has not been made publicly available by the producers. In this work, I aim to demonstrate the capabilities of optical trapping electrophoresis in surfactant-enriched environments by showing how meaningful insights can be extracted from measurements about the influence of OLOA 11000 on the charging behavior.

2.4.5 Charging mechanisms in nonpolar liquids with surfactants

Surfactant-enriched nonpolar colloids are widely used, even though the mechanisms by which the particles acquire their charge is not yet completely understood. The subject of charge in nonpolar liquids remains a topic of current scientific research, as is evidenced by three recent reviews on the matter[11, 12, 53]. While several distinct charging mechanisms have been allocated to different types of mixtures successfully, it is still often impossible to predict the charging mechanism of a certain mixture or even the charge of a colloidal particle in a mixture in advance.

Surfactants are known to participate in the surface charging mechanisms of colloidal particles. The surfactant molecules may facilitate the charging mechanism through stabilizing a counter-ion in the liquid and by stabilizing a charged site on the particle's surface. Below, I list some of the most commonly occurring particle charging mechanisms. The charging mechanism is explained and the role that surfactant plays is highlighted.

2.4.5.1 Acid-base mechanism

In the acid-base mechanism of particle charging, the charge originates from an interaction between acid and base molecules that involves the exchange of protons or electrons between these molecules. When a neutral inverse micelle approaches the surface of the particle, it can be adsorbed onto the particle, where it picks up a charge that is freed from an acid-base reaction. The now charged inverse micelle desorbs from the particle, which is left with an oppositely charged surface. This mechanism was first proposed by *Fowkes*[70, 71] and has been used to explain experimental observations of

silica surfaces in the presence of surfactants[24]. It is important to note that the charge in this mechanism is freed through the interaction between acid and basic species. A recent review article on acid-base interactions in nonpolar colloids is written by *Gacek* and *Berg*[15].

2.4.5.2 Preferential adsorption mechanism

At first glance, the preferential adsorption mechanism is the opposite of the acid-base reaction mechanism. Where inverse micelles function to carry charge away charge from the particle's surface in the acid-base mechanism, in the preferential adsorption mechanism a charged inverse micelle carries charge toward the particle. The charge contained within the inverse micelle is then adsorbed onto the particle, after which the neutral inverse micelle desorbs from the particle. In some cases the precise nature of the charge inside the inverse micelle can not be specified[72], while in others it can be theorized that the charge inside the inverse micelles comes from an ionized anionic surfactant molecule[73].

2.4.5.3 Site-binding mechanism

First proposed by *Kitahara* et al.[74] in a qualitative way, the site-binding model states that ionic species of polarity P from the liquid may be adsorbed to a site on the particle's surface S, forming SP. The liquid also contains ionic species N of opposite polarity with respect to P. These ions may in turn adsorb to SP, forming SPN. This model was elaborated by *Jenkins*[75] and has been used to explain the charging behavior of carbon black in nonpolar inks[76].

2.4.5.4 Surface dissolution

A colloidal particle can also acquire charge by dissociation of a surface ion. When that ion enters the core of an inverse micelle, it can be stabilized in the liquid. *Briscoe* and *Horn* argue that the dissolution of a surface ion requires the presence of trace amounts of water, because the hydration of a surface ion reduces the electrostatic attraction to the oppositely charged surface[77].

2.5 Charge measurement techniques

The study of electric phenomena in nonpolar liquids has yielded an array of measurement techniques from which much can be inferred about the interaction between surfactants and colloidal particles. Such techniques include conductometry[78, 79], transient current measurements[80, 81], small angle neutron scattering[82], atomic force microscopy[83] and others[10, 84].

While the aforementioned techniques certainly have their merit, a more thorough review of them is beyond the scope of this work. Here, I focus on modern techniques that can directly measure the charge or the ζ potential of colloidal particles, like optical trapping electrophoresis. I briefly explain the working principle behind these techniques and provide a comment on how it compares to OTE.

2.5.1 Optical tracking electrophoresis

In optical tracking electrophoresis, the movement of single particles is tracked with a camera. When an electric field is applied, the particle acquires a velocity v. From this, the electrophoretic mobility μ_e of the particle can be calculated, which is defined as:

$$\mu_e = \frac{v}{E} \qquad 2\text{-}24$$

The charge of the particle is calculated through the *Stokes-Einstein* relation, shown in equation 2-25:

$$\mu_e = \frac{Ze}{3\pi\eta d}, \qquad 2\text{-}25$$

where Ze is the particle's charge, η is the viscosity of the liquid and d the diameter of the particle. Formula 2-25 is valid in the limit of $\kappa d \gg 1$

The technique was pioneered by *Garbow* et al.[85] in aqueous systems. In a pure nonpolar liquid, *Strubbe* et al.[17] were able to discern discrete peaks in the histogram of the electrophoretic mobility of a single Silica sphere. They showed that the particle's charge exhibited discrete peaks, centered around

multiples of the elementary charge. This work featured the first time that the electric charge of a colloidal particle was measured with a resolution of 1 *e* and lower. Optical tracking electrophoresis is also referred to as nanoparticle tracking analysis or NTA by Malvern (formerly under Nanosight, acquired by Malvern in 2013), a company that produces a commercially available size and zeta-potential characterization tool based on this principle[86].

2.5.2 Blinking optical tweezers

When two like-charged particles are in close proximity, their counter-ion clouds overlap and the particles repel each other. In nonpolar liquids with low ionic strength, the velocity at which they move away from each other depends on their size, their charge, the *Debye* length and their separation. If these particles are placed close to each other and then released multiple times, the magnitude of the charge of the particles can be calculated from the trajectories they follow. This is exactly what is accomplished through blinking optical tweezers. Blinking optical tweezers can be seen as a special variant of optical tracking electrophoresis, because the position detection is achieved by centroid detection algorithms of video images.

Blinking optical tweezers was first introduced by *Crocker* and *Grier*[84, 87] and more recently employed by *Sainis* et al. for polystyrene latex particles in a microemulsion of AOT in hexadecane[18, 88].

Though the technique is very elegant, it offers little advantage over optical trapping electrophoresis. The polarity of the charge can not be determined through this technique and the charge is assumed to be constant in time and equal for both particles. It does however provide direct insight into the interparticle electric forces due to interacting double layers.

2.5.3 Laser Doppler electrophoresis & phase analysis light scattering

When a laser impinges on a moving object, the frequency of the scattered light is *Doppler* shifted. For laser scattering on a colloidal particle with a small velocity, the shift in laser frequency is proportional the velocity. The shift in frequency is measured by an optical interferometric technique. This is how

laser Doppler electrophoresis (LDE) measures the electrophoretic mobility of colloidal particles[19].

Phase analysis light scattering or PALS uses the same optical setup as laser Doppler electrophoresis, but instead of a frequency shift, the phase shift of the scattered light is determined. This technique was pioneered by *McNeil-Watson*[20], who later went on to work at Malvern where they developed the Zetasizer Nano which uses PALS.

2.5.4 Differential-phase optical coherence tomography

Differential-phase optical coherence tomography (DP-OCT) uses a broadband light source that is split into two parts, a reference beam that is modulated at high frequency (~50 kHz) and a beam that is directed towards the sample. The sample beam is separated into a horizontally and a vertically polarized beam, positioned at the center of the sample chamber and at the electrode-sample interface. When the horizontally and vertically polarized beams are then mixed with the modulated reference beam, they produce interference fringes that correspond to the moving particles and to the stationary electrode-sample interface respectively[21, 89].

2.5.5 Electroacoustics

The field of electroacoustics was pioneered by *Dukhin*[22]. There are two electroacoustic effects that are widely used to determine the zeta potential of colloidal particles. The first is the colloid vibration current. This occurs when an ultrasound wave travels through a colloidal suspension. As a result of the ultrasonic wave, particles are displaced relative to the surrounding liquid. Hence, the particle is also displaced from its counter-ion cloud. The particle and its counter-ion cloud then move to restore an equilibrium position. This process generates a measurable current from which the ζ potential of the particles can be calculated.

The second electroacoustic effect is the electric sonic amplitude, which is the reverse effect of the colloid vibration current. When an external oscillating electric field is applied, the particles move relative to the liquid, which generates an ultrasound wave.

A commercial characterization tool based on these principles is the Acoustosizer by Porotec. The AcoustoSizer is capable of both zetapotential and particle size analysis.

2.5.6 A case for optical trapping electrophoresis

In contrast to most other techniques, optical trapping electrophoresis does not have a commercial counterpart. That may be because it has some drawbacks; It requires very dilute particle systems to prevent freely moving particles from wandering into the trap, it is alignment intensive and is perhaps too expensive to commercially produce and sell.

That said, when it comes to particle charge characterization, OTE has much to offer. Because the entire laser beam is focused on a single particle, it offers very high resolution position measurements (1 nm) at high bandwidths (100 kHz) and because the particle is trapped, it can be studied over very long time intervals. It is one of only two techniques with the ability to detect single, elementary charging events. The long measurement times allow OTE to fully study charging and discharging rates as a function of the absolute charge value of the particle[90]. The optical trap lends further versatility, such as the possibility of applying a constant DC electric field while continuing charge measurement without any time limitation, which is used to great effect later in this work.

The only other technique to have demonstrated that it can achieve charge resolutions smaller than the elementary charge is optical tracking electrophoresis. Optical tracking electrophoresis is a straightforward method that in principle can be used on any type of colloidal suspension, but it has some drawbacks. First, the ability to detect single elementary charging and discharging events has only been demonstrated in pure nonpolar liquids. A surfactant-enriched liquid would give rise to increased electro-osmotic flow, which affects the mobility of the particle[91]. For instance, Z-NTA by Malvern measures the drift velocity of individual particles across a microfluidic channel and fits the parabolic electro-osmotic flow of the liquid and then subtracts the calculated electro-osmotic contribution for each particle. Second, the time during which a particle can be studied is limited by *Brownian* motion. After some time, the particle inevitably wanders out of the

field-of-view of the camera. Furthermore, because a camera is used to detect the particle's position, the position sampling rate is limited to the frame rate of the camera (~100 Hz).

Several parallels and contrasts could be noted between OTE and the other techniques, but there is one important distinction that sets OTE apart from them. LDE, PALS, DP-OCT and electroacoustics all acquire information on the average ζ potential of the entire ensemble of the colloidal particles in the liquid, whereas OTE is a single particle analysis tool. This difference assures that OTE can be used to probe certain aspects of the particle's ζ potential that the other techniques can't and vice versa. For instance, OTE is well suited for time- and location-dependent measurements to observe fluctuations in the charge.

2.6 Summary, setting and goals

Over the successive sections in this chapter, I provided both the underlying physics of optical trapping[32] and of electric phenomena in nonpolar colloidal systems with surfactants[72]. Colloidal particles tend to have a low net charge in pure nonpolar liquids[18, 92-94], surfactants are routinely added to stabilize the particle's charge[5, 6, 10, 95]. Though the relation between the charge density of the liquid and the surfactant concentration is well-established, the precise nature of the charging mechanisms that give rise to this charge are still a topic of current research efforts[13-16, 96, 97]. Some charging mechanisms have been observed experimentally. In this chapter, I discussed acid-base interactions[98], preferential adsorption[99, 100] and surface dissolution[77].

It is important to understand the interaction between surfactant molecules, free ions and particle surfaces, because this knowledge could be used to engineer better surfactants or to improve the performance of colloidal systems in existing applications. There exist many types of surfactants, particles and nonpolar liquids in a multitude of combinations. There also exists a large number of techniques that can be used to study a particle's charging behavior. Here, I discussed optical tracking electrophoresis[85], blinking optical tweezers[18], laser-Doppler electrophoresis[19] and phase

analysis light scattering[20], differential-phase optical coherence tomography[89] and electroacoustics[22].

Optical trapping electrophoresis is yet another technique that can provide insight into the charging behavior of colloidal particles, but it has one distinct difference that sets it apart: The ability to determine successive discrete charging and discharging events over extended periods of time. This ability is not shared with optical tracking electrophoresis, because while it can detect elementary charging events, the particles eventually wander out of the field-of-view, limiting measurement times[17]. Capillary electrophoresis is another technique that can resolve discrete charge peaks of colloidal entities. The peaks correspond to the number of elementary charges held by a group of proteins[101]. This technique requires the colloidal particles to maintain a fixed charge, so dynamic detection of single charging events is not an option.

It is my aim in this dissertation to show that this key feature of OTE, the ability to detect single charging and discharging events, enables it to gain new insights into the charging behavior of colloidal particles and to establish a protocol on how to do so.

Chapter 3.

Measurement & Analysis Method

3.1 Introduction

This chapter details the experimental setup and analysis method used to obtain the results reported in the following chapters of this thesis. This consists of two main parts.

In the first part, I describe the experimental setup. First I discuss the preparation of the microfluidic cells, then I explain how the position detection works and finally, an overview of the entire experimental setup is given.

In the second part, the analysis method to resolve the charge evolution for an optically trapped particle is discussed. This starts off with an analysis of the equation of motion that leads to the formula to compute the electric charge of a particle from the observed oscillatory motion. Then, the R^2 analysis method is explained and discussed. This section concludes with an overview of the analysis method.

3.2 Experimental setup

3.2.1 Microfluidic cell

In order to use or study a colloidal suspension with a microscope, the suspension has to be confined in a cell. Here I describe the fabrication and the configuration of the microfluidic cell that I have used. The cell consists of two ITO-coated glass plates that have been cleaned under cleanroom conditions and then glued together, while kept at a fixed distance by spacer balls.

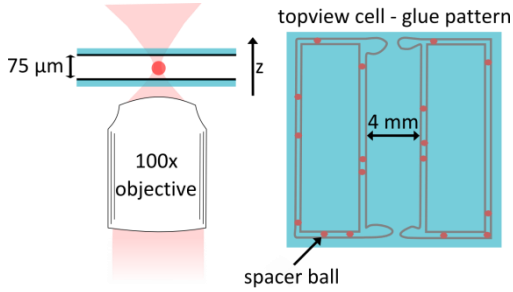

Figure 3-1 (left) The Laser light enters the sample from underneath and is focused inside the sample where it traps a colloidal particle. The glass plates of the microfluidic cell are coated with ITO (black), and the electric field will be applied along the *z*-direction. (right) Top view of the microfluidic cell with spacer balls mixed in the glue to separate the plates at a fixed distance.

Cleaning: The glass substrates (1 inch by 1 inch) are cleaned in three consecutive steps: the substrates are placed in a beaker, filled with DI water and detergent. This beaker is put into an ultrasonic bath filled with DI water. The ultrasound vibrations clean the substrates during 15 minutes. Afterwards, the substrates are blown dry with a nitrogen pressure gun. Then, this procedure is repeated with acetone, isopropanol and DI water consecutively. Then the glass plates are blown dry with a nitrogen gun and dried in the oven at 90°C for 4 hours[102, 103].

Glueing: UV curing glue is mixed with spherical spacer balls of the desired thickness. Here, I use spacers of 75 µm. Next, a glue dispenser (Nordson, DispenseMate) draws the double rectangular outline of the channel of the microfluidic cell onto the ITO-side of a clean glass plate, as shown in Figure 2-2. The rectangles are 4 mm apart. The second glass plate is placed on top and pressed down by a vacuum lock. The glue is cured under UV light for 60 s.

Materials: I use n-dodecane (Sigma Aldrich) and add micrometer sized PHSA-coated PMMA particles in weight fractions of 1/20000 wt%. The particles were provided by dr. *Andrew Schofield* and were synthesized as described in [26]. The particles have diameters of 0.998 µm and 0.498 µm (polydispersity unknown) In some experiments, I also use the commercial surfactant OLOA 11000 in varying concentrations that range from 0.001 wt% to 0.05 wt% in

dodecane. Above the CMC, the surfactant molecules form spherical inverse micelles with a diameter of 5.3 nm[104]. Prior to an experiment, the beaker containing the solution is placed in an ultrasonic bath for 5 seconds and then mixed for 30 seconds with a vortex mixer (Lab Dancer, VWR) to homogenize the suspension.

If long measurement times are desired, the entrances of the microfluidic channel have to be narrowed to slow down the evaporation of the solvent. This is accomplished by introducing glue at the edges of each opening. The glue is sucked in by capillary force. When the width is reduced to 1 mm, the glue is cured by UV light for 60 s.

The benefit of this preparation scheme over previous microfluidic cells used for OTE charge measurements in general[45, 90, 92] and elementary charge detection in particular[17, 90], is twofold. First, the cleanroom conditions ensure a clean and easily reproducible microfluidic environment. Second, because the electric field is perpendicular to the cell wall, electro-osmotic effects are prevented. This is especially important when considering higher charge density liquids, such as surfactant-enriched colloids.

3.2.2 Position detection

In this section I describe the part of the experimental setup that involves the position detection of the optically trapped colloidal particle. The particle's position is imaged onto the detector in a technique that is based on the detection by *Gittes* and *Schmidt*[105], which is widely used for position detection of trapped particles.

3.2.2.1 Position measurements

An optically trapped colloidal particle is confined to a small unit of space (displacements typically < 100 nm) for up to several hours by a 975 nm laser that has 60 mW of power in the sample. Aside from containing the movement of the particle to a small volume, the trapping laser can also be employed to measure the particle's position. As mentioned in section 2.3.2, a small displacement of the particle, results in a small deflection of the beam, proportional to that displacement. This way, the movement of the particle is recorded in the deflections of the laser beam by a quadrant photodiode

(QPD, Thorlabs PDQ80A). This technique that measures fluctuations of the deflected beam over time, to track the particle's position. The two main advantages of this technique over detection of images with a camera, are the higher readout speeds (100 Khz vs 100 Hz) and superior measurement accuracy.

Figure 3-2 shows the schematic representation of the setup. The laser beam is focused in the sample by a 100 times objective and is then collected by the condenser lens. The beam is again collimated after passing through the condenser lens. Then, the beam is focused by the imaging lens on to the QPD.

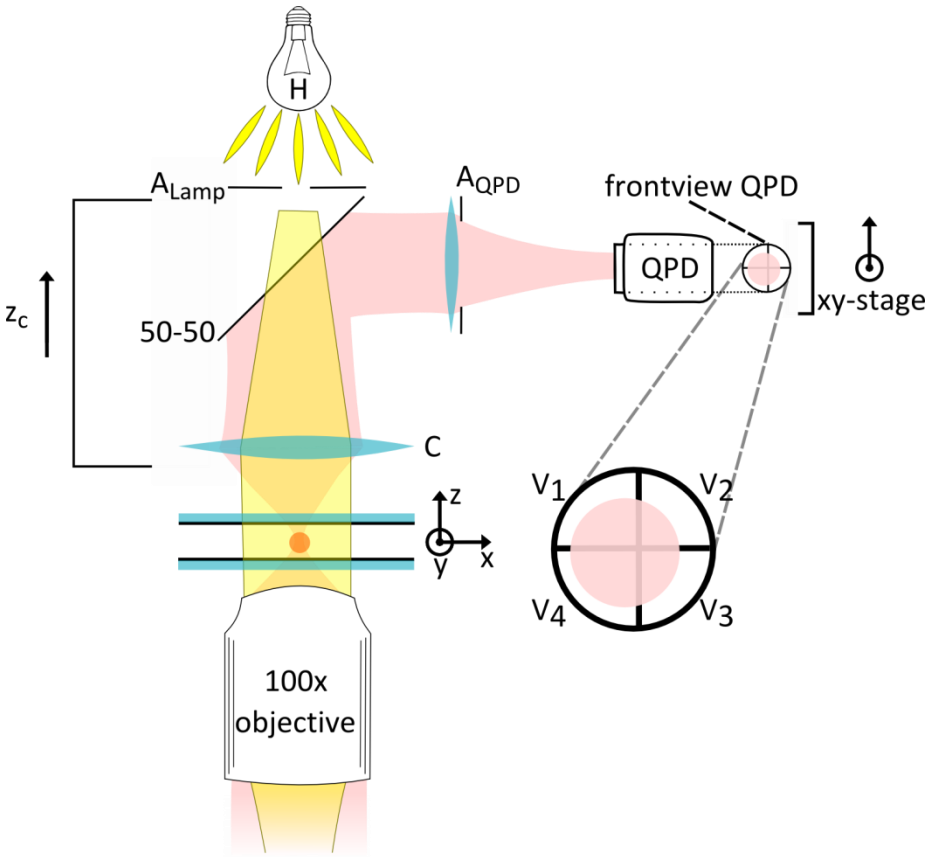

Figure 3-2 Schematic representation of the experimental. The QPD is mounted on a xy-stage that moves in the directions perpendicular to the propagation direction of the incoming beam. The upper part of the setup, consisting of the condenser lens, the 50-50 beam splitter, the

imaging lens and its aperture A_{QPD} and the QPD, is mounted on a translation stage that can move in the direction z_C as indicated. The lamp (L) is used for alignment purposes.

The QPD consists of 4 photodiodes and relays four voltage signals (V_1, V_2, V_3, V_4) to the data acquisition device which is linked to a computer where the data is stored. The voltage signal transferred from each photodiode is proportional to the incident light on its respective quarter of the QPD. The lens configuration in the position detection setup is such, that a small displacement of the trapped bead, lateral with respect to the laser propagation direction, results in a proportional displacement of the beam spot on the QPD. So that a displacement of the particle is translated into a corresponding set of output voltages from the QPD.

Specifically, for small displacements, the relation between the displacement of the particle (Δx, Δy, Δz) and the recorded QPD voltages (V_1, V_2, V_3, V_4) is linear and is given by equations 3-1 to 3-3. The z direction is indicated in Figure 3-2 and is along the propagation direction of the laser. x and y are the lateral directions, perpendicular to z and to each other.

$$x = \beta_x (V_1 + V_2 - V_3 - V_4) = \beta_x V_x \qquad 3\text{-}1$$

$$y = \beta_y (V_1 - V_2 - V_3 + V_4) = \beta_y V_y \qquad 3\text{-}2$$

$$z = \beta_z (V_1 + V_2 + V_3 + V_4) = \beta_z V_z \qquad 3\text{-}3$$

β_x, β_y and β_z are conversion factors in SI unit m/V. For a well aligned system, β_x and β_y are approximately equal. In what follows, I explain how the formula for β_z is obtained. This derivation is based on [106]. Formulas for β_x and β_y can be found entirely analogously.

The analytical formula to calculate β_z is obtained through *Fourier* analysis of equation 2-20. The *Fourier transform* is defined as

$$\hat{Z}(f) = \int_{-\infty}^{+\infty} z(t) e^{-i2\pi ft} dt, \qquad 3\text{-}4$$

where $\hat{Z}(f)$ is the *Fourier transform* of $z(t)$. Applying this transformation to equation 2-20 yields

$$\hat{Z}\left(-i2\pi f\gamma+\kappa\right)+Q_{\text{part}}E_0\delta\left(f-f_E\right)=\hat{F}_B, \qquad 3\text{-}5$$

For frequencies where $f \neq f_E$, this simplifies to

$$\hat{Z}_k\left(-i2\pi\gamma f+\kappa\right)=\hat{F}_B \qquad 3\text{-}6$$

$$\Rightarrow\left|\hat{Z}\right|^2=\frac{\left|\hat{F}_B\right|^2}{\left(4\pi^2\gamma^2f^2+\kappa^2\right)}=\frac{\left|\hat{F}_B\right|^2}{4\pi^2\gamma^2\left(f^2+f_c^2\right)} \qquad 3\text{-}7$$

Equation 3-7 follows from the modulus squared of equation 3-6, which is referred to as the power spectrum $\left|\hat{Z}\right|^2=S_{ZZ}$. Also in equation 3-7, the corner frequency $f_c=\kappa/2\pi\gamma$ is introduced, which marks the point in the frequency domain where the contribution of the optical trapping force and the viscous drag force are equal.

The power spectral density of the stochastic force $\left|\hat{F}_B\right|^2$ is $2k_BT\gamma$ as shown in section 2.2.1, with k_B the *Boltzmann* constant and T the temperature in Kelvin. Note that in the first 10 to 20 s the temperature of the particle can increase by several degrees Celcius under the influence of an AC field[107]. By introducing this into equation 3-7 the final form of the power spectrum S_{ZZ} is reached:

$$S_{ZZ}=\frac{k_BT}{2\pi^2\gamma\left(f^2+f_c^2\right)} \qquad 3\text{-}8$$

In my experiments, typical values for the corner frequency hover around f_c ≈ 10 Hz. For values of the frequency much higher than the corner frequency $f \gg f_c$, The power spectrum can be approximated as

$$S_{ZZ}=\frac{k_BT}{2\pi^2\gamma f^2} \qquad 3\text{-}9$$

For high frequencies, the expected value of the power spectral density multiplied by the frequency squared is a constant $f^2 S_{ZZ} = \frac{k_B T}{2\pi^2 \gamma}$. This value can be used to convert the measured voltage V_z of the QPD to the z displacement by equation 3-10, which has been derived by Flyvbjerg[108]:

$$z = \sqrt{\frac{S_{ZZ} f^2}{S_{VV,z} f^2}} V_z = \sqrt{\frac{k_B T}{2\pi^2 \gamma S_{VV,z} f^2}} V_z \qquad 3\text{-}10$$

Which provides the formula for the conversion coefficient β_z (in m/V) in equation 3-1 to 3-3, to convert the voltages that are obtained from the QPD to particle displacement in meter.

$$\beta_z = \sqrt{\frac{k_B T}{2\pi^2 \gamma S_{VV,z} f^2}}, \qquad 3\text{-}11$$

where $S_{VV,z} f^2$ is the high-frequency plateau value of the power spectral density of the QPD voltage signal multiplied with the frequency squared. By implementing the value of β_z into equations 3-1 to 3-3, I can trace the position of an optically trapped particle with nanometer precision at a rate of 100 kHz.

3.2.2.2 Alignment procedure

The previous section explains the analysis procedure by which the position is measured and converted from Volt to meter, in the implicit assumption that the setup is properly aligned. In practice, prior to the start of any experiment, the laser needs to be realigned. This calls for a consistent and standardized alignment method, to ensure position detection measurements of optimal quality and reproducibility.

The laser alignment of the back focal plane interferometry setup from Figure 3-2 follows the following steps:

- Trap a colloidal particle inside the microfluidic cell in the absence of an electric field
- Open the program on the computer that provides

- a life feed of the power spectrum in x-, y- and z-directions
- the sum voltage of the QPD averaged over 1 second: V_z
- a life feed of the x and y position of the laser beam V_x and V_y
- The modulus of the cross spectrum correlations between V_z and V_x, $\left|\langle V_x, V_z \rangle\right| = \left|\hat{V}_x \hat{V}_z^*\right|$, and between V_z and V_y, $\left|\langle V_y, V_z \rangle\right| = \left|\hat{V}_y \hat{V}_z^*\right|$, where $\hat{V}_i$ is the discrete *Fourier* transform of V_i and the symbol * denotes that $\hat{V}_i^*$ is the complex conjugate of $\hat{V}_i$.

- Open both the aperture of the lamp, A_{lamp}, and the aperture of the QPD, A_{QPD}.
- Slightly reduce the opening of the aperture of the lamp A_{lamp} and move the z-stage of the microscope, z_C, until you find the position of z_C with that gives the brightest field. Repeat this several times until the aperture of the lamp is nearly closed and you can observe the contour of the aperture A_{lamp} on the camera image.
  The aim of this step is to make the focal planes of the condenser lens (C) and the 100 X objective lens coincide perfectly. In this way the condenser lens converts the strongly diverging trapping beam into a perfectly parallel laser beam.
- When no aperture is present before the QPD, the entire beam is captured by the QPD and the sum of the four quadrants will be constant, so no z-signal is detected.
  Therefore, the opening of the A_{QPD} is reduced until the z-signal produces a power spectrum (as introduced in [109]).
  The QPD in my experiments can produce an output from 0 V to 5 V. Ideally, the value of V_z should be halfway in this range. If the signal is too high, a better value can be accomplished by further reducing A_{QPD} and vice versa.

- Move the xy translation stage of the QPD until both V_x and V_y are on average zero.
- From this point, move the translation stage along x_{QPD} until the modulus of the cross correlation $\left|\langle V_x, V_z \rangle\right|$ is minimized. Do the same for y_{QPD}.

The program should now provide a life feed of a clean power spectrum in all three directions. The laser is now properly aligned and the experiment can start.

Note that this alignment procedure is assuming some degree of prior alignment. This procedure only covers the alignment that needs to be repeated before every experiment, not the complete alignment of the optical trapping setup.

The *Fourier* spectrum of the cross correlation between two voltage signals mentioned in the alignment procedure is defined as the product of the *Fourier* spectrum of one signal with the complex conjugate of the *Fourier* spectrum of the second. I used voltage signals of time interval of 1 s.

3.2.3 Setup - Optical trapping electrophoresis

In Figure 3-3, the full experimental setup is presented that is used to obtain the main results from this thesis. The position detection system from section 3.2.2 is integrated in this setup. Figure 3-3 further also depicts the light path of the halogen lamp (H) to the camera.

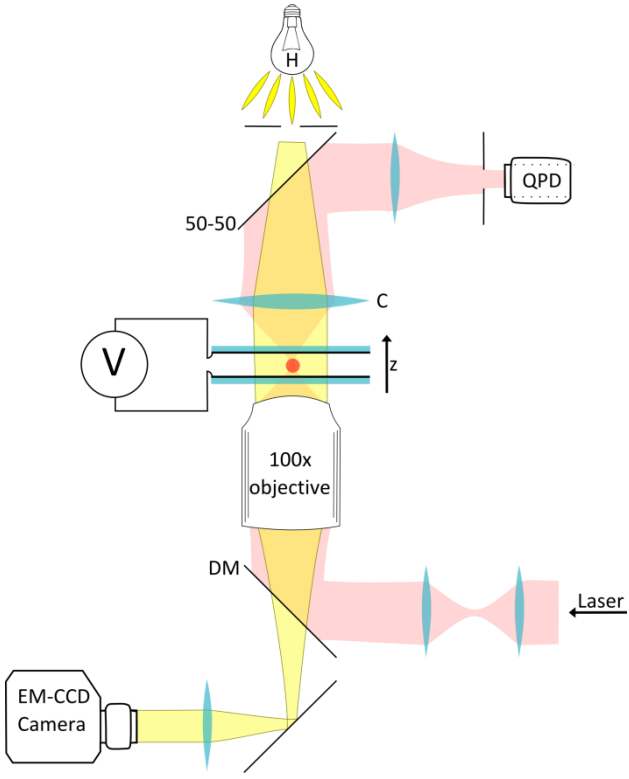

Figure 3-3 Full schematic overview of the OTE setup, showing the path of the IR laser beam (pink) that traps the particle and arrives at the QPD and the path of the white illumination (yellow) from the lamp to the EM-CCD camera.

The setup is built around an inverted optical microscope (Nikon Eclipse TI), which is used to simultaneously visualize and probe a single colloidal particle as shown in Figure 3-3. A 975 nm (IR) laser beam with 60 mW power is coupled into the microscope by a dichroic mirror (DM) and is focused by a 100 X oil immersion objective (Nikon, Plan Fluor 100X, numerical aperture 1.3). Two Indium-Tin-Oxide (ITO) covered glass plates are separated by a distance of approximately 75 µm by spacers in UV curable glue, and the volume between the electrodes is for example filled with a PMMA dispersion. The laser is focused in the mid-plane between the two electrodes where a single PMMA particle is optically trapped. The forward scattered light is collected by the condenser (C), reflects off a 50-50 beamsplitter and impinges onto the QPD. Section 3.2.2.1 details how the QPD works.

The halogen lamp (H) illuminates the sample under Köhler illumination. The white light travels through the sample in the opposite direction as the laser beam and forms an image of the particle on an Andor iXon+ EM-CCD camera. The camera is used to confirm trapping of a single particle and to align the laser inside the sample.

Measurements are executed with a sinusoidal voltage difference (V) applied across the ITO electrodes at frequencies ranging from 250 Hz to 5 kHz and voltage amplitudes ranging from 25 V to 200 V. As the electrodes are spaced 75 µm apart, typical amplitudes of the electric field are around 1 V/µm.

3.3 Analysis method

The first sections of this chapter focuses on the experimental side of the method. Here, I elaborate on the analysis method which consists of two parts.

In the first part, the converted QPD signal is used to calculate a first estimate of the electric charge of the particle.

If I observe that the normalized charge of the particle $Q_j(t)/e$ makes discrete jumps with the size nearly equal to one, but the values are not clustered around integer values, I calculate a correction factor u to remedy this and obtain the final charge values $Q_f(t) = Q_j(t)/u(t)$.

3.3.1 Calculation of the charge

Section 2.3 detailed how the movement of a particle can be tracked in time with nm resolution. Here, I delve into the analysis of how to calculate the particle's charge from that recorded movement. This analysis follows the work *Beunis* et al in [90] (supplementary online material).

In the presence of a sinusoidal electric field $E(t) = E_0 \cos(2\pi f_E t)$, a particle with a fixed charge Q_{part} is subject to a force proportional to its charge, $F_E = Q_{\text{part}} E(t)$. Section 2.3 concluded with equation of motion 2-17 which is repeated below.

$$Q_{\text{part}}E(t)+\sqrt{2k_BT\gamma}\xi(t)-\gamma\dot{z}-\kappa z=0 \qquad 3\text{-}12$$

Because the particle's equation of motion is a linear differential equation, the solution can be considered as the sum of an oscillatory motion with amplitude proportional to its charge (due to the sinusoidal force F_E) and a *Brownian* motion due to the random force.

The charge is calculated from one window of N measurements z_n, with $n=1,2,\ ..\ ,N$, of the position z at times t_n. I define z_n as the position z of the particle at time t_n, $z_n=z\left(t_n\right)=z\left(n\Delta t_s\right)$. In this work, the value of N is taken to be 100,000. As the acquisition frequency of the QPD is $f_{\text{s}}=100\ kHz=1/\Delta t_s$, this implies that the charge is sampled at a frequency of $f_{\text{Q}}=1\ Hz=1/\Delta t_Q$. Equation 3-12 is transformed into a difference equation by solving it in the interval $t_n\le t<t_{n+1}$

$$z_{n+1}=$$
$$z_n\mathrm{e}^{-\omega_c\Delta t_s}+Q_{\text{part}}E_0\int_{t_n}^{t_{n+1}}\cos\left(2\pi f_E t'\right)\mathrm{e}^{-\omega_c\left(t_{n+1}-t'\right)}dt'+\sqrt{\left(1-\mathrm{e}^{-2\omega_c\Delta t_s}\right)\frac{D}{2\pi f_c}}\xi_n\ , \qquad 3\text{-}13$$

where $\omega_c=2\pi f_c=\kappa/\gamma$ and ξ_n is defined as

$$\xi_n=\sqrt{\frac{\omega_c}{1-\mathrm{e}^{2\omega_c\Delta t_s}}}\int_{t_n}^{t_{n+1}}\xi\left(t'\right)\mathrm{e}^{-\omega_c\left(t_{n+1}-t'\right)}dt' \qquad 3\text{-}14$$

Introducing the *Discrete Fourier transform* (DFT) $\hat{z}_k=\Delta t_s\sum_{n=1}^{N}z_n\mathrm{e}^{\mathrm{i}\omega_k t_n}$, with $\omega_k=2\pi f_k=2\pi\mathrm{k}/\left(N\Delta t_s\right)$, equation 3-13 is transformed into

$$\hat{z}_k=\sqrt{\frac{D}{\omega_c}}\frac{\sqrt{1-\mathrm{e}^{-2\omega_c\Delta t_s}}}{\mathrm{e}^{-\mathrm{i}\omega_k\Delta t}-\mathrm{e}^{-\omega_c\Delta t_s}}\hat{\xi}_k+$$
$$\frac{Q_{\text{part}}E_0}{2\left(\omega_c^2+\omega_E^2\right)}N\Delta t\left(\left(\omega_c+\mathrm{i}\omega_E\right)\delta\left(\omega_k-\omega_E\right)+\left(\omega_c-\mathrm{i}\omega_E\right)\delta\left(\omega_k+\omega_E\right)\right) \qquad 3\text{-}15$$

where δ is the *Dirac-delta* function that is equal to one if its argument is zero and is equal to zero otherwise and $\hat{\xi}_k$ is the DFT of the Gaussian process and satisfies $\langle \xi_k \rangle = \langle \xi_k^* \rangle = 0$, $\langle \xi_k \xi_k \rangle = 0$ and $\langle \xi_k \xi_k^* \rangle = N \Delta t_s$.

From equation 3-15 I can calculate an estimate Q_j of the charge Q_{part} as a weighted sum of the real and imaginary parts of the DFT

$$Q_j = \frac{2\gamma f_Q}{E_0}\left(\omega_c \,\mathrm{Re}\left(\hat{z}_E\right) + \omega_E \,\mathrm{Im}\left(\hat{z}_E\right)\right), \qquad 3\text{-}16$$

where $\hat{z}_E$ is the frequency component for which $f_k = f_E$. The expected value of the estimate indeed equals the charge $\langle Q_j \rangle = Q_{\text{part}}$. The standard deviation on this estimate is:

$$\sigma\left(Q_j\right) = \frac{2\sqrt{k_B T \gamma f_Q \alpha_E}}{E_0} \qquad 3\text{-}17$$

α_E is a factor that takes into account anti-aliasing that is caused by the finite sampling rate.

$$\alpha_E = \frac{\left(\omega_c^2 + \omega_E^2\right)\left(1 - \mathrm{e}^{-2\omega_c \Delta t_s}\right)\Delta t_s}{2\omega_c\left(1 - 2\cos\left(\omega_E \Delta t_s\right)\mathrm{e}^{-\omega_c \Delta t}\mathrm{e}^{-2\omega_c \Delta t_s}\right)} \qquad 3\text{-}18$$

To resolve the elementary charge in the charge evolution of a particle, the following condition has to be met:

$$SNR = \frac{\mathrm{e}E_0}{2\sqrt{k_B T \gamma f_Q \alpha_E}} > 1 \qquad 3\text{-}19$$

Here, the amplitude of the electric field is typically on the order of $E_0 = 1\ \mathrm{V/\mu m}$ and the charge sampling frequency is $f_Q = 1\ \mathrm{Hz}$, so for a micrometer sized particle in dodecane ($\eta_{\text{dodecane}} = 1.34\ \mathrm{mPa\,s}$ at room temperature), the signal-to-noise ratio is $\frac{\mathrm{e}E_0}{2\sqrt{k_B T \gamma f_Q \alpha_E}} = 11.1$, which amply satisfies the required condition.

In this section, in deriving the relevant equations, I distinguished between the estimate of the charge Q_j and the particle's charge itself Q_{part}. In the continuation of this document, I will no longer make this distinction and refer to the calculated value of the charge as Q_j, unless otherwise specified.

3.3.2 R^2-method of adjusting the charge

In the previous section, I discussed how the position of the particle is tracked with the QPD and how the QPD signal is converted from Volt to meter through equation 3-3. Then, a thorough analysis of the particle's equation of motion led to a formula to calculate a first estimate of the charge Q_j. However, Figure 3-4 shows that while an experiment may meet the criterion for resolving the elementary charge (equation 3-19), the values of the normalized charge Q_j/e are not necessarily clustered around integer numbers. This is likely because the estimate of the charge Q_j depends on my estimate of both the electric field E and the *Stokes* drag coefficient γ. Fluctuations in the conversion coefficient β_z and small mechanical variations in the setup may also contribute to this effect. This is why I employ the R^2-method of adjusting the charge. This method is based on [110]. Figure 3-4 is an excerpt of a longer measurement and shows the final 400 s of charge data.

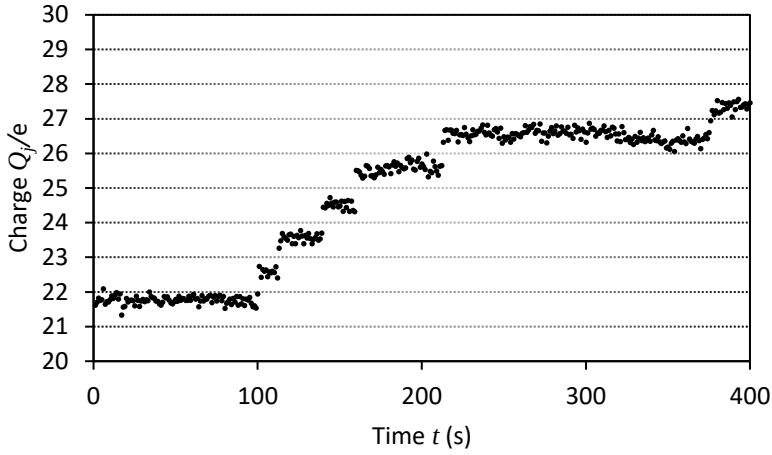

Figure 3-4 Time evolution of the charge Q_j for a 1 μm PHSA-coated PMMA particle in dodecane during 400 s with electric field amplitude $E = 0.67\ \mathrm{V/\mu m}$ and frequency $f = 2.5\ \mathrm{kHz}$. Though the signal to noise ratio is larger than 1, $\mathrm{SNR} = 7.4 > 1$, the values of the normalized charge are not clustered around integer values.

Consider a charge measurement where the normalized charge values Q_j/e, unlike those from Figure 3-4, are clustered around multiples of the elementary charge. Then I can rewrite the normalized charge Q_j/e at time $t = t_i$ as

$$\frac{Q_j(t_i)}{e} = Z_i + \varepsilon_i, \qquad 3\text{-}20$$

where Z_i is the integer number of elementary charges on the particle and ε_i is the deviation from the integer Z_i. So that for most normalized charge values it can be stated that

$$\frac{Q_j(t_i)}{e} - \left[\frac{Q_j(t_i)/e}{Z_i}\right] Z_i = \varepsilon_i < 0.5 \qquad 3\text{-}21$$

Where the bracket notation $\left[\ \right]$ denotes rounding to the nearest integer. The deviation ε_i is mainly due to *Brownian motion*.

Now reexamine the values of the normalized charge Q_j/e in Figure 3-4. They are systematically smaller than the nearest integer number and the offset increases as the value of the charge increases. This indicates that the separation between the experimentally observed normalized charges u is slightly smaller than 1. The normalized charge values here can be better described by:

$$\frac{Q_j(t_i)}{e} = Z_i u + \varepsilon_i \qquad 3\text{-}22$$

And

$$\frac{Q_j(t_i)}{e} - \left[\frac{Q_j(t_i)/e}{Z_i u}\right] Z_i u = \varepsilon_i \ < 0.5 \qquad 3\text{-}23$$

To find the optimal value of u, I perform a parameter sweep of u over a certain interval (for example between 0.9 and 1.1 or between 0.25 and 2) and calculate the R^2 function for a time centered around t

$$R^2(t,u) = \sum_{i=-n}^{n}\left(\frac{Q_j(t+i\Delta t)}{e} - u_j\left[\frac{Q_j(t+i\Delta t)/e}{u}\right]\right)^2, \qquad 3\text{-}24$$

where $2n\Delta t+1$ is the total size of the time window centered around the normalized charge value Q_j/e. This function can not be computed for the first and the final n data points. The R^2 function was introduced by *Strubbe* in [17, 110].

The R^2 function is expected to go through a local minimum for the optimal value of u. This is shown in Figure 3-5, which displays $R^2(u)$ for t = 100 s from Figure 3-4 with n = 100.

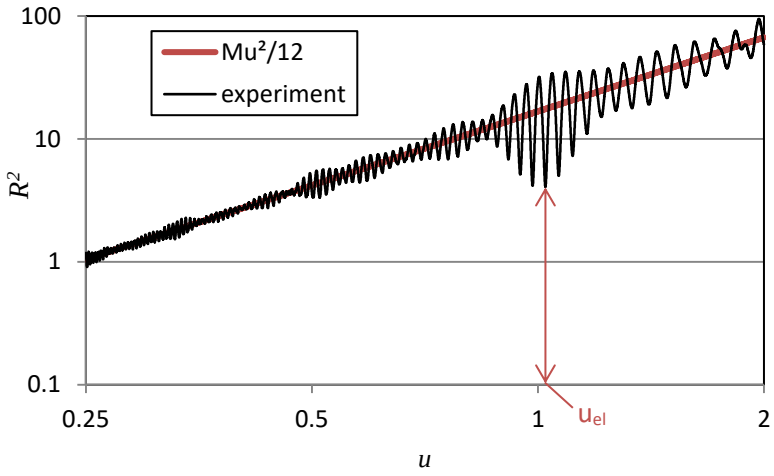

Figure 3-5 Analysis of the deviation of the normalized charge from Figure 3-4. $R^2(t,u)$ from equation 3-24 is calculated for the data from Figure 3-4 for t =100 s (black). The straight line (red) shows the quadratic expectancy $Mu^2/12$, with $M = 2n+1$, for random charge data. Values of this graph that are below this line suggest clustering of the charge data around multiples of u. The local minimum corresponding to the elementary spacing between the charge levels is u_{el} =1.023.

The graph on Figure 3-5 plots the R^2 function together with its quadratic expectancy of random data $Mu^2/12$, where $M = 2n+1$. At u = 1.023, the local minimum that corresponds to the mean separation between normalized charge clusters can be identified, which I call u_{el}. Notice that the difference between adjacent peaks of u_{el} is quite small. I will come back to this observation later in section 3.3.2.2.

I can now define a flattened and normalized R^2 function, which I shall refer to as R^2_-:

$$R^2_-(t,u) = \frac{12}{M^2}\sum_{i=-n}^{n}\left(\frac{Q_j(t+i\Delta t)}{e} - u_j\left[\frac{Q_j(t+i\Delta t)/e}{u}\right]\right)^2 \Big/ u^2 \qquad 3\text{-}25$$

The advantage of R_{-}^{2} is that a local minimum stands out more strongly against a constant curve than versus a quadratic curve as in R^2.

The value for u_{el} in Figure 3-5 is calculated for t = 100 s, but it can be obtained for any data point of the measurement. In Figure 3-6 R_{-}^{2} is shown for the experiment from Figure 3-4 for n = 250, for t varying from 0 s to 150 s (note that the measurement starts I fact at t = -250 s, but not all the data is shown), and for u ranging from 0.25 to 2. One sustained dip can be observed in the figure near u = 1. This dominant valley in the graph is the time evolution of u_{el}, which should yield a quasi-continuous $u_{el}(t)$. The local maxima surrounding this minimum for this experiment lie at 0.97 and 1.00.

In Figure 3-7, $u_{el}(t)$ is plotted in black for the 150 seconds, corresponding to the first 150 seconds of the experiment in Figure 3-4. A discontinuous jump can be observed at t = 130 s. In order to obtain the running local minimum in the graph from Figure 3-6, the R_{-}^{2} is calculated again with bounds u = 0.97-1.00. The minimal value of u in this interval is shown in red.

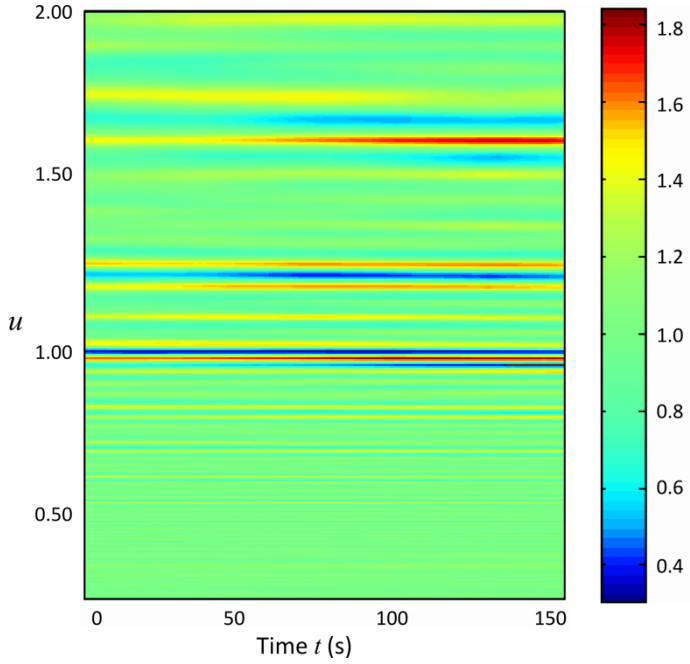

Figure 3-6 The R^2_- function over time for the experiment in Figure 3-4 with n = 250. A pronounced local minimum is found near u = 1 over the entire experiment. Starting around t = 100 s, a second local minimum appears next to the first local minimum.

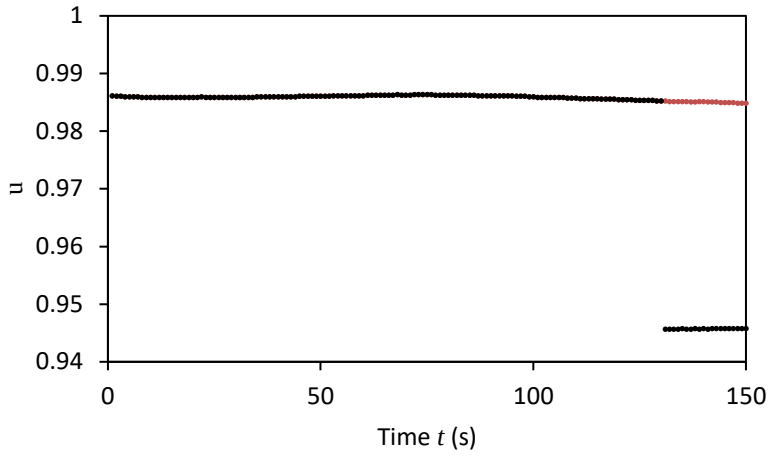

Figure 3-7 Time evolution of $u_{el}(t)$ from Figure 3-6. (black) A discontinuous jump at t = 130 s indicates that the local minimum from that point onward does not lie in the dominant valley observed in Figure 3-6. (red) By calculating R^2_- within bounds u =0.97 - 1.00, the appropriate value for $u_{el}(t)$ can be obtained consistently.

Now that bounds for $u(t)$ have been established in case of a very large time window n = 250, this can be taken advantage of to calculate R^2_- for progressively smaller time windows n = 100 s, 50 s, 25 s. The result is shown in Figure 3-8.

Figure 3-9 shows the original normalized charge data Q_j/e from Figure 3-4 together with the final normalized charge data $Q_f(t)/e$, which is defined as

$$Q_f(t) = Q_j(t)/u(t)_{el,n=25}, \qquad 3\text{-}26$$

where $u(t)_{el,n=25}$ is $u(t)_{el}$ with n = 25. Note that $Q_f(t)$ has 25 data points less, due to the size of the time window used to calculate $u(t)_{el,n=25}$. Due to the form of the definition of $Q_f(t)$, I will refer to $u(t)_{el}$ as the correction factor.

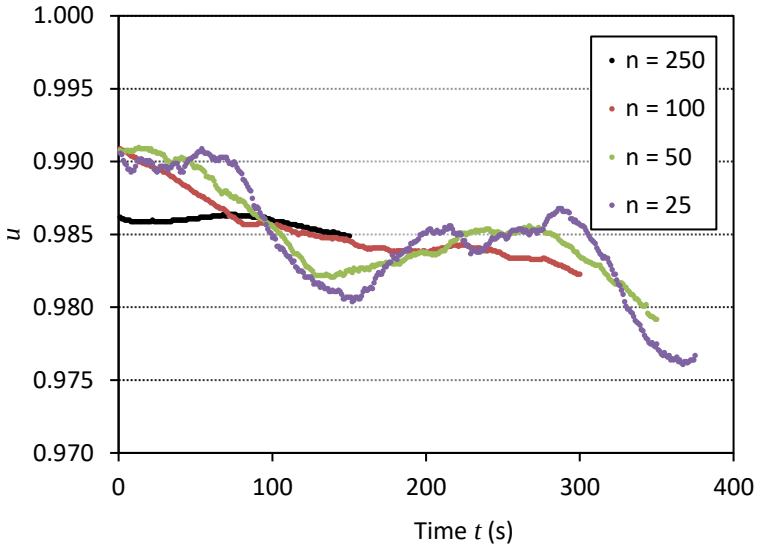

Figure 3-8 Correction factor $u_{el}(t)$ calculated through R_{-}^{2} for time windows with half width $n\Delta t$ = 250 s, 100 s, 50 s and 25 s. For $n\Delta t$ becoming progressively smaller, the fluctuation in $u_{el}(t)$ increases. Note that the fluctuations remain below a few %.

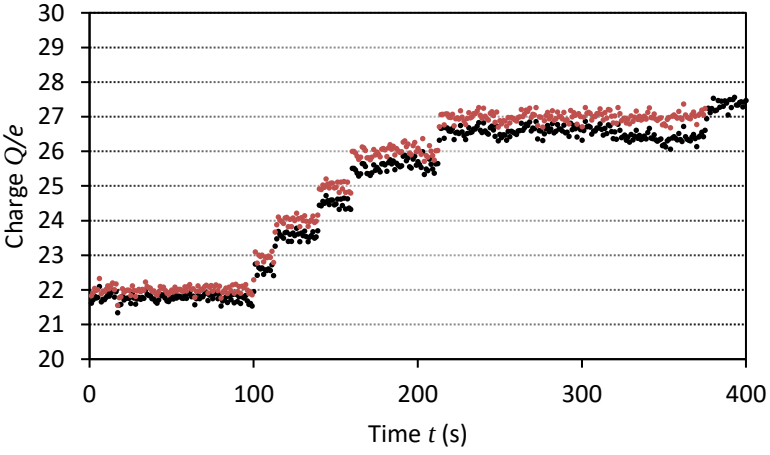

Figure 3-9 Normalized charge data before (Q_j/e, black) and after (Q_j/e, red) correction with the correction factor $u(t)$ calculated by the R_{-}^{2} method with n = 25 s.

By reducing the size of the time window $n\Delta t$, the normalized charge data points are better reduced to their corresponding integers. Also, less data has to be discarded at the beginning and the end of the experiment. It is therefore advantageous to use a small time window.

If the selected time window is too small however, data points can be directed towards an incorrect integer. This is prevented by checking for discontinuous variations. This is accomplished by checking the progression of $u_{el}(t)$ with the condition that for any t it is valid that:

$$\left| \frac{Q_j(t)}{u_{el}(t)e} - \frac{Q_j(t)}{u_{el}(t+1)e} \right| < 0.5 \qquad \text{3-27}$$

This formula checks whether the difference between consecutive values of the correction factor $u_{el}(t)$ are large enough to project the same normalized charge value corresponding to the first correction factor to different integer values after rounding.

3.3.2.1 R^2 and measurement variance

Consider equation 3-24 of the R^2 function expressed for final normalized charge Q_f/e at time t for $u = u_{el}$. Here, it is applied to final normalized charge data, so that $u = u_{el} = 1$. This yields

$$R^2(t,1) = \sum_{i=-n}^{n} \left(\frac{Q_f(t+i\Delta t)}{e} - 1 \left[\frac{Q_f(t+i\Delta t)/e}{1} \right] \right)^2 \qquad \text{3-28}$$

Since $u = u_{el} = 1$, the normalized charge can be written as $Q_f/e = Z_i + \varepsilon_i$. Which simplifies 3-28 to

$$R^2(t,1) = \sum_{i=-n}^{n}\left(Z_i u_{el} + \varepsilon_i - \left[\frac{Z_i + \varepsilon_i}{1}\right]\right)^2$$

$$= \sum_{i=-n}^{n}\left(Z_i + \varepsilon_i - Z_i - u_{el}\left[\varepsilon_i\right]\right)^2 \quad , \qquad \text{3-29}$$

$$= \sum_{i=-n}^{n}\left(\varepsilon_i - \left[\varepsilon_i\right]\right)^2 = \sum_{i=-n}^{n}\left(\varepsilon_i\right)^2$$

since $\left[\varepsilon_i / u_{el,i}\right] = 0$.

This means that the value for $R^2\left(Q_f,1\right)$ is directly related to the variance σ^2 of the fluctuations around integer values of the measurement.

$$R^2(t,1) = \sum_{i=-n}^{n}\left(\varepsilon_i\right)^2 = M\sigma_R^2 \qquad \text{3-30}$$

To verify this result, I compare the value of the R^2 function at the local minimum at u = 0.984 in Figure 3-5 with the variance of the corrected normalized charge in Figure 3-9. This respectively yields σ_R^2 = 0.02 and σ^2 = 0.018.

3.3.2.2 Local minima of R^2 around u_{el}

In Figure 3-5, it is shown that the R^2 function follows a quadratic trend on average. But aside from the position of u_{el}, little else can be inferred from the fluctuations of the graph. It can be observed however that for values of u around u_{el}, R^2 goes through a series of local maxima and minima that are progressively less pronounced.

It is crucial that the u_{el} is assigned to the appropriate local minimum. The aim of this section is to understand what determines the number of local minima of R^2 around u_{el}. To that effect I investigate the curvature around the local minimum corresponding to u_{el} by once again considering equation

3-24, now for small deviations of u_{el}, $\left[u_{el}-\Delta u, u_{el}+\Delta u\right]$ with $\Delta u \ll 1$, for the final normalized charge Q_f/e at time $t=t_i$.

$$
\begin{aligned}
R^2(t,1) &= \sum_{i=-n}^{n}\left(\frac{Q_f(t+i\Delta t)}{e}-(1+\Delta u)\left[\frac{Q_f(t+i\Delta t)/e}{(1+\Delta u)}\right]\right)^2 \\
&\approx \sum_{i=-n}^{n}\left((Z_i+\varepsilon_i)-(1+\Delta u)\left[(Z_i+\varepsilon_i)(1-\Delta u)\right]\right)^2 \\
&= \sum_{i=-n}^{n}\left((Z_i+\varepsilon_i)-(1+\Delta u)\left[Z_i-\Delta u Z_i+\varepsilon_i-\Delta u\varepsilon_i\right]\right)^2 \qquad , \qquad \text{3-31} \\
&\approx \sum_{i=-n}^{n}\left((Z_i+\varepsilon_i)-(1+\Delta u)\left(Z_i-\left[\Delta u Z_i+\varepsilon_i\right]\right)\right)^2 \\
&= \sum_{i=-n}^{n}\left(\varepsilon_i-\Delta u Z_i-(1+\Delta u)\left[\Delta u Z_i+\varepsilon_i\right]\right)^2
\end{aligned}
$$

where the *Taylor expansion* $\frac{1}{(1+\Delta u)} \approx 1-\Delta u$ is used and the term $\Delta u\varepsilon_i$ has been neglected.

From equation 3-31, I gather that for small deviations Δu around u_{el}, the curvature of the R^2 function increases with increasing charge number Z_i of the particle. That indicates that a higher mean charge leads to a higher number of local minima surrounding u_{el}. In fact, this is to be expected: The difference between factors that project a number to its nearest integer and its second nearest integer are closer together when the absolute value of that number is larger.

The other parameter in the R^2 function is the time window $(2n+1)\Delta t$. I would expect that, as the size of the time window increases and more values of the charge are taken into account, the R^2 function should make a more accurate calculation of u_{el}.

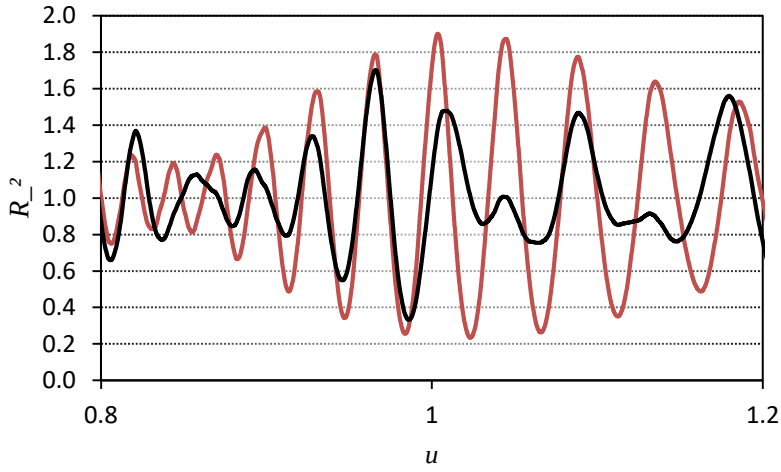

Figure 3-10 The R_{-}^{2} function in function of u for n = 250 (black) and n = 100 (red). The data from the red curve is also shown in Figure 3-5 where it is expressed by the R^2 function. The red curve has a higher number of local minima. The lowest minima of the two curves do not coincide. The black curve, with highest n, assigns u_{el} to the correct local minimum.

From Figure 3-10 it can be observed that a lower number for n results in a larger number of local minima. This confirms that a higher number for n can more reliably lead to the correct value of u_{el}.

Therefore, when the global minimum $u_{el}(t)$ switches between two local minima, the most appropriate local minimum to follow is obtained by increasing the time window for R_{-}^{2} and to pick the local minimum that is dominant in the time interval where the particle's charge is smaller.

3.3.3 Summary of the analysis method

The relevant formulas and analysis tools to properly evaluate the charge of a colloidal particle have been laid out extensively over the course of this chapter. Therefore, as a summary in brief, I provide a graphical overview of the entire process below in Figure 3-11.

First, the voltage data of the QPD is converted to z-position data by calculating the conversion coefficient through equation 3-11.

Next, the particle's charge Q_j is calculated every second by formula 3-16, by using 100 000 z-positions in a 1 s time interval. The resulting $Q_j(t)$ is measured over an interval of hundreds of seconds.

Then, I calculate the correction factor $u_{el}(t)$ based on formula 3-25 as a function of time t. First for large values of n, to ensure identifying the correct local minimum of R_-^2. Then, I calculate $u_{el}(t)$ for progressively smaller values of n, within well-defined bounds of u.

Finally, the corrected charge data $Q_f(t)/e$ is obtained by dividing the initial estimation of the charge $Q_j(t)$ by the corresponding correction factor $u_{el}(t)$.

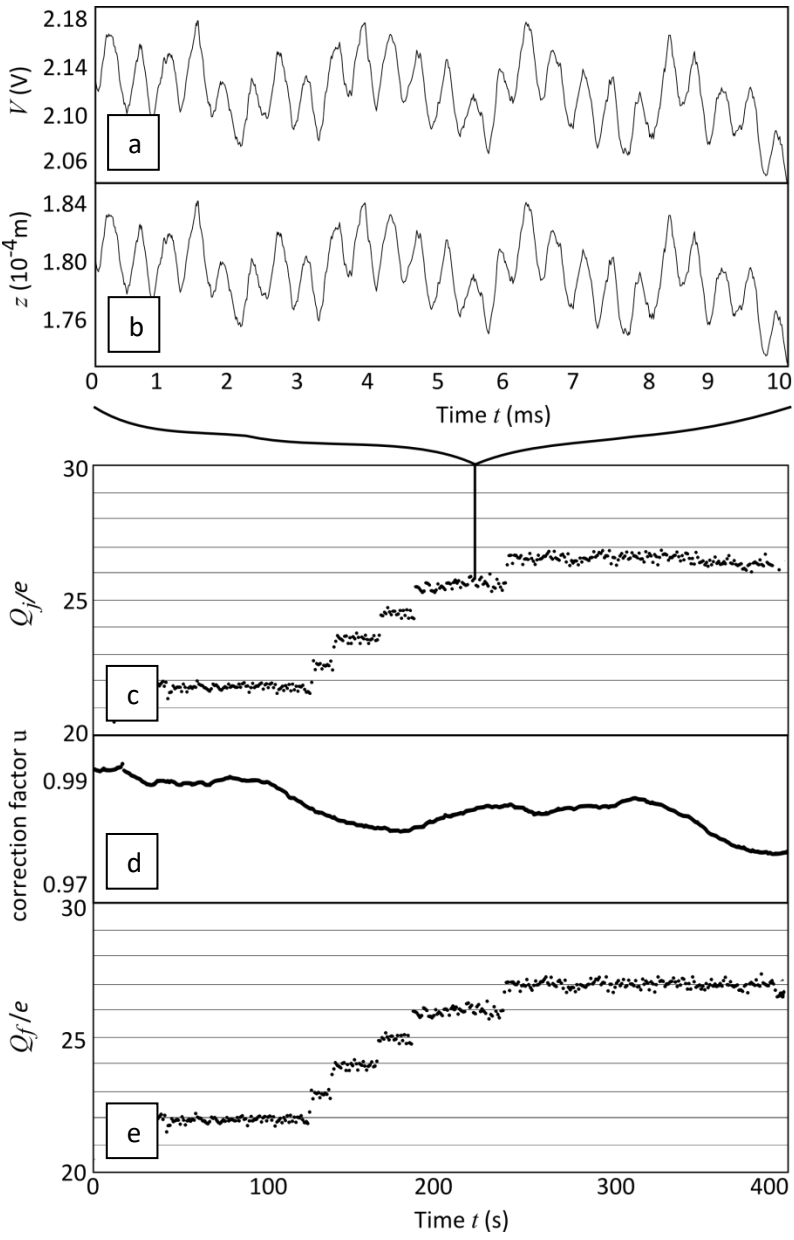

Figure 3-11 Consecutive steps in the analysis method are shown. The QPD voltage signal (a) is converted to position data (b). The charge $Q_j(t)$ (in e) (c) is calculated for every set of 100k data points, which corresponds to 1000 ms. The normalization factor $u_{\mathrm{el}}(t)$ (d) is calculated. The charge evolution is then scaled to obtain $Q_f(t)$ (e).

In this chapter, it was necessary to provide a subscript to the charge in order distinguish between different charges that were used such as Q_{part}, Q_j and Q_f. In the following chapters I will present experimental data and as such I will only present the final normalized charge which I equate to the particle's charge. Since it is no longer necessary to explicitly state this every time, I will only talk about the charge and the subscripts can be dropped by defining the charge as $Q = Q_f = Q_{\text{part}}$.

Chapter 4.

Electric Field-Induced Charging

4.1 Introduction

The motivation for developing OTE mainly draws from the desire to understand the mechanisms by which surfactants stabilize charge on colloidal particles in nonpolar liquids. Before I study the influence of surfactants however, this chapter focuses on the charging behavior of single colloidal PHSA-coated PMMA microparticles in pure dodecane. In chapter Chapter 5, I will study how the charging behavior of single particles is modified by the presence of surfactant at different concentrations.

Optical trapping electrophoresis is well suited for single particle measurements over long time intervals with high resolution. The goal of any such measurement is to investigate which mechanisms govern the charging behavior of the colloidal particles and how the particles behave in the presence of an electric field. Therefore, ideally, the technique itself does not interfere with the charging behavior that is being measured.

In this chapter, I present the charge evolution of single colloidal PHSA-coated PMMA particles in pure dodecane. I observe that these particles accumulate positive surface charge over time when a voltage is applied. This is a phenomenon that has not been previously detected in similar systems[18, 90, 92, 93, 111]. The rest of the chapter is dedicated to characterizing the nature of this new phenomenon, which I dub 'electric field-induced charging'. Through an array of different experiments I narrow down the driving factors of this behavior and offer a plausible mechanism for the nature of the reaction that fits well with the presented observations.

4.2 Electric field-induced charging

In Figure 4-1, the normalized charge evolution Q/e of single colloidal PHSA-coated PMMA particles with a diameter of d = 1 µm is shown. The particles oscillate in the optical trap under electric field and frequency sets: (E = 1.33 V/µm, f = 2.5 kHz), (E = 0.67 V/µm, f = 2.5 kHz) and (E = 0.67 V/µm, f = 5 kHz).

Under these conditions, it is possible to measure the charge of the particle with elementary charge resolution so that individual charging and

discharging events can be detected. By my definition, N_{el} single (dis)charging events occur when the difference of 2 consecutive data points of the normalized charge Q/e, each rounded to their respective nearest integer, is equal to N_{el} and N_{el} is non-zero, $\left[Q(t)/e\right]-\left[Q\left(t+\Delta t_Q\right)/e\right]=N_{el}\neq 0$, where $[\ ]$ denotes rounding to the nearest integer and Δt_Q is the size of time window for which one calculation of the charge is made. When N_{el} = 2, this is interpreted as two elementary charging events. Here, Δt_Q = 1 s.

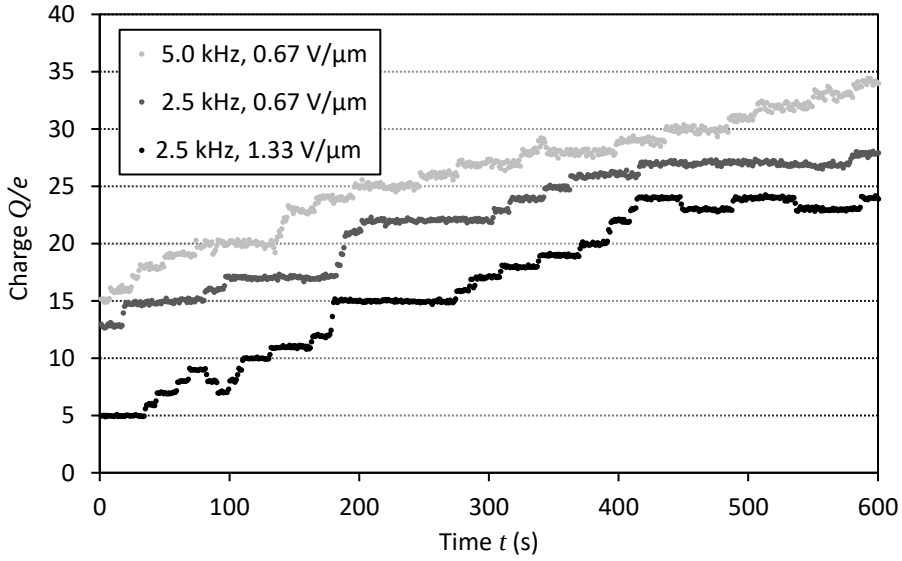

Figure 4-1 Evolution of the normalized charge Q/e for three 1 μm PHSA-coated PMMA particles in dodecane during 600 s under (5 kHz, 0.66 V/μm), (2.5 kHz, 0.66 V/μm), and (2.5 kHz, 1.33 V/μm) with one charge measurement per second.

The measurements in Figure 4-1 reveal a common pattern. All 3 particles start off with a small net charge, $|Q/e|$ < 20, and they slowly accumulate net positive charge over time during the experiment. Measurements on other particles with different sets of applied electric field amplitude E and frequency f reveal a similar trend, where the net charge of the particle rises over a long time interval.

In order to understand the mechanism behind this charging mechanism, I study the impact of different measurement settings on the several aspects of this phenomenon. These results are shown in the subsequent sections of this chapter.

4.3 Effect of amplitude and frequency

I study the charge evolution of several individual particles for varying combinations of the amplitude and the frequency of the electric field (E, f). Both parameters are varied over one order of magnitude. The applied voltage ranges from V = 0.33 V/µm to 2.67 V/µm and the frequency from f = 250 Hz to 5 kHz.

The result of these measurements is summarized in Figure 4-2. The charge of a single colloidal particle is measured over time for each set of the measurement parameters, the amplitude and the frequency of the electric field (E, f), in the graph. As a measure for the speed of the induced charging mechanism, I define the charging speed, $\Delta Q/\Delta t$, which is the difference between the final charge value Q_{final}/e and the initial normalized charge value Q_i, $\Delta Q = Q_{\text{final}} - Q_i$, divided by the total measurement time Δt. The charging speed is proportional to the area of the disks in Figure 4-2. For E = 1.67 V/µm, I could not achieve measurements with elementary charge resolution for frequencies f = 500 Hz and 250 Hz, because the particles escaped the optical trap.

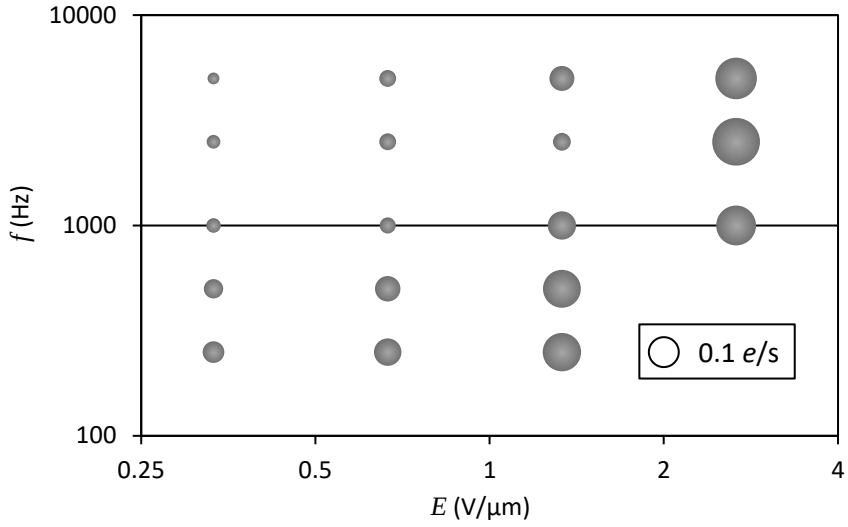

Figure 4-2 Dependence of the charging rate of 1 µm PHSA-coated PMMA particles on the amplitude E and the frequency f of the applied electric field in dodecane. The rate is proportional to the disk size. For reference, the circle in the caption represents a charging rate of 0.1 *e*/s.

From Figure 4-2, it can be observed that there is at least one parameter that has a strong correlation with the charging rate, which is the amplitude of the electric field E. The influence of the frequency on the charging rate is less strong. To further examine how the charging rate depends on the voltage and the frequency, the charging rates from Figure 4-2 are displayed in function of the amplitude and the frequency of the electric field separately in Figure 4-3 and Figure 4-4 respectively.

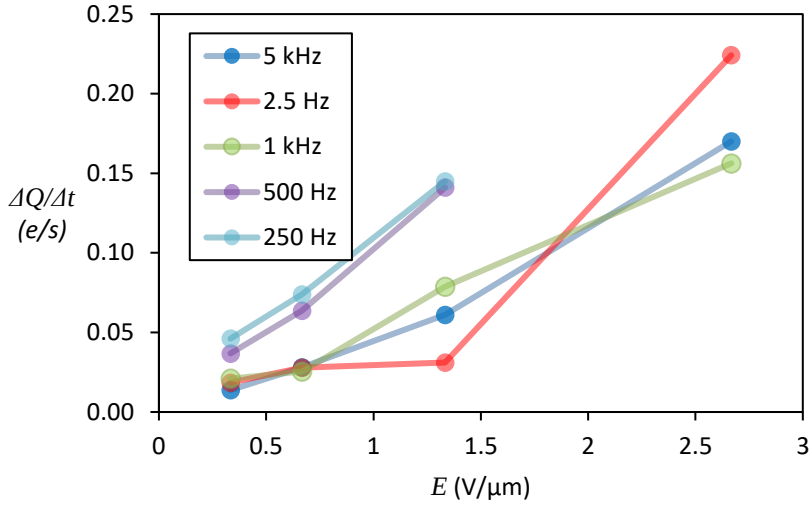

Figure 4-3 Average charging rate of 1 µm PHSA-coated PMMA particles in dodecane as a function of the amplitude of the applied electric field for frequencies f = 250 Hz, 500 Hz, 1 kHz, 2.5 kHz and 5 kHz.

Figure 4-3 shows the charging rate of the 1 µm PHSA-coated PMMA particles in dodecane from Figure 4-2, expressed as a function of the amplitude of the electric field E. Results of measurements at the same electric field frequency are coupled with straight lines. For each of these sets, a roughly linear correlation is observed between the charging rate of the particle and the amplitude of the applied electric field. If the amplitude of the electric field is increased with an order of magnitude, the charging rate is as well. This strongly indicates that the electric field E is a driving factor behind this phenomenon.

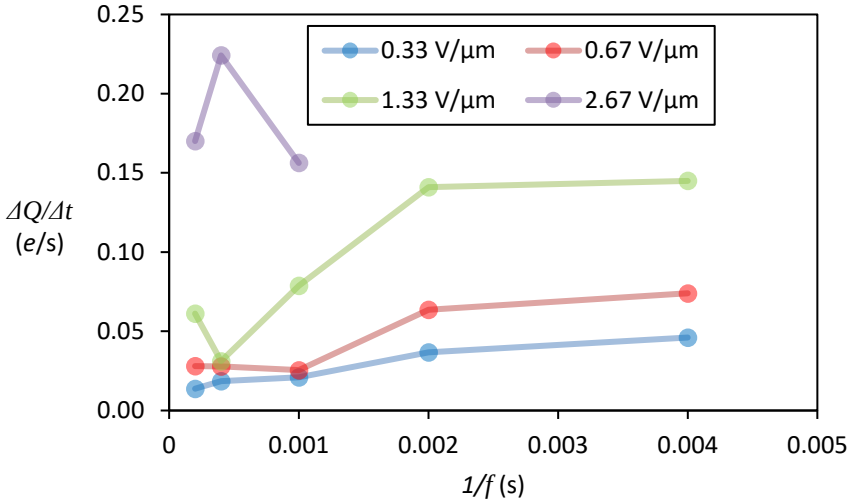

Figure 4-4 Charging rate of 1 µm PHSA-coated PMMA particles in dodecane as a function of the frequency of the applied field for electric field amplitudes E = 0.33 V/µm; 0.67 V/µm, 1.33 V/µm and 2.67 V/µm.

Figure 4-4 shows the charging rate of the 1 µm PHSA-coated PMMA particles in dodecane from Figure 4-2 expressed as a function of the inverse of the frequency of the electric field $1/f$. It appears that the charging rate is larger for smaller frequencies, though the effect on the charging rate is less pronounced with respect to the effect of the amplitude of the electric field.

Additional information can be extracted from the distribution of the times in between consecutive charging events. Figure 4-5 presents a histogram of the time between consecutive elementary charging or discharging events for 1 µm PHSA-coated PMMA particles in dodecane. The histogram shows the combined data for several particles that are probed at E = 0.67 V/µm, with differing frequencies, because no individual measurement has enough data to give an accurate representation of the phenomenon. The influence of the field frequency is neglected. The linear slope in the semi-logarithmic plot reveals that the charging and discharging events follow a Poisson process[90]. This means that consecutive charging events are uncorrelated. The mean time in between charging events is influenced by the total net

charge of the colloidal particle however. This is elaborated upon in the section 4.4.

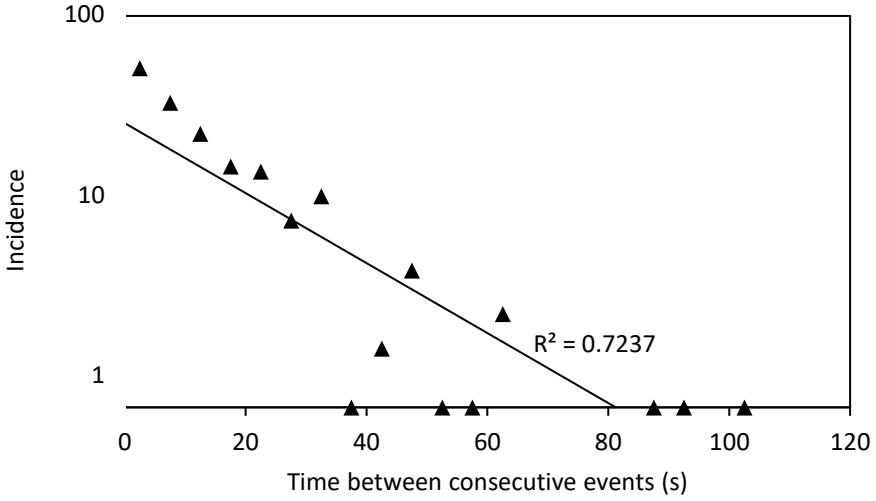

Figure 4-5 Histogram of the time between consecutive (dis)charging events for 1 µm PHSA-coated PMMA particles with E = 1.33 V/µm. Data from measurements with frequencies f = 250 Hz, 500 Hz, 1 kHz, 2.5 kHz and 5 kHz are combined. The time between consecutive events is distributed in bins with a width of 5 s. The logarithmic representation of the incidence as a function of the time between consecutive charging events reveals an exponential relation between these two parameters.

The logarithmic distribution of the incidence of the time between consecutive events shown in Figure 4-5 is fitted to a linear regression. The residual square error (R^2) of the fit is 0.72, indicating that the linear regression is a good approximation to the experimental data.

4.4 Saturation

In order to investigate saturation effects in the charging, I measured the charge of a 1 µm particle in a E = 1.33 V/µm field at f = 5 kHz over an extended period of 3 hours. The result is shown in Figure 4-7.

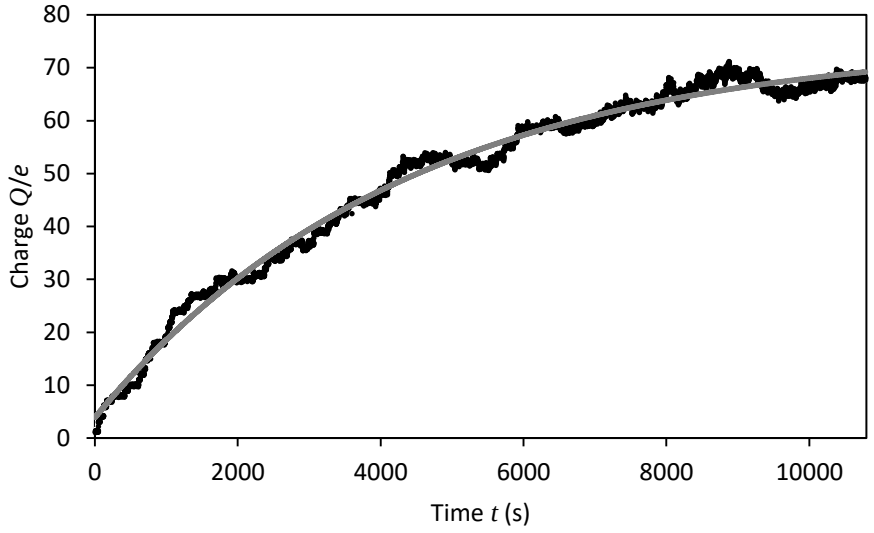

Figure 4-6 (black) The charge evolution of a single PMMA particle over a 3 hour time period with E = 1.33 V/µm and f = 5 kHz. The charging rate slows down as the particle approaches its maximum charge. (grey) Theoretical fit to the experimental data.

From Figure 4-7 it is clear that the charging rate slows down over time. The observations can be explained by a mechanism in which the charging rate is proportional to the amplitude of the electric field, as was observed in Figure 4-3, and proportional with the difference to the final charge. This is expressed by equation 4-1:

$$\frac{dQ(t)}{dt} = \alpha E\left(Q_f - Q(t)\right), \qquad 4\text{-}1$$

where $Q(t)$ is the time dependent charge, α is a proportionality factor, E is the amplitude of the electric field and Q_f is the final charge value. The solution of $Q(t)$ is given in equation 4-2

$$Q(t) = Q_f - \left(Q_f - Q_i\right)\mathrm{e}^{-\alpha E t}, \qquad 4\text{-}2$$

where Q_i is the initial charge value. Fitting the data from Figure 4-6 to equation 4-2 (with E = 1.33 V/µm) yields Q_i = 3.87 *e*, Q_f = 73.2 *e* and α = 1.91*10^{-10} m/Vs, which yields a characteristic time constant $1/\alpha E$ = 3937 s. This fit is included in Figure 4-6.

In this model, the charging rate after 15 minutes is a factor 1.25 lower than the initial charging rate. Hence, for measurements that do not last longer than 15 minutes, the charging rates can be approximated to be constant. The measurements shown in previous sections of this chapter or in the following sections fall in this category.

4.5 Size matters

Figure 4-7 displays the average charging rate of 3 PHSA-coated PMMA particles with a diameter of d_1 = 424 nm at f = 5 kHz and E = 1.33 V/µm plotted together with the data of the particles from Figure 4-2 in section 4.3 that were probed under electric fields from E =0.33 V/µm to E = 2.67 V/µm at f = 5 kHz. On average, the charging rate from these three experiments is $\Delta Q/\Delta t$ = 0.013 *e*/s. This charging rate is 4.3 times smaller than the expected value from the linear fit to the 1 µm sized particles which is $\Delta Q/\Delta t$ = 0.056 *e*/s. The ratio of the surface areas of these particles is *ratio* = d^2/d_1^2 = 5.5, where d = 1 µm. This suggests that the charging rate varies proportionally with the surface area of the colloidal particle rather than for example proportionally with the radius.

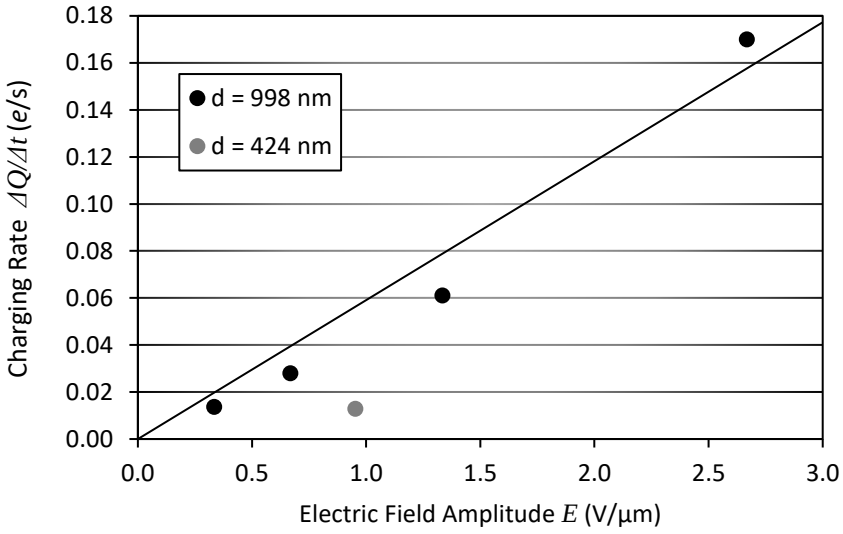

Figure 4-7 Charging rate of 1 µm sized particles (black) as a function of the applied field amplitude at f = 5 kHz, and the mean charging rate of three 424 nm particles (grey) at E = 0.95 V/µm and f = 5 kHz. The charging rate differs by a factor 4.3. This is approximately equal to the ratio of their surface areas, which is 5.5.

Though the data indicates that the charging rate varies proportionally with the particle's surface area, for now, due to the low volume of data points, it can not be concluded definitively to be the case. It is possible to determine this relation with a higher degree of certainty, but this avenue was not pursued any further, because all three possible charging mechanisms are expected to show the same behavior. Therefore, further narrowing down the relation between the particle's size and its charging rate does not offer any additional benefit.

4.6 Voltage switched off

By switching the voltage off for a certain time interval, while maintaining the optical trap, I can study the relaxation of the charge Q/e. Figure 4-8 shows the charge of one particle over time while the voltage is intermittently switched on and off. No charge data can be obtained when the oscillating voltage is switched off. The charge is measured three times for 10 minutes

with an amplitude of E = 1.33 V/µm and f = 2.5 kHz and a DC offset of 1 V (E_{DC} = 0.0133 V/µm). Between the first and the second measurement, the AC and DC voltage is switched off for 10 minutes and between the second and the third measurement, the voltage is switched off for 1 hour. It can be observed that the charge remains constant during the 10 minute waiting period and increases by 1 elementary charge during the one hour waiting period. There is no particle charge value during the off-periods, because an electric field is required to obtain such a value.

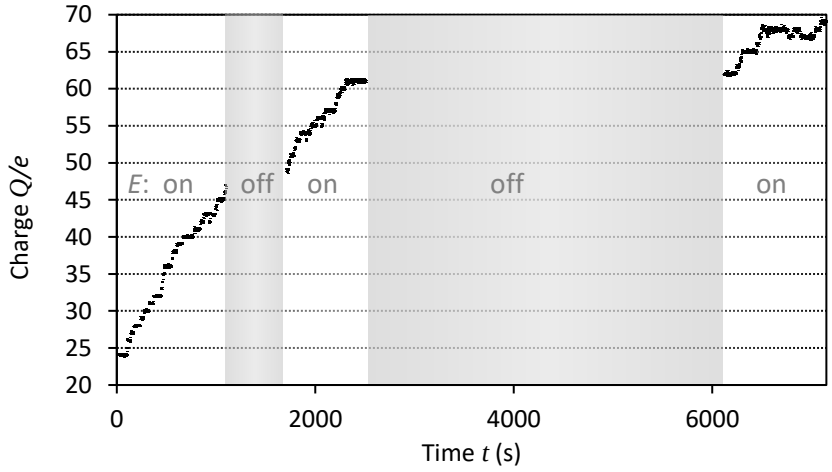

Figure 4-8 The charge evolution of a single PMMA particle over time with the electric field on or off with E = 1.33 V/µm at f = 2.5 kHz and E_{DC} = 0.0133 V/µm. In between measurements, the charge of the particle does not decrease.

4.7 Al_2O_3 coating

Under the influence of a high electric field, an electrode is capable of injecting charge into a dielectric liquid[112]. In order to eliminate charging through injection of charged species at the electrodes, the electrodes are covered with a physical, non-conducting barrier. This is achieved by coating the ITO electrodes with an Al_2O_3 layer of 100 nm. Figure 4-9 displays the charging of a 1 µm sized particle at E = 1.33 V/µm and f = 5 kHz in a device with coated electrodes. It is clear that the charge of the particle is increasing in a similar way (although slower) as without coating. This means that the increase in

positive charge of the particle is not related to injection of charges from the electrodes.

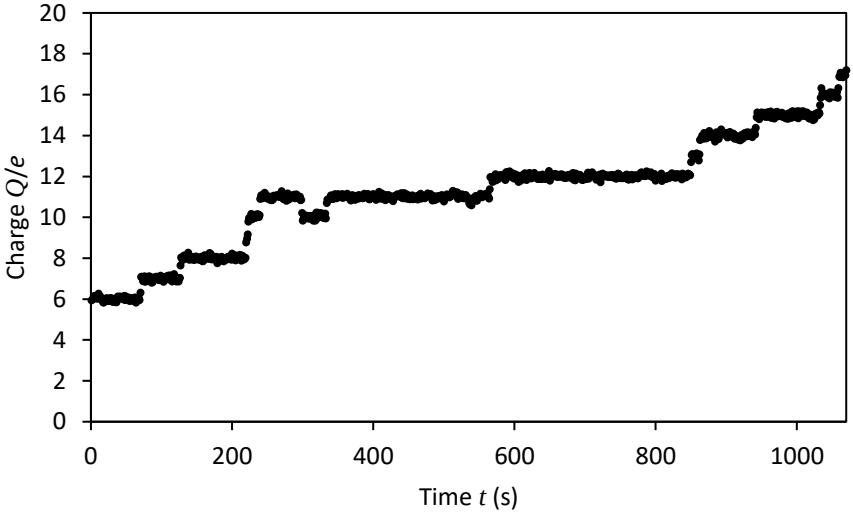

Figure 4-9 The evolution of the normalized charge Q/e of a 1 µm particle at E = 1.33 V/µm and f = 5 kHz in a device with 100 nm Al_2O_3 coating on the electrodes. The charging rate is about 0.01 *e*/s.

4.8 DC-effect

In previous sections, the effect of variations in the amplitude and frequency of the electric field on the charging rate of PHSA-coated PMMA particles in dodecane has been investigated. It was also found that the particles retain their acquired charge level when the electric field is no longer present. Here, I look for the effect that a superimposed DC field exerts on this charging mechanism. To that effect, the measurement sweep from section 4.3 is revisited with a DC voltage of V_{DC} = 1 V over the 75 µm wide channel, which corresponds to a DC electric field of E_{DC} = 0.0133 V/µm. A 1 V DC offset voltage is sufficiently large to deplete the bulk of the microfluidic channel of freely diffusing ions[80]. This has a serious implication to the charging mechanism. For instance, if the charging mechanism would involve the interaction of a surface site with free ionic species from the bulk, the reaction

mechanism is expected to come to a halt when the liquid is depleted from ionic species.

The results of this set of experiments is shown in red in Figure 4-10 and is plotted over the corresponding results from section 4.3 in Figure 4-2, shown in grey.

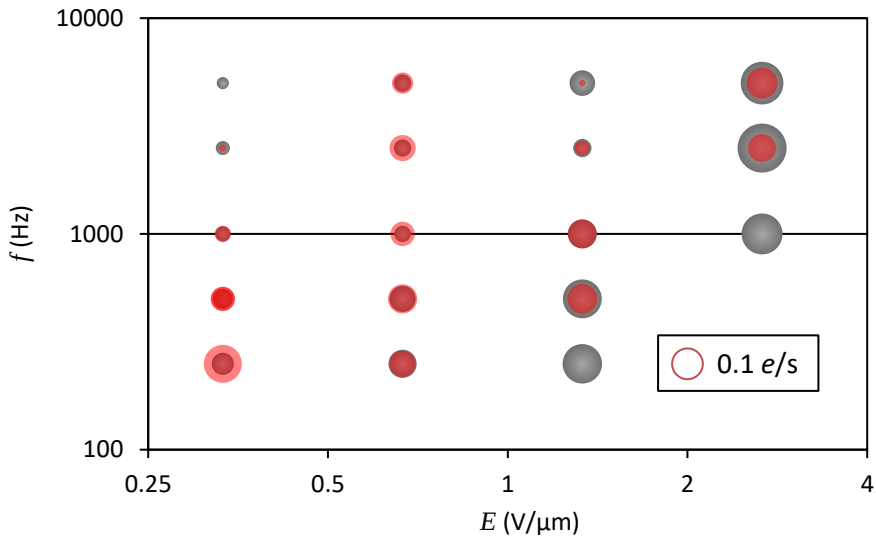

Figure 4-10 Dependence of the charging rate of 1 µm PHSA-coated PMMA particles on the amplitude E and the frequency f of the applied electric field in dodecane with a DC field component E_{DC} = 0.0133 V/µm in red and without DC component E_{DC} = 0 V/µm in grey (behind) from Figure 4-2. The rate is proportional to the disk size. For reference, the red (in front) circle in the caption represents a charging rate of 0.1 *e*/s.

It can be observed that the charging rates of the measurements where a DC voltage is present are approximately equal to the corresponding charging rates of the measurements where no DC voltage was applied. For the DC measurements, the same trends appear to be present in the charging rate with respect to the amplitude and the frequency of the electric field. A single anomaly stands out at frequency f = 5 kHz and amplitude E = 1.33 V/µm, where the charging rates of the 2 sets are off by a factor > 10.

It appears that the application of an offset voltage of 1 V, that depletes the bulk of the liquid from ions, does not significantly alter the governing reaction mechanism. This further demonstrates that the observed electric field-induced charging mechanism does not involve a reaction with freely diffusing ionic species from the bulk.

4.9 Discussion

I have presented experiments that reveal electric field-induced charging of colloidal particles in a nonpolar liquid. The charge of a colloidal particle that is optically trapped and subjected to AC electric fields with amplitudes around E = 1 V/μm and frequencies around f = 1 kHz, gradually increases over time. These experiments give insight in the parameters that drive the mechanism. In this section I will present three mechanisms by which charge can arrive at or leave from the particle. Since the charging events follow a Poisson process the focus is on uncorrelated charging mechanisms. Then, I discuss how well these mechanisms comply with my observations. A schematic representation of the three charge mechanisms is shown in Figure 4-11Figure 4-1.

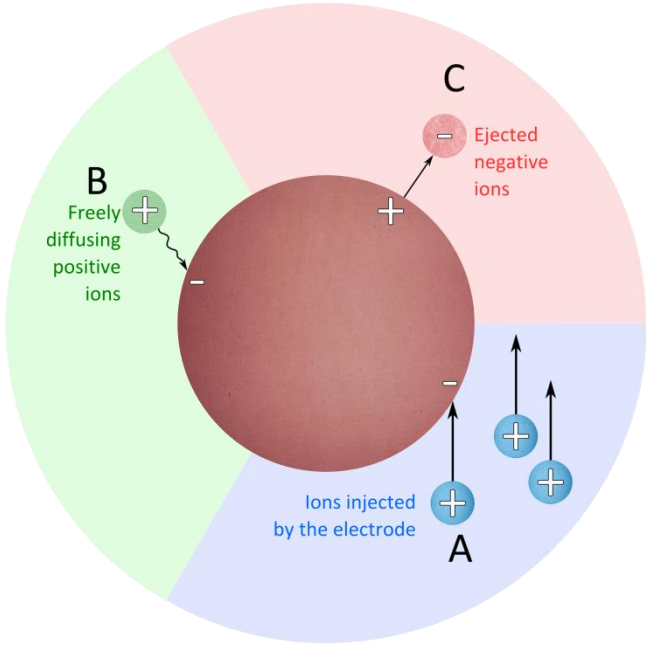

Figure 4-11 Schematic representation of 3 possible charging mechanisms.

When a voltage is applied over two electrodes that are separated by a nonpolar liquid medium, charged ions can be formed at the interface with the electrode and injected into the medium[113]. In mechanism A, positively charged ions that originate from the electrodes collide with the trapped particle. A fraction of these collisions results in bonding with the particle, causing the surface charge to increase over time. Mechanism B assumes that the particle has negatively and positively charged sites on its surface and that freely diffusing positive ions bond with the oppositely charged negative sites, while the positive sites on the particle do not undergo any reaction. Because the reaction neutralizes negative sites, but not positive ones, net positive charge builds up on the particle. In mechanism C, the particle surface contains negatively charged ions that can desorb from the particle under high electric fields (~1 V/µm). When the negative ions leave the particle, the particle's net charge has increased. I expect the applied fields to be insufficiently strong to disrupt covalent or ionic bonds, so the type of bond that holds these negative ions to the surface can be a weak hydrogen bond or electrostatic attraction with a positively charged site on the particle.

In section 4.7, I presented an experiment where the electrodes are covered with an Al_2O_3 coating and observed that, although the rate of the electric field-induced charging was slower for this measurement, it was still present. This indicates that mechanism A can not solely responsible for the induced charging phenomenon.

Mechanism B can also be discarded because the colloidal particles would have started charging before they were introduced into the microfluidic channel and they would have reached their saturation charge before I started measuring. For mechanism B to be eligible, the ions would need to be introduced into the liquid when the mixture enters the microfluidic channel, for instance by trace amounts of ionic molecules on the channel's electrodes. In section 4.6, I observed that charging effectively stops in the absence of an electric field. This can be expected for mechanism C, but not for B. If electric field-induced charging originates from particle interaction with only the positive ions from the bulk as in mechanism B, then the phenomenon is not expected to require an AC electric field to drive it, because an AC field does not steer positive ions towards negative surface sites. This means that under mechanism B, I do not expect a dependency on the amplitude or the frequency of the AC electric field and I do expect the mechanism to carry on when the voltage is switched off. This in direct contrast with my observations, where I have demonstrated a strong correlation between the charging rate and the amplitude of the electric field and no induced charging when the voltage is switched off. Mechanism B is further disqualified by the measurement results from section 4.8 where it was observed that the charging rate is not significantly influenced by a DC electric field that is sufficiently strong to deplete the bulk of the liquid from charged ionic species. Since the reaction rate continues unperturbed in the absence of ionic species, mechanism B can be confidently rejected.

Mechanism C can account for all observations from the presented experiments. If the particle charging originates from negative ions that are stripped away from the particle by high electric fields, then the charge should remain stable when the field is not present as was observed. Moreover, a higher electric field amplitude means that the negative ions are pulled by a

stronger electric force. Therefore, a higher field amplitude should induce a higher charging rate, as is observed. Furthermore, if it is assumed that the number of negative ions that are involved in this mechanism is constant per unit area, then the charging rate has to scale quadratically with the radius of the particle, which is in agreement with the results of section 4.5.

By conducting a measurement over a 3 hour time period, I was able to show that the induced charging phenomenon is in the end a self-limiting reaction. This observation was to be expected for any mechanism. For mechanism C in particular, the implication is that it becomes increasingly harder for negative ions to escape the inward electrostatic pull of the particle as its positive charge increases. This effect is in good agreement with a theoretical fit, based on the assumption that the charging rate is proportional to the difference between the actual charge and the charge that is finally obtained.

Because an electric field dependent dissociation mechanism (mechanism C) can adequately explain all observations, this prompts a new question: What is the chemical structure of the ejected ion? For now, I can not definitively identify the ion. Trace amounts of water offer one plausible origin of the charge[114, 115], as for the samples in the current study no additional drying steps have been implemented. Charging of particles can also be caused by the presence of unreacted monomer[116] or cleaving of functional groups such as the PHSA tails.

4.10 Conclusions

When applying OTE to PHSA-coated PMMA microparticles in pure dodecane, I came across unanticipated charging behavior. I observed that the charge of the particles increased slowly over time. I conducted a series of experiments to test the influence of several measurement parameters: the amplitude and frequency of an applied AC field, the presence of a DC field, the size dependency of the charging rate, the effect of a dielectric coating on the electrodes and the saturation effect. This ensemble of measurements has led me to conclude that this electric field-induced charging phenomenon is best explained by an electro-activated surface dissolution mechanism.

Chapter 5.

Surfactants & Particle Charging

5.1 Introduction

In Chapter 4, I comprehensively studied the charging behavior of PHSA-coated PMMA particles in dodecane and through an ensemble of experiments I was able to provide insight into the charging mechanism. In this chapter, I study how the charging behavior of these particles changes when surfactant is introduced. The influence of added surfactant on the dynamic charging of PMMA particles is investigated with precision higher than the elementary charge. This represents the first time that charge measurements are carried out in surfactant-enriched nonpolar liquids with a charge resolution smaller than a single elementary charge. Since colloidal particles in nonpolar liquids are seldom used without surfactants, this signifies an important step forward in the pursuit of fully understanding charging behavior of colloidal particles in general and for optical trapping electrophoresis in particular.

I study the charging of single PMMA particles in dodecane for different concentrations of the commercial surfactant OLOA 11000. The studied concentrations span from 0.001 wt% to 0.05 wt%, which encompasses the CMC which lies around 0.005 wt%[81]. The charging behavior above and below this concentration is observed to be distinctly different. Also, I present particle charge measurements that are carried out both in the absence and in the presence of a small DC offset to the applied electric field (V_{DC} = 1 V, E_{DC} = 0.0133 V/µm). The application of a small DC voltage offset expands the range of concentrations at which the charge of a particle can be measured with elementary charge resolution.

The experimental results are divided in four separate subsections. First, charge measurements in solutions close to the CMC with DC offset are discussed. These measurements show a particle charge that fluctuates around a mean charge value. Second, I present the charge measurement of a particle in a solution below the CMC, first with and then without DC electric field. Here, the particle's charge is not stable and positive charge accumulates on the particle over time, in a similar way as discussed in Chapter 4. In the third section, the influence of the DC offset is discussed. In

the fourth subsection, trends in the charging behavior of colloidal particles with 1 V DC offset as a function of the surfactant concentration are analyzed.

Some of the observations that are presented in this chapter are not in line with earlier publications, such as the papers by Strubbe et al.[17] and Beunis et al.[90]. Therefore, before I can delve into the experimental results, I have to address some key differences between these experiments and the earlier ones.

5.2 Particle charge fluctuations close to the CMC with DC offset

Figure 5-1 displays the variation of the charge of a single particle over time in a mixture of 0.0046 wt% OLOA in dodecane which is near the CMC. The applied electric field has an amplitude of E = 1.33 V/µm and a frequency of f = 5 kHz and a DC offset of E_{DC} = 0.0133 V/µm. The charge histogram reveals the discrete nature of the charge and that there is an approximately normal distribution around an average value of -12 e.

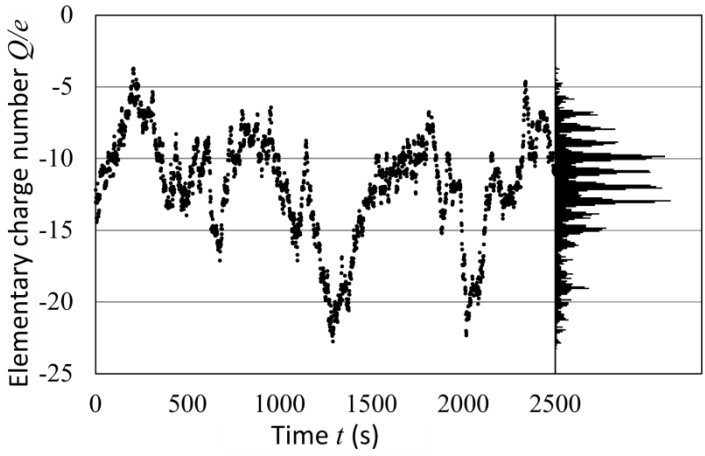

Figure 5-1 (left) Time evolution of the normalized charge Q/e for a single PMMA particle in dodecane with 0.0046 wt% OLOA 11000 during 2500 s (one charge measurement per second). The charge fluctuates around the average value of -12 *e*. (right) Charge histogram from 2500 values, 10 intervals per unit charge, showing the discrete nature of the particle charge.

To determine the number of charging events, the normalized charge Q/e is rounded to the nearest integer value. When two consecutive integer values are not equal, this represents a charging event. The time sequence of Figure 5-1 contains 499 charging (or discharging) events which are defined with an accuracy of 1 s, the time interval for each charge measurement. Charging events much faster than 1 s can be ruled out if there is a clear local minimum corresponding to the elementary charge detected in R^2-function.

The average time in between consecutive charging events in Figure 5-1 is 5.01 s. Figure 5-2 displays the histogram of the time between consecutive charging events for the time sequence in Figure 5-1. The linear slope in the semi-logarithmic plot (inset) reveals that the charging and discharging events follow a Poisson distribution (similar as observed in [90]). This signifies that consecutive charging events are uncorrelated.

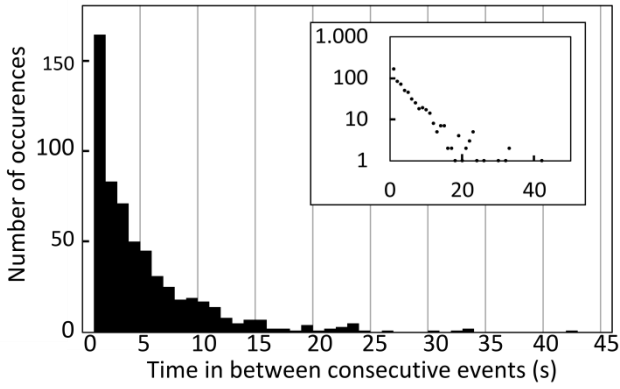

Figure 5-2 Histogram of the 499 time intervals in between consecutive charging events of a 1 µm PMMA particle in dodecane with 0.0046 wt% OLOA 11000 during 2500 s (corresponding to Figure 5-1). The average value is 5.01 s. Inset: the histogram shown in a semi-logarithmic diagram.

5.3 Particle charging below the CMC with DC offset

For surfactant concentrations below 0.003 wt%, the charging mechanism is different than for concentrations around the CMC (0.005 wt%) shown in the previous section. A representative measurement at 0.0015 wt% is shown in

Figure 5-3. It is evident that the charge does not fluctuate around a mean value. Instead, the charge steadily increases over time (in Figure 5-3 there is only one exception around 400 s), similar as reported in Chapter 4. It is also apparent that the charging frequency is lower: there are only 28 events over 1600 s, yielding an average time in between consecutive charging events of 57 s.

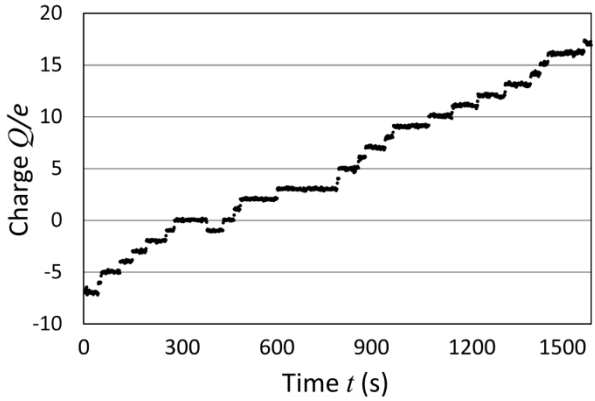

Figure 5-3 Time evolution of the charge of a d = 1 μm PMMA particle dispersed in dodecane with 0.0015 wt% of OLOA 11000 with E = 1.33 V/μm at f = 5 kHz and E_{DC} = 1 V DC offset. The particle charge increases at about 1 elementary charge per 57 s.

A similar behavior is observed for all measurements with OLOA concentrations well below the CMC. The charge becomes more positive and the mean time between events is larger than 10 s.

5.4 Particle charging without DC offset

The variation of the charge of PMMA particles in different surfactant concentrations has also been investigated in the absence of an electric DC offset. For concentrations below 0.003 wt% OLOA 11000 in dodecane, the presence of a DC offset has no significant influence on the charging dynamics. In Figure 5-4, the particle charge is shown in function of time over a 600 s interval for a mixture with 0.0015 wt% OLOA 11000 in dodecane, without DC offset. The particle charge increases monotonously (as in Figure 5-3) and the mean time between events is more than 10 s.

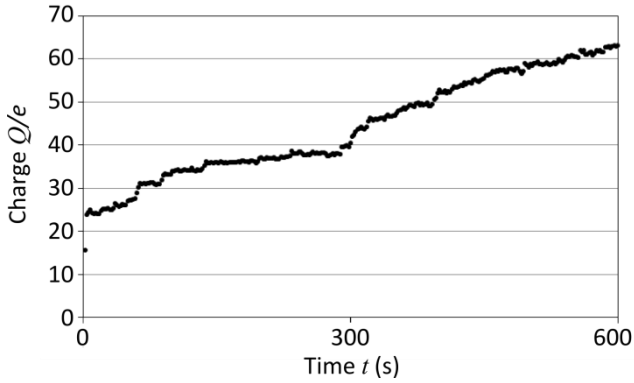

Figure 5-4 Time evolution of the charge of a PMMA particle dispersed in dodecane with 0.0015 wt% of OLOA 11000 with E = 1.33 V/µm at f = 5 kHz and E_{DC} = 0 V DC offset.

When the surfactant concentration is increased to 0.003 wt%, the DC component has an important effect on the charging behavior. To illustrate this, the charge of the same particle is measured over 600 s for different DC values in Figure 5-5, starting with 0 V/µm and increasing stepwise by 0.25 V/µm. In between the measurements, the particle is kept trapped while short-circuiting the electrodes during 600 s in order to let it return approximately to the same initial charge value.

Note that the system already displays markedly different behavior at a surfactant concentration of wt% 0.0015 than is the case in pure dodecane (no surfactant). While the particle still undergoes electric field-induced charging at a similar rate, the charge now returns to approximately the same initial value in the absence of an electric field. This demonstrates the involvement of surfactant in the particle's discharging mechanism.

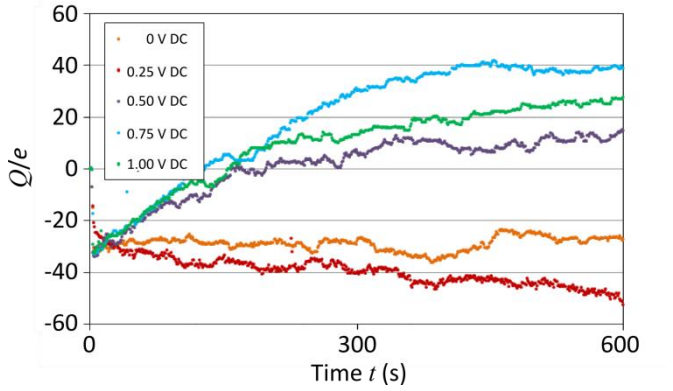

Figure 5-5 The charge of a PMMA particle in dodecane with 0.003 wt% OLOA 11000 with E = 100 V at f = 5 kHz. The particle charge is measured for 5 different values of the DC offset from 0 V DC up to 1 V DC over 75 µm (This corresponds to electric fields from 0 V/µm DC to 0.0133 V/µm DC). All measurements are performed on the same particle. The elementary charge resolution is not obtained for measurements with E_{DC} < 0.0067 V/µm (V_{DC} = 0.5 V). For these measurements, the mean value of the correction factor from the other measurements with E_{DC} ≥ 0.0067 V/µm (V_{DC} = 0.5 V) is used in this graph. Note that for the first data points some measurements show anomalous behavior. This is because the voltage amplifier is switched on manually after several seconds.

Two different charging behaviors can be observed. When the applied DC field is below E_{DC} < 0.0067 V/µm (V_{DC} < 0.5 V), The charge Q fluctuates around a mean (negative) charge. A similar behavior was observed for measurements where a DC voltage was applied, at slightly higher surfactant concentrations as shown in Figure 5-1. When the DC electric field is increased to E_{DC} = 0.0067 V/µm (V_{DC} = 0.5 V) or higher, the charge increases over time.

Another important distinction between E_{DC} < 0.0067 V/µm (< V_{DC} = 0.5 V) and E_{DC} ≥ 0.0067 V/µm (≥ V_{DC} = 0.5 V) is that for small DC voltages the particle charge can no longer be observed with elementary charge resolution because the charge data is noisier. By applying a DC field, I can extend the surfactant concentration range in which single elementary charging events can be detected.

5.5 Influence of surfactant

Despite the difference in charging behavior below and above the CMC, some trends are visible over the entire concentration range. Figure 5-6 shows charge measurements for 12 different surfactant concentrations, with the size of each dot being proportional with the fraction of time that the particle carried the indicated charge. For all measurements a DC offset of V_{DC} = 1 V is applied (E_{DC} = 0.0133 V/µm). Below the CMC (red vertical line) the final charge (red dot) is typically higher than the initial charge (blue dot), which corresponds to measurements where the charge increases monotonously. Above the CMC, the charge fluctuates around an average value. It is therefore speculated that the presence of inverse micelles can stabilize the charging and discharging processes.

For surfactant concentrations above the CMC, the time evolution is entirely different and the charge distribution obtain a Gaussian-like shape. Charges are mostly negative and there does not seem to be a correlation between the mean charge and the concentration of surfactant.

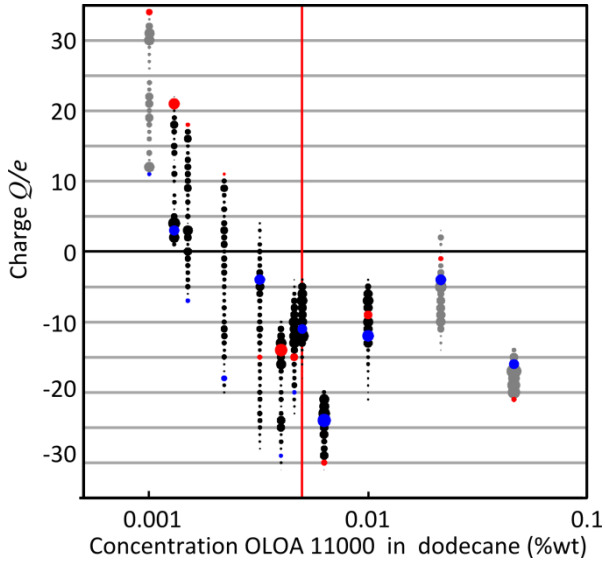

Figure 5-6 Variation of the particle charge with time for different concentrations of the surfactant OLOA 11000, all measured with V_{DC} = 1 V DC offset (E_{DC} = 0.0133 V/µm). The

blue and red dot correspond to the initial and final value of the particle charge. The area of each dot is proportional to the relative fraction of the time that the particle carried the indicated charge in that measurement. The red vertical line at 0.005 wt% indicates the CMC. For the measurements with black dots, the AC electric field has a E = 1.33 V/μm amplitude at 5 kHz and for measurements with grey dots the AC electric field is E = 2 V/μm at 2 kHz.

Inverse micelles are known to play an important role in charge stabilization[59, 117]. It is also well known that the addition of surfactant increases the concentration of charged and uncharged inverse micelles in nonpolar solvents[10, 118]. Therefore, if the particle charging is related to interactions with charged or uncharged inverse micelles, one can expect that the increase of surfactant concentration should be accompanied with a decrease in the average time in between consecutive charging events. This is indeed observed in Figure 5-7. The average time interval between successive charging events drops by an order of magnitude when the concentration is increased from the lowest to the highest concentration. Note that at surfactant concentrations below the CMC, it is possible that the charging and discharging events are mediated by pre-micellar aggregates.

The charge is calculated once every second, which means that charging time intervals shorter than 1 s (which may be present at higher concentrations) cannot be detected. Once the concentration of surfactant exceeds the CMC, the charging frequency appears to plateau, though the volume of data is not sufficiently large to support this conclusion.

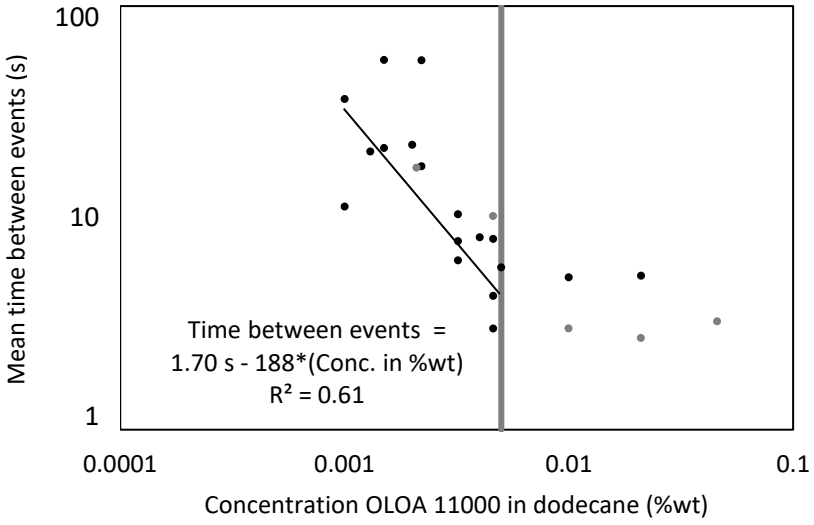

Figure 5-7 Mean time between consecutive charging events as a function of the weight fraction of surfactant, measured while applying a V_{DC} = 1 V DC offset (E_{DC} = 0.0133 V/µm). The vertical line at 0.005 wt% indicates the value of the CMC. For black dots, the applied electric field is E = 1.33 V/µm at 5 kHz and E = 2 V/µm at 2 kHz for the grey dots.

A linear regression is fit to the data points on the mean time between consecutive events corresponding to concentrations of OLOA 11000 in dodecane below the critical micelle concentration at 0.005 wt%. The data corresponding to higher surfactant concentrations is not taken into account for multiple reasons. Firstly, because these concentrations lie above the CMC and therefore it is not unreasonable to expect a change in the charging behavior. Secondly, due to the low number of data points. And thirdly, as explained earlier, because the mean time between consecutive events lies close to the charge calculation frequency. The linear regression has a negative slope of 188*(concentration in wt%) and has an R^2 value of 0.61, which indicates that an increase in the surfactant concentration is strongly correlated to an increase the charging frequency.

5.6 Discussion

Before delving into the physical implications of the presented experiments, it is useful to note that there are some important distinctions to make with respect to previous experimental work. With respect to the earlier work from Strubbe [17] there are two important differences. First, the particles that were investigated in this paper were freely diffusing, hence the experiments were much shorter, and it was harder to detect whether the particles undergo certain charging effects. Second, the particles in [17] are silica particles. The different chemical composition may cause particles to behave differently. The differences with the work of Beunis [90] lie mainly in the fabrication method of the microfluidic cell. In this work, the cell consists of two ITO-covered glass plates that have been cleaned in a cleanroom with DI-water, RBS, acetone, isopropanol and again with DI-water. On the other hand, in the double folded aluminum foil strips that serve as electrodes in [90] the device could not be cleaned this way. Because the aim is to work in pure dodecane, not being able to clean the devices is a likely source of contamination. It appears that the results from [90] are similar to the results that I present for high concentrations of surfactant, solidifying this assumption. In [92], prof. Roberts et al. also measure the charge of single PMMA particles with optical trapping electrophoresis in pure dodecane. They do not report on the charge evolution of these particles over long time intervals, but note that the distribution of the initial charge value is very small ($|E| \leq 20e$) and is on average slightly negative. Here too, the initial charge value is small, though the mean initial charge is slightly positive.

The experiments in this chapter lead me to conclude that the charging behavior of PMMA particles is different below and above the CMC, and the presence of a DC electric field has an influence on the charging behavior. First I discuss the charging behavior of particles below the CMC.

The charging behavior of PMMA particles in dodecane with surfactant concentrations lower than 0.003 wt%, below the CMC of 0.005 wt%, exhibits a clear trend (see Figure 5-3 and Figure 5-4). During application of an AC field, the charge on the particle becomes more positive. When a DC voltage of V_{DC}

= 1 V (E_{DC} = 0.0133 V/µm) is applied across the electrodes, the bulk is completely depleted of ionic particles such as charged premicellar aggregates, just as is observed in the case of charged inverse micelles[119]. Under these conditions, a similar increase of the particle charge is observed as in the case without DC electric field. This observation of a similar charging with or without DC electric field disfavors a charging mechanism in which a PMMA particle adsorbs positively charged ions preferentially from its environment, since in the presence of a DC electric field the concentration of positive charges near the particle is considerably lower than without DC electric field. Instead, supported by measurements without surfactant showing similar charging behavior (not shown), it rather suggests that a PMMA particle sheds negative charges over time (see Figure 5-8 a) due to the large AC electrical fields in the order of MVm^{-1}. Such a field-induced, non-equilibrium charging process does not involve surfactant molecules.

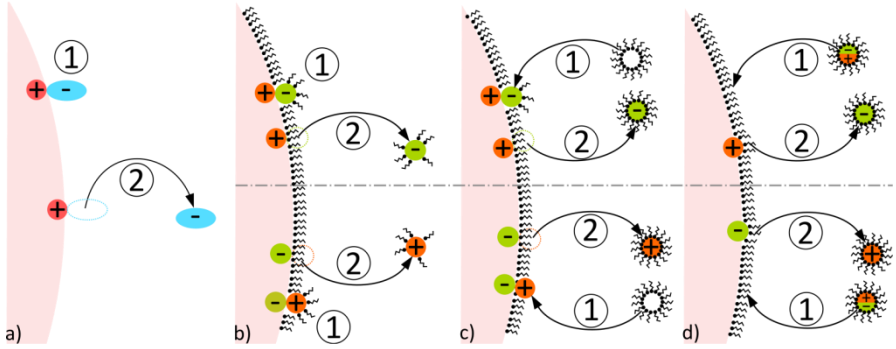

Figure 5-8 Charging mechanisms. a) In a field-induced charging mechanism, negatively charged surface groups are stripped from the particle. b) Surfactant molecules facilitate surface charging and discharging and form premicellar aggregates containing ionic molecules. c) and d) Neutral inverse micelles charge or discharge the particle by either supplying or removing ionic molecules.

The increase of surfactant concentration from 0.001 wt% to 0.003 wt% results in a decrease in the mean time between elementary (dis)charging events for particles that are monitored under E = 1.33 V/µm AC field with a V_{DC} = 1 V DC offset (E_{DC} = 0.0133 V/µm). The higher frequency of charging and discharging events for higher surfactant concentrations reveals that

there is a second mechanism that involves surfactant molecules, shown in Figure 5-8 b. Here, positively (top) or negatively (bottom) charged species stabilized by surfactant molecules are removed from the particle in the presence of a field. Note that it in case of a zwitterionic surfactant, it is possible that a dissociated ion from a surfactant molecule is adsorbed to the particle's surface with the oppositely charged surfactant ion being stabilized in the bulk of the liquid by inverse micelles. The inverse process in which stabilized charges are adsorbed onto the particle surface is ignored here, because the bulk concentration of such free charges is extremely low. Therefore, the proposed charging below the CMC is a combination of field-induced stripping of negative charge and surfactant-mediated removal of charge. The surfactant concentration also has an effect on the initial charge of the colloidal particle (see Figure 5-6). For very low surfactant concentrations, the initial charge is positive (~10 *e*). For concentrations above 0.002 wt% OLOA 11000 in dodecane, the initial charge is negative (~-10 *e*).

The application of a DC offset decreases the noise in the charge data. In the measurements shown in Figure 5-5, the standard deviation of the normalized charge data around integer values increases when the DC voltage decreases from σ_{1V} = 0.16 *e* for V_{DC} = 1 V (E_{DC} = 0.0133 V/µm) to $\sigma_{0.5V}$ = 0.43 *e* for V_{DC} = 0.5 V (E_{DC} = 0.0067 V/µm). Because both measurements are performed on the same particle with identical laser alignment, the increase in the standard deviation can be solely attributed to the decrease in DC electric field. I assume that the noise in the motion of the PMMA particle is related to the (variable) interaction with a small number of charged molecules or charged premicellar aggregates below the CMC and by charged inverse micelles above the CMC. This interaction leads to the well-known retardation effect when a large number of charges are present. It has been shown that by applying a DC offset voltage, charges can be stripped off from the double layer around a particle, leading to a reduction of the retardation force[120]. In the limit of low particle charges the interaction between a particle and a low number of countercharges can lead to fluctuations in its motion. By applying a DC offset, practically all charges move to the neighborhood of the

the electrode with opposite polarity and less charges are present near the PMMA particle, such that the noise in the charge measurement reduces. The range of surfactant concentrations where the particle's charge can be measured with unitary resolution is then extended from about 0.004 wt% to 0.05 wt%, which is one order of magnitude above the CMC.

Charge measurements of particles in solvents with surfactant concentrations larger than 0.003 wt% do not show an increase of charge. Instead, the particle charge fluctuates around a mean charge value and the charging/discharging events are more frequent than at lower concentrations. At these surfactant concentrations inverse micelles are present in the bulk liquid. Due to the DC offset, the bulk is depleted of charged inverse micelles and the concentration of newly generated charges negligible[80]. This introduces two additional mechanisms through which surfactant can contribute to particle charging and discharging by supplying as well as removing ionic species from the particle surface, as shown in Figure 5-8 c and d. Here, charge-regulation could play an important role. In thermodynamic equilibrium the particle charge will then fluctuate around an equilibrium value. If the particle charge deviates from the average value, electrostatic interaction will favor those processes of charging leading towards the average value. Therefore, even if the mechanisms from Figure 5-8 a and b are still occurring, the dominant effect would likely be the charge stabilization due to inverse micelles of Figure 5-8 c and d. From the exponential shape of the histogram of times in between consecutive charging events, it is clear that the charging/discharging is a Poisson process, indicating that successive charging events are uncorrelated.

In summary, three mechanisms have been proposed to explain charging below and above the CMC: the field-induced stripping of negative charges from the PMMA particle when an AC electric field is applied, surfactant-mediated charge desorption and charging mediated by inverse micelles.

5.7 Conclusions

I demonstrated for the first time that OTE can be used to detect single, elementary charging events on colloidal particles in nonpolar liquids with

surfactants present. I showed that an increase in the surfactant concentration leads to changes in the probabilities of different charging mechanisms, when compared to particle charging in a surfactant-free medium.

It could be observed that the charging and discharging rate of PHSA-coated PMMA particles increases by an order of magnitude for surfactant concentrations of OLOA ranging from 0.001 wt% to 0.005 wt% under electric fields of ~1.33 V/µm at 5 kHz and 0.01 V/µm DC, as shown in Figure 5-7. Around that surfactant concentration and under the same conditions, the charge of the particle stabilizes and fluctuates around a negative mean value (Figure 5-6).

The presence of a DC field has a pronounced effect on both the charging mechanism and on the detection of elementary events. This is evidenced by Figure 5-3 and Figure 5-4. In case no DC field is applied I could not attain single event detection with OTE at these surfactant concentrations, but I did observe that the charge stabilizes at lower concentrations than is the case when a DC field is applied (Figure 5-5). This gives a clue that charged species, possibly charged inverse micelles, play an important role in the charging mechanism.

Chapter 6.

Conclusions & Future Prospects

In this concluding chapter I emphasize the innovations that I implemented and how they contributed to the technique or to the scientific community. I also give an outlook on the next stage in optical trapping electrophoresis. For that reason, this chapter is split into two parts.

In the first part, I provide a summary of the important innovations that have been introduced to optical trapping electrophoresis with respect to previous iterations of the technique and their significance, as well the expansions to the analysis method. Then, I will frame the significance of the experimental results in the wider context of current scientific research.

The second part of this chapter aims to give an outlook on what lies ahead for optical trapping electrophoresis as a technique. I propose a novel analysis method that is only applicable to particle charge data measured with a charge resolution smaller than a single elementary charge, and I propose an experiment that would use optical trapping electrophoresis.

6.1 Optical trapping electrophoresis

In this work, several important innovations have been implemented in the technique of optical trapping electrophoresis. These have been mentioned in previous chapters, though they were not explicitly labeled as such. Here I provide an overview of these innovations together with guiding comments as to why they present improvements in my view.

6.1.1 Fabrication process and design of the microfluidic cell

This dissertation builds on previous work by *Beunis* et al. [90]. The electrodes in that work consisted of two folded strips of aluminum foil and the glass plates that sealed the cell were glued around it. The fabrication did not take place under cleanroom conditions.

Here, I use ITO covered glass plates that are glued together with UV curing glue that contains spherical spacer balls of known diameter, a process that is routinely used for creating single pixel cells for liquid crystals[121]. This fabrication method offers several advantages:

- The ITO covered glass plates can be cleaned following a standard procedure[121].
- The thickness of the cell can be chosen by the size of the spacer balls.
- The electric field is uniform across the entire cell.
- Because the electric field is perpendicular to the cell walls, there is no build-up of electro-osmotic flow.

The last point is a significant benefit for measurements in surfactant-enriched systems where strong electro-osmotic flow can be superimposed on the particle's motion.

This design has another consequence that sets this work apart from previous iterations of optical trapping electrophoresis[45, 90, 92, 106]. Here, the direction of the electric field is along the propagation direction of the trapping beam. Because I use the trapping beam for detection as well, in contrast to *Beunis* et al. [90], the challenging alignment that requires the focus of the detection beam to coincide with the focus of the trapping beam is bypassed.

6.1.2 Alignment method

The development of a proper alignment procedure may be easily overlooked. It is nonetheless a crucial aspect in constructing an experimental setup that can achieve a charge resolution smaller than a single elementary charge. While it is evident that the laser should be properly aligned to reach optimal and reproducible measurement conditions, it is not immediately obvious how this is achieved.

In this work I have developed an alignment procedure to be followed prior to every experiment. I state from my observations that two factors are of paramount importance in the alignment procedure. First, that the back focal plane of the condenser lens and the front focal plane of the 100 X objective coincide perfectly. Second, that it is more important to reduce cross-correlation between QPD voltages $\left(V_z, V_x\right)$ and $\left(V_z, V_y\right)$ than to have the laser beam impinge exactly on the center of the QPD.

6.1.3 Analysis procedure

The analysis method is strongly based on past research, from the analysis of particle motion in an optical trap[122], to the R^2-method[17, 90]. This analysis method is explored further here. I show how the time evolution of a flattened R^2-function can be used to find the accurate local minimum. The algorithm to determine the appropriate correction factor is developed in this work. Through local analysis of the behavior of the R^2-function around this minimum, extra insight is provided while also justifying the procedure of finding that minimum.

6.1.4 Electric field-induced charging

Experiments on colloidal PMMA particles in dodecane resulted in a qualitatively different behavior than the previous study[90]. This could be explained by the difference in fabrication method that is applied. The effect was not reported by *Roberts* et al. [92] who performed similar measurements, though they do report similar initial conditions of the PMMA particles.

I demonstrate how optical trapping electrophoresis can be used to study charging phenomena by testing the influence on a number of varying measurement conditions:

- the amplitude and the frequency of the electric field
- the presence of a DC field
- particle size
- relaxation when the voltage is switched off
- saturation effect after long time interval
- covering the electrodes with a dielectric coating

By looking at combinations of these factors, I was able to gain insight in this previously unreported charging phenomenon which I dubbed electric field-induced charging[123]. The ensemble of experimental results led me to conclude that the electric field-induced charging effect is likely an electro-activated surface dissolution mechanism. Because a number of experiments

were carried out in the absence of surfactants, I was able to conclude that surfactants are not essential for this charging phenomenon.

6.1.5 Single charging events in a surfactant-enriched liquid

By virtue of the improved method, I was able, for the first time, to resolve single elementary charging and discharging events for colloidal particles below and above the critical micelle concentration (CMC)[124].

I demonstrated that even below the CMC, the surfactant plays an important role in the charging behavior. When the surfactant concentration approaches the CMC, the initial particle charge switches polarity. Around the CMC, the charge is stabilized and the electric field-induced charging effect is no longer the dominant mechanism. Because these measurements were executed in the presence of a DC electric field, this proves that neutral inverse micelles do play a role in the charging mechanism.

6.2 Future prospects

In this section, I want to provide a possible roadmap for the future of OTE. The selected list of suggestions are important examples of how this can be achieved, but do not comprise an exhaustive list. I comment on how OTE can be improved, what new experiments can be carried out and suggest a new analysis method for elementary charging and discharging data.

6.2.1 Increase of the unitary measurement range

Perhaps the most obvious future work is to increase the concentration range of surfactant in which OTE can still detect single charging and discharging events on colloidal particles, both in the presence and in the absence of a DC electric field. This could be achieved in several ways.

One possibility is to retreat from the approximation in which the trapping force is assumed perfectly linear and instead completely characterize the trap.

Another route is to work with optical traps that have stronger trapping forces. Since there exists a reciprocity between the detection resolution and the stiffness of the trap κ [125], stronger beams go hand in hand with higher

detection resolution. This can be accomplished with more power, but also through the use of non-Gaussian beams[125].

6.2.2 Acid-base versus preferential adsorption

Acid-base reactions and preferential adsorption of charged inverse micelles are commonly used to explain the charging behavior of colloidal particles in nonpolar media even though it is not always possible to pin down which mechanism is the dominant one. OTE has the potential to create a litmus test to distinguish between these two mechanisms.

An important difference between these two mechanisms is that acid-base reactions rely solely on neutral inverse micelles that become charged after taking up an ionic molecule from the particle's surface which they then carry away from the particle, whereas preferential adsorption consists of the adsorption of charged species delivered by charged inverse micelles. Therefore, the charging rate of preferential adsorption should come to a halt when a DC voltage is applied that depletes the bulk of charged inverse micelles and acid-base reactions should carry on (ideally unperturbed).

Here, I propose a new experiment with OTE that has the potential to offer direct insight into the active charging mechanisms by which a surfactant can charge a colloidal particle and where it is not required to resolve elementary events to do so. First, I will explain how I propose to conduct the experiment and then how the results can be interpreted.

The experiment requires a microfluidic device with three channels: one channel with pure dodecane and particles, a middle channel with pure dodecane and one channel with dodecane mixed with surfactant. Each of the three channels has flow that is sufficiently strong to prevent strong mixing of their respective contents. The experiment consists of three main steps:

1. A particle is trapped and brought over to the middle channel. The middle channel without particles prevents other, untrapped colloidal particles from entering the optical trap and prematurely stopping the experiment.

2. An electric field is applied with an AC component so the particle's charge Q_1 can be measured with OTE and a DC component that is sufficiently strong so that the bulk of the surfactant-enriched flow channel is depleted from ionic species. The particle is brought over to the surfactant-enriched flow channel with the DC field still present. (Charge measurements during movement will likely be unreliable.)
3. Wait for several minutes (until the particle's charge has entered a new dynamic equilibrium).
4. Measure the charge Q_2 of the particle through OTE.
5. Release the particle and trap a different particle to repeat the experiment without a DC field. This results in particle charges Q_3 and Q_4.

A schematic representation of the flow cell is shown in Figure 6-1.

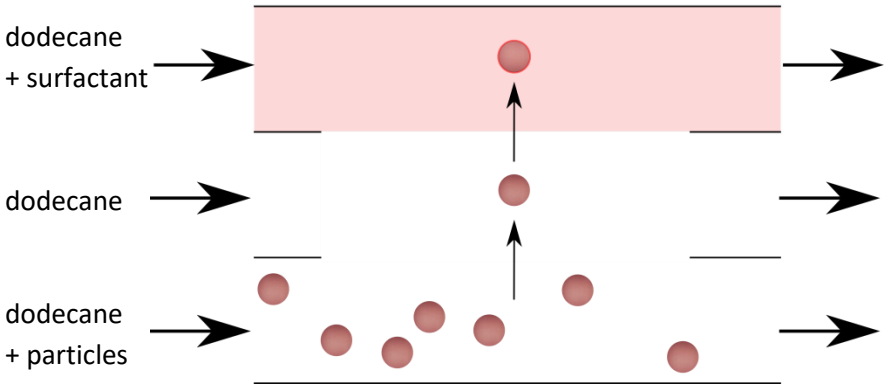

Figure 6-1 Schematic representation of a flow cell with three microfluidic channels. The bottom channel contains dodecane mixed with colloidal particles, the middle channel contains dodecane and the top channel contains dodecane with surfactant. The top and bottom substrates are coated with ITO so that an electric field can be applied. In this experiment: ① A particle is trapped and transported to the middle channel. ② An AC electric field is applied to measure the particle's charge with OTE and a DC electric field is applied to remove ionic species from the bulk of the liquid in the surfactant-enriched top channel. The particle is now moved to the top channel (DC field still present). ③ Wait for several minutes. ④ Measure the particle's charge again. ⑤ Release the particle and repeat the experiment with another particle. This time without a DC field.

Now four charges are measured Q_1, Q_2, Q_3 and Q_4 and together they contain significant information on how the surfactant influences the charging mechanism of the particle. After all, the aim of this experiment is to exploit a key difference in the acid-base and preferential adsorption mechanisms:

- In an acid-base charging mechanism, neutral inverse micelles approach the particle, adsorb onto the surface where they take up an ion and then the newly charged inverse micelle leaves.
- In preferential adsorption, a charged inverse micelle approaches the particle and it leaves its ionic content behind at the particle's surface.

Now, because a DC electric field was applied sufficiently strong to remove all ionic species from the bulk of the liquid, it is not possible for the particle to acquire any charge due to preferential adsorption. Therefore, if $|Q_1| \ll |Q_2|$, it can be concluded that the particle did not acquire charge by preferential adsorption but more likely due to an acid-base charging mechanism. On the other hand, if $|Q_1| \approx |Q_2|$ and $|Q_3| \ll |Q_4|$, this is a strong indication that the particle acquires charge through preferential adsorption.

There exist two obvious ways to expand this experiment:

1. Instead of waiting for several minutes, the particle's charge could be monitored continuously. In the process, the rate at which the particle charges can be measured. In the case that $|Q_1| \ll |Q_2|$ and $|Q_3| \ll |Q_4|$, it could be very interesting to check whether particles acquire charge at the same rate. If the transition from $|Q_1| \to |Q_2|$ happens much faster than the transition from $|Q_3| \to |Q_4|$, this would seem to indicate that in the absence of a DC field, preferential adsorption is the dominant mechanism, but that it is also not the only mechanism that is present.
2. A logical extra step can be added after step 4 where the particle is transported back to the middle channel and the particle's charge is

measured again. It can now be measured whether the particle can retain its acquired charge.

This experiment seems to have enormous potential and while the fabrication stage is more challenging, the experiments offer to be much more accessible since it does not require the detection of elementary charging and discharging events.

6.2.3 Noise induced escape rate

The electric field-induced charging mechanism which has been discussed at length in Chapter 4 is a likely form of ion dissociation that is aided by applying an AC electric field. Because OTE can resolve single charging events, I have been able to determine how the reaction rate is influenced by the presence of an electric field or by the particle's size. Even though these parameters influence the reaction rate, the process remains a stochastic process. This stochastic element is likely because an amount of energy is required to escape the particle's surface. This energy can be generated by thermal motion of the liquid molecules, which is a stochastic process.

Taking this into account, the analysis of electric field-induced charging could be taken one step further by proposing a formula for the potential well. This formula could be a combination of *Van der Waals* forces and electrostatic forces. Once a formula for the potential well is established, the escape rate can be calculated by *Kramer's*[126] method or by a more recent variation of it[127].

Chapter 7.

References

1. Comiskey, B., et al., *An electrophoretic ink for all-printed reflective electronic displays.* Nature, 1998. **394**(6690): p. 253-255.
2. Chen, Y., et al., *Flexible active-matrix electronic ink display.* Nature, 2003. **423**(6936): p. 136-136.
3. Pearlstine, K., L. Page, and L. Elsayed, *Mechanism of Electric Charging of Toner Particles in Nonaqueous Liquid with Carboxylic-Acid Charge Additives.* Journal of Imaging Science, 1991. **35**(1): p. 55-58.
4. Rosenholm, J.B., *Solvent and surfactant induced interactions in drug dispersions.* Colloids and Surfaces a-Physicochemical and Engineering Aspects, 2010. **354**(1-3): p. 197-204.
5. Strubbe, F., et al., *Generation current of charged micelles in nonaqueous liquids: Measurements and simulations.* Journal of Colloid and Interface Science, 2006. **300**(1): p. 396-403.
6. Kornbrekke, R.E., I.D. Morrison, and T. Oja, *Electrophoretic Mobility Measurements in Low Conductivity Media.* Langmuir, 1992. **8**(4): p. 1211-1217.
7. Hsu, M.F., E.R. Dufresne, and D.A. Weitz, *Charge stabilization in nonpolar solvents.* Langmuir, 2005. **21**(11): p. 4881-4887.
8. Smith, P.G., et al., *Effect of surface hydrophilicity on charging mechanism of colloids in low-permittivity solvents.* Journal of Physical Chemistry C, 2007. **111**(2): p. 840-848.
9. Espinosa, C.E., et al., *Particle Charging and Charge Screening in Nonpolar Dispersions with Nonionic Surfactants.* Langmuir, 2010. **26**(22): p. 16941-16948.
10. Guo, Q., V. Singh, and S.H. Behrens, *Electric Charging in Nonpolar Liquids Because of Nonionizable Surfactants.* Langmuir, 2010. **26**(5): p. 3203-3207.
11. Dukhin, A. and S. Parlia, *Ions, ion pairs and inverse micelles in non-polar media.* Current Opinion in Colloid & Interface Science, 2013. **18**(2): p. 93-115.
12. Lyklema, J., *Principles of interactions in non-aqueous electrolyte solutions.* Current Opinion in Colloid & Interface Science, 2013. **18**(2): p. 116-128.
13. Lee, J., et al., *Mechanisms of Particle Charging by Surfactants in Nonpolar Dispersions.* Langmuir, 2015. **31**(44): p. 11989-11999.
14. Hao, T., *Exploring the charging mechanisms in non-aqueous multiphase surfactant solutions, emulsions and colloidal systems via conductivity behaviors predicted with eyring's rate process theory.* Physical Chemistry Chemical Physics, 2016. **18**(1): p. 476-491.

15. Gacek, M.M. and J.C. Berg, *The role of acid-base effects on particle charging in apolar media.* Advances in Colloid and Interface Science, 2015. **220**: p. 108-123.
16. Smith, G.N., J.E. Hallett, and J. Eastoe, *Celebrating Soft Matter's 10th Anniversary: Influencing the charge of poly(methyl methacrylate) latexes in nonpolar solvents.* Soft Matter, 2015. **11**(41): p. 8029-8041.
17. Strubbe, F., F. Beunis, and K. Neyts, *Detection of elementary charges on colloidal particles.* Physical Review Letters, 2008. **100**(21).
18. Sainis, S.K., J.W. Merrill, and E.R. Dufresne, *Electrostatic Interactions of Colloidal Particles at Vanishing Ionic Strength.* Langmuir, 2008. **24**(23): p. 13334-13347.
19. Tucker, I.M., et al., *Laser Doppler Electrophoresis applied to colloids and surfaces.* Current Opinion in Colloid & Interface Science, 2015. **20**(4): p. 215-226.
20. McNeil-Watson, F., W. Tscharnuter, and J. Miller, *A new instrument for the measurement of very small electrophoretic mobilities using phase analysis light scattering (PALS).* Colloids and Surfaces a-Physicochemical and Engineering Aspects, 1998. **140**(1-3): p. 53-57.
21. Smith, P.G., et al., *Electrophoretic mobility measurement by differential-phase optical coherence tomography.* Journal of Physical Chemistry C, 2007. **111**(6): p. 2614-2622.
22. Dukhin, A.S. and P.J. Goetz, *Acoustic and electroacoustic spectroscopy.* Langmuir, 1996. **12**(18): p. 4336-4344.
23. Guo, Q., et al., *Surfactant mediated charging of polymer particles in a nonpolar liquid.* Journal of Colloid and Interface Science, 2013. **392**: p. 83-89.
24. Poovarodom, S. and J.C. Berg, *Effect of particle and surfactant acid-base properties on charging of colloids in apolar media.* Journal of Colloid and Interface Science, 2010. **346**(2): p. 370-377.
25. Gacek, M., G. Brooks, and J.C. Berg, *Characterization of Mineral Oxide Charging in Apolar Media.* Langmuir, 2012. **28**(5): p. 3032-3036.
26. Antl, L., et al., *The Preparation of Poly(Methyl Methacrylate) Lattices in Nonaqueous Media.* Colloids and Surfaces, 1986. **17**(1): p. 67-78.
27. Khademi, M., et al., *Zeta Potential of Poly(methyl methacrylate) (PMMA) in Contact with Aqueous Electrolyte-Surfactant Solutions.* Langmuir, 2017. **33**(40): p. 10473-10482.
28. Smith, G.N., et al., *Charging Poly(methyl Methacrylate) Latexes in Nonpolar Solvents: Effect of Particle Concentration.* Langmuir, 2017. **33**(47): p. 13543-13553.

29. Duplantier, B., *Brownian motion, "Diverse and undulating".* Einstein, 1905-2005: Poincare Seminar 2005, 2006. **47**: p. 201-293.
30. Einstein, A., *Zur Quantentheorie der Strahlung.* Physikalische Zeitschrift, 1917. **18**: p. 121-128.
31. Maiman, T.H., *Stimulated Optical Radiation in Ruby.* Nature, 1960. **187**: p. 493–494.
32. Ashkin, A., *Acceleration and Trapping of Particles by Radiation Pressure.* Physical Review Letters, 1970. **24**(4): p. 156-&.
33. Ashkin, A., et al., *Observation of a Single-Beam Gradient Force Optical Trap for Dielectric Particles.* Optics Letters, 1986. **11**(5): p. 288-290.
34. Chu, S., et al., *Experimental-Observation of Optically Trapped Atoms.* Physical Review Letters, 1986. **57**(3): p. 314-317.
35. Kawata, S., et al., *Finer features for functional microdevices - Micromachines can be created with higher resolution using two-photon absorption.* Nature, 2001. **412**(6848): p. 697-698.
36. Ashkin, A., J.M. Dziedzic, and T. Yamane, *Optical Trapping and Manipulation of Single Cells Using Infrared-Laser Beams.* Nature, 1987. **330**(6150): p. 769-771.
37. Ono, M., et al., *Mitotic tethers connect sister chromosomes and transmit "cross-polar" force during anaphase A of mitosis in PtK2 cells.* Biomedical Optics Express, 2017. **8**(10): p. 4310-4315.
38. Diekmann, R., et al., *Nanoscopy of bacterial cells immobilized by holographic optical tweezers.* Nature Communications, 2016. **7**.
39. Wang, S.F., et al., *Reflection Microspectroscopic Study of Laser Trapping Assembling of Polystyrene Nanoparticles at Air/Solution Interface.* Journal of Physical Chemistry C, 2016. **120**(29): p. 15578-15585.
40. Varney, M.C.M., N.J. Jenness, and I.I. Smalyukh, *Geometrically unrestricted, topologically constrained control of liquid crystal defects using simultaneous holonomic magnetic and holographic optical manipulation.* Physical Review E, 2014. **89**(2).
41. Ruffner, D.B. and D.G. Grier, *Optical Conveyors: A Class of Active Tractor Beams.* Physical Review Letters, 2012. **109**(16).
42. Ribezzi-Crivellari, M., J.M. Huguet, and F. Ritort, *Counter-propagating dual-trap optical tweezers based on linear momentum conservation.* Review of Scientific Instruments, 2013. **84**(4).
43. Kawauchi, H., et al., *Calculation of optical trapping forces on a dielectric sphere in the ray optics regime produced by a radially polarized laser beam.* Optics Letters, 2007. **32**(13): p. 1839-1841.

44. Harada, Y. and T. Asakura, *Radiation forces on a dielectric sphere in the Rayleigh scattering regime.* Optics Communications, 1996. **124**(5-6): p. 529-541.
45. Garbow, N., M. Evers, and T. Palberg, *Optical tweezing electrophoresis of isolated, highly charged colloidal spheres.* Colloids and Surfaces a-Physicochemical and Engineering Aspects, 2001. **195**(1-3): p. 227-241.
46. Debye, P., Hückel, E., *ON THE THEORY OF ELECTROLYTES. I. FREEZING POINT DEPRESSION AND RELATED PHENOMENA.* Physikalische Zeitschrift, 1923. **24**(9): p. 185-206.
47. Derjaguin, B., Landau, L., *Theory of the stability of strongly charged lyophobic sols and of the adhesion of strongly charged particles in solutions of electrolytes.* Acta Physico Chemica URSS, 1941. **14**(633).
48. Verwey, E.J.W.O., J. Th. G., *Theory of the stability of lyophobic colloids.* Elsevier, 1948.
49. Stern, O., *Zur theorie der elektrolytischen doppelschicht.* Z. Elektrochem. Angew. Phys. Chem., 1924. **30**: p. 508-516.
50. Delgado, A.V., et al., *Measurement and interpretation of electrokinetic phenomena.* Journal of Colloid and Interface Science, 2007. **309**(2): p. 194-224.
51. Lobaskin, V., et al., *Electrophoresis of colloidal dispersions in the low-salt regime.* Physical Review Letters, 2007. **98**(17).
52. Strubbe, F., et al., *Electrokinetics of colloidal particles in nonpolar media containing charged inverse micelles.* Applied Physics Letters, 2008. **93**(25).
53. Smith, G.N. and J. Eastoe, *Controlling colloid charge in nonpolar liquids with surfactants.* Physical Chemistry Chemical Physics, 2013. **15**(2): p. 424-439.
54. Romero-Cano, M.S., et al., *Colloidal stabilization of polystyrene particles by adsorption of nonionic surfactant - II. Electrosteric stability studies.* Journal of Colloid and Interface Science, 1998. **198**(2): p. 273-281.
55. Sainis, S.K., et al., *Electrostatic interactions of colloidal particles in nonpolar solvents: Role of surface chemistry and charge control agents.* Langmuir, 2008. **24**(4): p. 1160-1164.
56. Klinkenberg A, v.d.M.J.L., *Electrostatics in the petroleum industry: the prevention of explosion hazards.* Elsevier, 1958.
57. Rabinow, B.E., *Nanosuspensions in drug delivery.* Nature Reviews Drug Discovery, 2004. **3**(9): p. 785-796.

58. Wang, Y.C., et al., *Stability of nanosuspensions in drug delivery.* Journal of Controlled Release, 2013. **172**(3): p. 1126-1141.
59. Vanderhoeven, P.H.C. and J. Lyklema, *Electrostatic Stabilization in Nonaqueous Media.* Advances in Colloid and Interface Science, 1992. **42**: p. 205-277.
60. Kim, Y.D., *A surfactant bridge model for the nonlinear electrorheological effects of surfactant-activated ER suspensions.* Journal of Colloid and Interface Science, 2001. **236**(2): p. 225-232.
61. Percin, G., T.S. Lundgren, and B.T. Khuri-Yakub, *Controlled ink-jet printing and deposition of organic polymers and solid particles.* Applied Physics Letters, 1998. **73**(16): p. 2375-2377.
62. Graydon, O. and J. Heikenfeld, *Bright future for electronic paper.* Nature Photonics, 2009. **3**(5): p. 304-304.
63. Karvar, M., et al., *Investigation of Various Types of Inverse Micelles in Nonpolar Liquids Using Transient Current Measurements.* Langmuir, 2014. **30**(41): p. 12138-12143.
64. Gacek, M.M. and J.C. Berg, *Effect of surfactant hydrophile-lipophile balance (HLB) value on mineral oxide charging in apolar media.* Journal of Colloid and Interface Science, 2015. **449**: p. 192-197.
65. Schmidt, J., et al., *Conductivity in nonpolar media: Experimental and numerical studies on sodium AOT-hexadecane, lecithin-hexadecane and aluminum(III)-3,5-diisopropyl salicylate-hexadecane systems.* Journal of Colloid and Interface Science, 2012. **386**: p. 240-251.
66. Karvar, M., et al., *Transport of Charged Aerosol OT Inverse Micelles in Nonpolar Liquids.* Langmuir, 2011. **27**(17): p. 10386-10391.
67. Bleier, B.J., et al., *Droplet-based characterization of surfactant efficacy in colloidal stabilization of carbon black in nonpolar solvents.* Journal of Colloid and Interface Science, 2017. **493**: p. 265-274.
68. Yezer, B.A., et al., *Use of electrochemical impedance spectroscopy to determine double-layer capacitance in doped nonpolar liquids.* Journal of Colloid and Interface Science, 2015. **449**: p. 2-12.
69. Gacek, M.M. and J.C. Berg, *Effect of synergists on organic pigment particle charging in apolar media.* Electrophoresis, 2014. **35**(12-13): p. 1766-1772.
70. Fowkes, F.M., et al., *General Discussion.* Discussions of the Faraday Society, 1966(42): p. 243-+.
71. Pugh, R.J., T. Matsunaga, and F.M. Fowkes, *The Dispersibility and Stability of Carbon-Black in Media of Low Dielectric-Constant .1. Electrostatic and Steric Contributions to Colloidal Stability.* Colloids and Surfaces, 1983. **7**(3): p. 183-207.

72. Roberts, G.S., et al., *Electrostatic charging of nonpolar colloids by reverse micelles.* Langmuir, 2008. **24**(13): p. 6530-6541.
73. McNamee, C.E., Y. Tsujii, and M. Matsumoto, *Interaction forces between two silica surfaces in an apolar solvent containing an anionic surfactant.* Langmuir, 2004. **20**(5): p. 1791-1798.
74. Kitahara, A., et al., *Concentration Effect of Surfactants on Zeta-Potential in Non-Aqueous Dispersions.* Colloid and Polymer Science, 1977. **255**(11): p. 1118-1121.
75. Jenkins, P., et al., *The electrochemistry of nonaqueous copper phthalocyanine dispersions in the presence of a metal soap surfactant: A simple equilibrium site binding model.* Journal of Colloid and Interface Science, 1999. **211**(2): p. 252-263.
76. Sugita, T. and T. Ohshimay, *Evaluation of Electrophoretic Migration of Submicron Particles in a Microgap by Optical and Current Responses.* Japanese Journal of Applied Physics, 2010. **49**(12).
77. Briscoe, W.H. and R.G. Horn, *Direct measurement of surface forces due to charging of solids immersed in a nonpolar liquid.* Langmuir, 2002. **18**(10): p. 3945-3956.
78. Fuoss, R.M. and L. Onsager, *Conductance of Unassociated Electrolytes.* Journal of Physical Chemistry, 1957. **61**(5): p. 668-682.
79. Shilov, V.N., Y.B. Borkovskaja, and A.S. Dukhin, *Electroacoustic theory for concentrated colloids with overlapped DLs at arbitrary kappa a - I. Application to nanocolloids and nonaqueous colloids.* Journal of Colloid and Interface Science, 2004. **277**(2): p. 347-358.
80. Strubbe, F., M. Prasad, and F. Beunis, *Characterizing Generated Charged Inverse Micelles with Transient Current Measurements.* Journal of Physical Chemistry B, 2015. **119**(5): p. 1957-1965.
81. Neyts, K., et al., *Charge transport and current in non-polar liquids.* Journal of Physics-Condensed Matter, 2010. **22**(49).
82. Smith, G.N., et al., *Interaction between Surfactants and Colloidal Latexes in Nonpolar Solvents Studied Using Contrast-Variation Small-Angle Neutron Scattering.* Langmuir, 2014. **30**(12): p. 3422-3431.
83. Luderitz, L.A.C. and R. von Klitzing, *Interaction forces between silica surfaces in cationic surfactant solutions: An atomic force microscopy study.* Journal of Colloid and Interface Science, 2013. **402**: p. 19-26.
84. Crocker, J.C. and D.G. Grier, *Microscopic Measurement of the Pair Interaction Potential of Charge-Stabilized Colloid.* Physical Review Letters, 1994. **73**(2): p. 352-355.

85. Garbow, N., et al., *High-resolution particle sizing by optical tracking of single colloidal particles.* Physica a-Statistical Mechanics and Its Applications, 1997. **235**(1-2): p. 291-305.
86. Griffiths, D., et al., *Zeta Potential Measurement of Nanoparticles by Nanoparticle Tracking Analysis (NTA).* Nanotechnology 2011: Advanced Materials, Cnts, Particles, Films and Composites, Nsti-Nanotech 2011, Vol 1, 2011: p. 4-7.
87. Evans, D.J., A.D. Hollingsworth, and D.G. Grier, *Charge renormalization in nominally apolar colloidal dispersions.* Physical Review E, 2016. **93**(4).
88. Sainis, S.K., V. Germain, and E.R. Dufresne, *Statistics of particle trajectories at short time intervals reveal fN-scale colloidal forces.* Physical Review Letters, 2007. **99**(1).
89. Patel, M.N., et al., *Electrophoretic mobility of concentrated carbon black dispersions in a low-permittivity solvent by optical coherence tomography.* Journal of Colloid and Interface Science, 2010. **345**(2): p. 194-199.
90. Beunis, F., et al., *Beyond Millikan: The Dynamics of Charging Events on Individual Colloidal Particles.* Physical Review Letters, 2012. **108**(1).
91. Burgreen, D. and F.R. Nakache, *Electrokinetic Flow in Ultrafine Capillary Slits.* Journal of Physical Chemistry, 1964. **68**(5): p. 1084-&.
92. Roberts, G.S., et al., *Direct measurement of the effective charge in nonpolar suspensions by optical tracking of single particles.* Journal of Chemical Physics, 2007. **126**(19).
93. Auer, S., W.C.K. Poon, and D. Frenkel, *Phase behavior and crystallization kinetics of poly-12-hydroxystearic-coated polymethylmethacrylate colloids.* Physical Review E, 2003. **67**(2).
94. Merrill, J.W., S.K. Sainis, and E.R. Dufresne, *Many-Body Electrostatic Forces between Colloidal Particles at Vanishing Ionic Strength.* Physical Review Letters, 2009. **103**(13).
95. Smith, G.N., et al., *The effects of counterion exchange on charge stabilization for anionic surfactants in nonpolar solvents.* Journal of Colloid and Interface Science, 2016. **465**: p. 316-322.
96. Kemp, R., et al., *Nanoparticle Charge Control in Nonpolar Liquids: Insights from Small-Angle Neutron Scattering and Microelectrophoresis.* Langmuir, 2010. **26**(10): p. 6967-6976.
97. Noel, A., et al., *Tridodecylamine, an efficient charge control agent in non-polar media for electrophoretic inks application.* Applied Surface Science, 2018. **428**: p. 870-876.

98. Liu, H.L., et al., *Charging behavior of carbon black in a low-permittivity medium based on acid-base charging theory.* Journal of Materials Chemistry C, 2015. **3**(16): p. 3980-3988.
99. Smith, G.N., et al., *Surfactants with colloids: Adsorption or absorption?* Journal of Colloid and Interface Science, 2015. **449**: p. 205-214.
100. Poovarodom, S., S. Poovarodom, and J.C. Berg, *Effect of alkyl functionalization on charging of colloidal silica in apolar media.* Journal of Colloid and Interface Science, 2010. **351**(2): p. 415-420.
101. Carbeck, J.D., et al., *Protein charge ladders, capillary electrophoresis, and the role of electrostatics in biomolecular recognition.* Accounts of Chemical Research, 1998. **31**(6): p. 343-350.
102. Kim, K., K. Ihm, and B. Kim, *Surface Property of Indium Tin Oxide (ITO) After Various Methods of Cleaning.* Acta Physica Polonica A, 2015. **127**(4): p. 1176-1179.
103. Castano-Alvarez, M., et al., *Critical points in the fabrication of microfluidic devices on glass substrates.* Sensors and Actuators B-Chemical, 2008. **130**(1): p. 436-448.
104. Parent, M.E., et al., *Influence of Surfactant Structure on Reverse Micelle Size and Charge for Nonpolar Electrophoretic Inks.* Langmuir, 2011. **27**(19): p. 11845-11851.
105. Gittes, F. and C.F. Schmidt, *Interference model for back-focal-plane displacement detection in optical tweezers.* Optics Letters, 1998. **23**(1): p. 7-9.
106. Galneder, R., et al., *Microelectrophoresis of a bilayer-coated silica bead in an optical trap: Application to enzymology.* Biophysical Journal, 2001. **80**(5): p. 2298-2309.
107. Brans, T., et al., *Joule heating monitoring in a microfluidic channel by observing the Brownian motion of an optically trapped microsphere.* Electrophoresis, 2015. **36**(17): p. 2102-2109.
108. Tolic-Norrelykke, I.M., K. Berg-Sorensen, and H. Flyvbjerg, *MatLab program for precision calibration of optical tweezers.* Computer Physics Communications, 2004. **159**(3): p. 225-240.
109. Rohrbach, A. and E.H.K. Stelzer, *Three-dimensional position detection of optically trapped dielectric particles.* Journal of Applied Physics, 2002. **91**(8): p. 5474-5488.
110. F., S., *Electrokinetics and charging mechanisms of colloidal particles in nonpolar liquids.* Ph.D. thesis, 2008-2009.

111. Smith, G.N., et al., *Electrolyte-induced Instability of Colloidal Dispersions in Nonpolar Solvents.* Journal of Physical Chemistry Letters, 2017. **8**(19): p. 4668-4672.
112. Russel, M.K., P.R. Selvaganapathy, and C.Y. Ching, *Effect of electrode surface topology on charge injection characteristics in dielectric liquids: An experimental study.* Journal of Electrostatics, 2014. **72**(6): p. 487-492.
113. Beunis, F., et al., *Electric charging of inverse micelles in a nonpolar liquid with surfactant.* Colloids and Surfaces a-Physicochemical and Engineering Aspects, 2014. **440**: p. 10-19.
114. Gacek, M., et al., *Effects of Trace Water on Charging of Silica Particles Dispersed in a Nonpolar Medium.* Langmuir, 2012. **28**(31): p. 11633-11638.
115. Morrison, I.D., *Electrical Charges in Nonaqueous Media.* Colloids and Surfaces a-Physicochemical and Engineering Aspects, 1993. **71**(1): p. 1-37.
116. van der Linden, M.N., et al., *Charging of Poly(methyl methacrylate) (PMMA) Colloids in Cyclohexyl Bromide: Locking, Size Dependence, and Particle Mixtures.* Langmuir, 2015. **31**(1): p. 65-75.
117. Ryoo, W., et al., *Electrostatic stabilization of colloids in carbon dioxide: Electrophoresis and dielectrophoresis.* Langmuir, 2005. **21**(13): p. 5914-5923.
118. Dukhin, A.S. and P.J. Goetz, *How non-ionic "electrically neutral" surfactants enhance electrical conductivity and ion stability in non-polar liquids.* Journal of Electroanalytical Chemistry, 2006. **588**(1): p. 44-50.
119. Verschueren, A.R.M., et al., *Screening and Separation of Charges in Microscale Devices: Complete Planar Solution of the Poisson-Boltzmann Equation.* Journal of Physical Chemistry B, 2008. **112**(41): p. 13038-13050.
120. Strubbe, F., et al., *Electrophoretic Retardation of Colloidal Particles in Nonpolar Liquids.* Physical Review X, 2013. **3**(2).
121. Aaboud, M., et al., *Precision measurement and interpretation of inclusive W+, W- and Z/gamma* production cross sections with the ATLAS detector.* European Physical Journal C, 2017. **77**(6).
122. Berg-Sorensen, K. and H. Flyvbjerg, *Power spectrum analysis for optical tweezers.* Review of Scientific Instruments, 2004. **75**(3): p. 594-612.

123. Schreuer, C., et al., *Electric field induced charging of colloidal particles in a nonpolar liquid.* Journal of Colloid and Interface Science, 2018. **515**: p. 248-254.
124. Schreuer, C., et al., *Single charging events on colloidal particles in a nonpolar liquid with surfactant.* Journal of Applied Physics, 2018. **123**(1).
125. Taylor, M.A., et al., *Enhanced optical trapping via structured scattering.* Nature Photonics, 2015. **9**(10): p. 669-+.
126. Hanggi, P., P. Talkner, and M. Borkovec, *Reaction-Rate Theory - 50 Years after Kramers.* Reviews of Modern Physics, 1990. **62**(2): p. 251-341.
127. Maier, R.S. and D.L. Stein, *Noise-activated escape from a sloshing potential well.* Physical Review Letters, 2001. **86**(18): p. 3942-3945.